Implementation of Optogenetic Voltage Sensor VSFP2.3 to Visualize Cardiac Excitation

Vom Promotionsausschuss der

Technischen Universität Hamburg-Harburg

zur Erlangung des akademischen Grades

Doktorin der Naturwissenschaften (Dr. rer. nat.)

genehmigte Dissertation

von

Mei-Ling Chang Liao

aus

Taipei, Taiwan

2014

Gutachter:

1. Prof. Dr. Wolfgang Krautschneider
2. Prof. Dr. Michael Morlock
3. Prof. Dr. Wolfram H. Zimmermann

Tag der mündlichen Prüfung: 8. April 2014

Table of content

Acknowledgement

I would like to thank my supervisors, Prof. Dr. Michael Morlock and Prof. Dr. Wolfram-Hubertus Zimmermann, for providing me the opportunity to work on this interesting topic and for their supervision and support. I would also like to thank my thesis committee, Prof. Dr. Wolfgang Krautschneider, for his valuable comments.

This project required many techniques and knowledge, which I couldn't accomplish solely on my own. I would like to thank the following people for their technical and intellectual assistance,

Prof. Thomas Knöpfel, Dr. Hiroki Mutoh, Yuka Iwamoto, and members in Prof. Knoepfel's group, for the help in the concept, establishing and screening for the transgenic mouse lines, as well as their warm hospitality during my stay in Japan.

Prof. Erich Wettwer, Dr. Teun de Boer for the help in patch clamp and preparing the knowledge for me to be an electrophysiologist.

Prof. Stefan Luther, Prof. Stephan Lehnart, Dr. Claudia Richter, Dr. Nour Raad and Dr. Bernhard Unsöld for the assistance in optical mapping and animal experiment.

Dr. Stephan Doeker for the excellent cloning instruction.

Dr. Kaomei Guan, Dr. Katrin Streckfuss-Bömeke, and Dr. Peter Christalla for the help in establishing the iPSC lines.

Our technical staff, Mrs. Ursel Leonhardt for taking care of the mice and genotyping, Mr. Roland Blume for the help in echocardiography.

Many thank to all the members and technical staff in the Institute of Pharmacology in the University Medical Center Goettingen for their assistance in many aspects. Special appreciation goes to Simin Chen, Dr. Poh Loong Soong, and Sumon Sur for the brainstorming and their invaluable friendship, which accompanied me through the ups and downs. An immense gratitude goes to my best friend, Yun-Shu Yang, who has helped me go through the bitter and sweet moment in all these years. Without whose spiritual inspiration, I wouldn't have gone so far.

Family is always the staunch backing of mine. Thanks to my adorable niece and nephew who have always brought me laughter and warmth. Thanks to my relatives back home who have help look after my parents while I am far away from home.

I would like to dedicate my thesis to my parents, Jing-Hsiu Yang, Kwui-Kun Chang Liao, and my brothers, Wan-Gong Chang Liao, Wan-Jun Chang Liao. Their unconditional love and support encourage me to pursue my dream and to stand up whenever I fall. My appreciation is beyond words.

Abstract

The initiation and propagation of electrical signals play a pivotal role in normal cardiac function. These are carried out by cardiomyocytes, the building blocks of the heart, which generate and conduct electrical signal from one cell to another, throughout the whole heart. The techniques used for investigating electrical activities in cardiomyocytes and hearts, such as applying electrodes and optical mapping, possess different advantages and disadvantages. Microelectrode recordings, for example, provide direct and faithful insight into changes in the current and membrane potential from single cardiomyocytes. The experimental procedure, however, is laborious and invasive, which prevents repeated recordings on the same cells at different time points. Optical mapping using flourescent dyes offers a non-invasive technique with higher spatial-temporal resolution. However, the fluorescent dyes used are usually toxic, and the distribution of the dyes could be inhomogeneous due to the complex tissue structure. Moreover, repeated and simultaneous recordings at different time points in living cell/tissue are most challenging. Thus, *in vivo* and long-term applications are limited in the abovementioned set up.

In this study, the hypothesis that a voltage sensitive fluorescent protein (VSFP2.3) is applicable for the visualization of cardiac excitability was tested. Optogenetic labeling with VSFP2.3 may overcome some of the aforementioned shortcomings. VSFP2.3 can be stably expressed in defined cell types by using cell type specific promoter elements, making it functional throughout lifetime. Combined with high speed and highly sensitive cameras, chronic studies in a noninvasive manner are feasible.

Firstly, a transgenic mouse model stably expressing VSFP2.3 under the control of the cardiac specific alpha myosin heavy chain promoter (αMHC) was established. The transgene did not impair myocardial structure and cardiac function. Adult cardiomyocytes isolated from these transgenic mice showed clear membrane labeling of VSFP2.3. The electrical activities from single VSFP2.3 cardiomyocytes and whole hearts were optically recorded with high sensitive cameras and photomultipliers and validated the use of this approach.

Secondly, double transgenic induced pluripotent stem cell (iPSC) lines carrying both neomycin resistant gene (neoR) and VSFP2.3 under the control of αMHC promoter were generated. NeoRVSFP iPSCs were differentiated into spontaneously beating cardiomyocytes. Changes in fluorescent signals were recorded from beating cardiomyocytes indicating the function of the protein. Engineered heart muscles (EHMs) generated from neoRVSFP iPSC-derived cardiomyocytes contracted spontaneously and responded to increasing extracellular calcium concentrations with an increase in force development. Fluorescent signals within EHMs were acquired successfully.

Collectively, this study demonstrated for the first time that a genetically encoded voltage sensor expressed in the mammalian heart can serve as a means to precisely assess cardiomyocyte excitability.

Zusammenfassung

Die Initiierung und Übertragung von elektrischen Signalen spielen eine essentielle Rolle für die normale Herzfunktion. Diese werden von Kardiomyozyten, den funktionellen Bausteinen des Herzens, generiert und von einer zur nächsten Zelle und somit durch das gesamte Herz weitergeleitet. Die derzeitigen Methoden zur Untersuchung von elektrischer Aktivität in Kardiomyozyten und des gesamten Herzens über Elektroden und optische Kartierung beinhalten verschiedene Vor- und Nachteile. Beispielsweise liefern Aufnahmen mittels Mikroelektroden direkte und vertrauensvolle Einblicke über Änderungen von Stromfluss und Membranpotenzial von vereinzelten Zellen. Allerdings ist das experimentelle Vorgehen umständlich und invasiv, welches wiederholte Aufnahmen derselben Zelle zu unterschiedlichen Zeitpunkten verhindert. Optische Kartierungen mittels Fluoreszenzfarbstoffen weisen dahingegen eine höhere räumlich-zeitliche Auflösung auf. Jedoch sind diese Farbstoffe, obwohl nicht-invasiv, im Allgemeinen toxisch; zudem kann die Verteilung der Farbstoffe aufgrund der komplexen Gewebestruktur inhomogen ausfallen. Darüber hinaus stellen wiederholte, simultane Aufnahmen zu verschiedenen Zeitpunkten von vitalen Zellen bzw. Geweben eine technische Herausforderung dar, so dass Studien *in vivo* und über einen langen Zeitraum stark limitiert sind.

In der vorliegenden Arbeit wurde die Hypothese untersucht, dass das spannungssensitive fluoreszierende Protein VSFP2.3 zur Visualisierung von kardialer, elektrischer Erregung anwendbar ist. Über optogenetische Markierungen mittels VSFP2.3 sollen die obengenannten Defizite umgangen werden. VSFP2.3 kann in definierten Zelltypen stabil exprimiert werden, indem zellspezifische Promotorelemente verwendet werden, wobei das Protein permanent funktional bleibt. Dies kombiniert mit Bildgebung über Hochgeschwindigkeits- und hochsensitive Kameras wird longitudinale, nicht-invasive Studien ermöglichen.

Zunächst wurde ein transgenes Mausmodell mit stabiler VSFP2.3-Expression unter der Kontrolle des kardial-spezifischen *α-Myosin Heavy Chain* (αMHC) Promotors etabliert. Das Transgen beeinträchtigte weder die Myokardstruktur noch die kardiale Funktion. Isolierte adulte Kardiomyozyten aus αMHCVSFP2.3-Mäuse wiesen eine

deutliche Membranmarkierung auf. Elektrische Aktivitäten dieser Zellen und vom gesamten Herzen konnten zeitlich und räumlich hochaufgelöst optisch erfasst werden.

Anschließend wurden doppelt-transgene induzierte pluripotente Stammzell-Linien (iPSC) generiert, die sowohl für das Neomycin-Resistenzgen (neoR) als auch für VSFP2.3 unter der Kontrolle des αMHC-Promotors kodierten: neoRVSFP-iPSC. Diese konnten erfolgreich zu spontan kontrahierenden Kardiomyozyten differenziert werden. Auch hier konnte nachgewiesen werden, dass sich VSFP2.3 in Herzmuskelzellen zur optischen Analyse der elektrischen Funktion eignet. Aus VSFP2.3 exprimierenden Herzmuskelzellen konnten schließlich spontan kontrahierende EHM (*Engineered Heart Muscle*) entwickelt werden. Auch in den EHMs konnten Fluoreszenzsignale erfolgreich aufgezeichnet werden.

Zusammenfassend demonstriert die vorliegende Arbeit erstmalig die Anwendung eines genetisch kodierten Spannungssensors im Säugerherzen. Damit wird die nicht-invasive Beurteilung der elektrischen Aktivität in Herzmuskelzellen *in vitro* und *in vivo* mit hoher zeitlicher und räumlicher Auflösung auch im longitudinalen Experiment möglich.

List of Figures

List of Tables

Abbreviations

ALP	alkaline phosphatase
αMHC	alpha myosin heavy chain (aka myh6)
APD	action potential durations
APs	action potentials
AV node	atrio-ventricular node
BCL	basic cycle lengths
BDM	2,3-butanedione 2-monoxime
BSA	bovine serum albumin
c-Myc	c-myc proto-oncogene
cDNA	complementary DNA
CFP	cyan fluorescent protein
CHD	coronary heart disease
CHF	congestive heart failure
Ci-VSP	*Ciona intestinalis*-Voltage-Sensor-containing Phosphatase
CICR	Calcium-Induced Calcium Release
CM	cardiaomyocytes
CSC	cardiac stem cells
CVD	cardiovascular diseases
CytoD	cytochalasin D

DAPI	4’, 6’-diamidino-2-phenylindole
DEPC	diethylpyrocarbonate
DMSO	dimethyl sulfoxide
DPBS	Dulbecco's phosphate buffered saline
E-C coupling	excitation-contraction coupling
EB	embryoid bodies
ECG	electrocardiogram
EHM	engineered heart muscle
EPC	endothelial progenitor cells
ESC	embryonic stem cells
EtBr	ethidium bromide
FBS	fetal bovine serum
FOC	force of contraction
FP	fluorescent protein
FRET	fluorescent resonance energy transfer
GAPDH	glyceraldehyde 3-phosphate dehydrogenase
GFP	green fluorescent protein
ICD	implantable cardiac defibrillator
iPSC	induced pluripotent stem cells
Klf4	Kruppel-like factor 4
MCS	multiple cloning site

MEA	multiple electrode arrays
MEFs	mouse embryonic fibroblasts
MMC	mitomycin-c
MOI	multiplicity of infection
MSC	mesenchymal stem cells
Nanog	transcription factor
neoR	neomycin resistance gene
Oct3/4	octamer binding transcription factor 3/4
P/S	penicillin/streptomycin
PCR	polymerase chain reaction
PMT	photomultiplier tube
RE	restriction enzyme
Rex 1	zinc finger protein-42 (aka Zfp42)
RMP	resting membrane potential
ROS	reactive oxygen species
RT	reverse transcription
RyR	ryanodine receptor
RyR2	ryanodine receptors 2 (cardiac isoform)
S/N	signal-to-noise ratio
SA node	sinoatrial node
SEM	standard error of mean

SKM	skeletal myoblasts
Sox2	sex determining region Y-box 2
SR	sarcoplasmic reticulum
SSEA-1	stage-specific embryonic antigen-1
TnC	troponin C
TTFs	tail tip fibroblasts
VSD	voltage-sensing domain
VSFP	voltage sensitive fluorescent protein
YFP	yellow fluorescent protein

1. Introduction

1.1 Heart diseases and tissue engineering based therapy

Cardiovascular diseases (CVDs), including hypertension, coronary heart disease (CHD), congestive heart failure (CHF), valvular defects, and congenital cardiovascular defects, are the main cause for morbidity and mortality worldwide. CVDs often occur with acute or chronic loss of critical amount of cardiomyocytes. Subsequently, the diseased heart undergoes remodeling process such as forming non-contractile scar tissue, dilated ventricle, wall thinning, and eventually lead to heart failure or death. Since cardiomyocytes are terminated differentiated cells that only have limited ability to regenerate once they are injured, the loss of myocardium is nearly irreversible. Medication and implanted assist devices can partially improve the cardiac function, but the function of the damaged myocardium cannot be revived. Heart transplantation is the ultimate way to fully restore the cardiac function; however, this approach is limited by the availability of organ and the rejection complications.

Therapeutics based on cell transplantation has emerged as an approach for repairing myocardium since the past decades. Several types of donor cells, including fetal cardiomyocytes, skeletal myoblasts (SKMs), endothelial progenitor cells (EPCs), mesenchymal stem cells (MSCs), embryonic stem cells (ESCs), and more recently, cardiac stem cells (CSCs), have been used as the sources for the cardiac regeneration by direct injection to the injured site or by inducing paracrine effects. Given the potential of unlimited self-renewal and the possibility to differentiate into all cell types, ESCs are considered as the best candidate for cell therapy. However, the infinite proliferation of ESCs leads to high risk of teratoma formation[1, 2], which is the major concern of ESCs-based cell therapy. An alternative promising approach is to differentiate ESCs into cardiomyocytes *in vitro*, and replenish the injured myocardium with ESC-derived cardiomyocytes. Although the risk of tumor formation can be averted, the ethical issue still remains the key point of contention. Besides, considering the amount of cardiomyocytes loss due to diseases or injury, the low efficiency of cardiac differentiation and low cell number that retains and engrafts with native myocardium after transplantation are the main obstacles as well.

A major breakthrough to bypass the ethical issue of using ESCs was the discovery of converting somatic cells such as fibroblasts into ESC-like pluripotent state by introducing four transcription factors: Oct4, Sox2, Klf4, and c-Myc[3]. These induced pluripotent stem cells (iPSCs) can be derived from one's own cell, which can be used for the generation of patient-specific stem cell lines. The patient-specific stem cell lines provide models for the study of certain disease conditions, and assays for drug screening. In addition, since iPSCs are derived from the subjects of interest, the immune rejection complications may be reduced[4].

In order to compensate for the massive loss of myocardium during CVDs, large quantities of cardiomyocytes and high survival rate after implantation are required. The generation of 3-dimensional cardiac tissue constructs *ex vivo* provides another solution for this demand. In general, heart muscle can be engineered *in vitro* by stacking cardiac cell monolayers (Fig. 1A)[5-7], seeding cardiac cells to decellularized native tissue (Fig. 1B)[8] or scaffolds (Fig. 1E and 1D)[9, 10], mixing cardiomyocytes with hydrogels to form engineered heart muscle (EHM) (Fig. 1C)[11], and using hydrogel as a vehicle for delivering cells to the injured sites (Fig. 1F)[12]. The cultivation and formation of functional EHM can be improved under certain condition such as electrical stimulation[13-15] and mechanical stimulation[16]. Beside therapeutic potentials, EHM can also be used as disease models and provide platforms for drug screening.

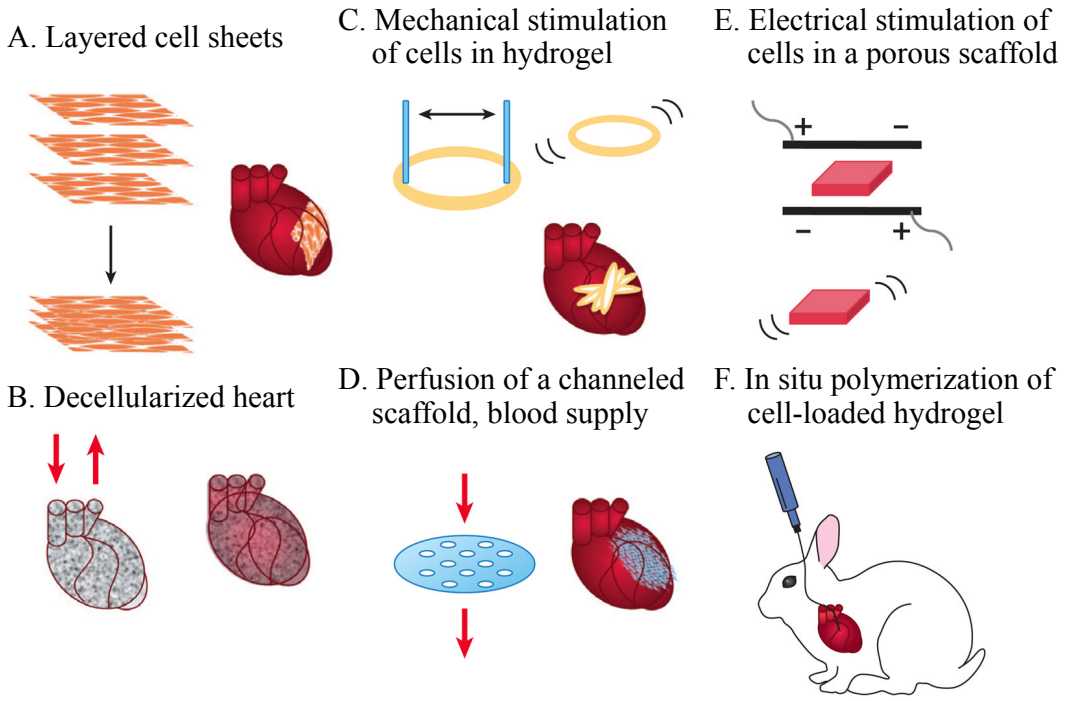

Fig. 1 Different approaches for heart muscle engineering[15].

The essential requirements for either cell therapy or cardiac tissue engineering are to restore normal structure and function of the injured myocardium. For this, electromechanical integration of the grafts with native myocardium is essential. Monitoring the electrical activities during cardiogenesis and within EHM during its *in vitro* assembly and in vivo integration will aid in understanding underlying mechanisms and ultimately facilitate cell and EHM engraftment.

1.2 Aims of the study

We hypothesize the genetically encoded voltage sensor proteins, VSFP2.3, can be engineered under the control of the cardiac specific alpha myosin heavy chain (αMHC) promoter and to be expressed exclusively in cardiomyocytes. Using this genetic engineering approach, we would be able to monitor the electrical activities of the heart, and heart muscle assembly in vitro, as well as the potentially EHM graft-host coupling.

The aims of the study were twofold:

(1) To establish a transgenic mouse model with cardiomyocyte-restricetd expression of VSFP2.3 for AP recordings on a cellular and whole heart level.
(2) To develop and characterize pluripotent stem cells with stable expression of VSFP2.3 in cardiomyocytes for the studies of cardiac regeneration and cardiac tissue engineering.

2. Background

2.1 Electrophysiology of the heart – from organ to cellular levels

The heart is one of the most important organs in the human body. It pumps blood to the whole body to provide oxygen and nutrient that are essential for maintaining daily life. The pumping function of the heart is controlled by the electrical signals (i.e. action potentials, APs) initiated from the sinoatrial (SA) node. Followed by a sequence of events, APs propagate and eventually trigger the contraction of the atria and ventricles through a process known as excitation-contraction coupling (E-C coupling). This process requires proper generation and conduction of the APs.

The SA node is a region of specialized cardiac muscle fibers located in the posterior wall of the right atrium of the heart. It serves as the natural pacemaker of the heart that generates the APs spontaneously and rhythmically. Besides the SA node, the constituent parts of the cardiac conduction system also include the atrio-ventricular (AV) node, the bundle of His, the left and right bundle branches, and the Purkinje fibers (Fig. 2). The electrical impulses from the SA node spread through both atria, which result in the contraction of the atria, and eventually reach the AV node. After a certain delay, the impulses continue to travel along the bundle of His, the bundle branches and then to the Purkinje fibers, triggering the contraction of the ventricles that propels the blood to the whole body. The delay in the AV node allows enough time for the atria to eject all the blood into the ventricles efficiently.

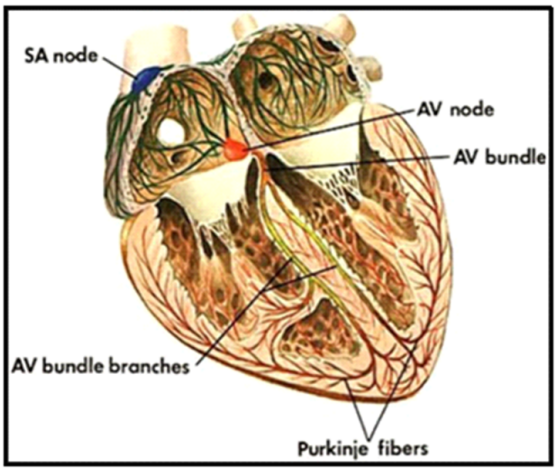

Fig. 2 The conduction system of the heart. The conduction pathway consists of five elements: 1. SA node; 2. AV node; 3. AV bundle (the bundle of His); 4. AV bundle branches; 5. Purkinji fibers[17].

Cardiac action potential

Cardiac cells are excitable cells that generate and conduct APs spontaneously or under electrical stimulation from adjacent cells. APs of the heart exhibit regional heterogeneity providing different electrical properties by different cell types. Nevertheless, cardiac APs can be classified into two major types, according to the cellular response to the electrical stimulation. The first type of APs, known as fast APs, is mainly found in the ventricles, atria, and the specialized conducting cells in Purkinje fibers. This type of APs consist of a rapid upstroke (phase 0), a brief partial repolarization (phase 1), a plateau (phase 2) and a slower repolarization (phase 3). The stable, flat interval between two APs with a stable resting membrane potential (RMP) is defined as phase 4 of the AP (Fig. 3). On the other hand, the second type of APs, slow APs, have much less steep phase 0, absence of phase 1, a short and slanted phase 2 which is not very distinguishable from phase 3. The RMP of slow APs is also less negative than fast APs. The slow response cells are primary found in nodal cells, i.e. SA node and AV node (Fig. 4).

The generation of cardiac APs involves complex processes of ions flux across cell membrane primary through ion channels passively or secondarily through ion pump or exchanger actively. This is due to the differences in ionic distribution between intracellular and extracellular environment, as well as the permeability of cell membrane to certain ions during various phases of APs. The major currents that are responsible for carrying out APs are sodium (Na^+), potassium (K^+), and calcium

(Ca^{2+}) currents, while others play minor roles. A typical ventricular AP consists of five phases (Fig. 3),

Phase 0: The rapid depolarization phase. Upon excitation, the fast Na^{+} channels open rapidly which results in a large influx of Na^{+} ions.

Phase 1: Partial repolarization phase. Activation of K+ channel leads to transient outward K+ current (I_{to}). This brief efflux of K+ regulates the action potential duration and the duration of phase 2.

Phase 2: Plateau phase. During this phase, Ca^{2+} enters the cell through Ca^{2+} channels, which are much slower than Na+ channels. The influx of Ca^{2+} is counterbalanced by the efflux of K^{+} ions through different K^{+} channels.

Phase 3: Repolarization phase. When the efflux of K^{+} starts to exceed the influx of Ca^{2+}, the repolarization begins. The inwardly rectified K^{+} current mainly contributes to repolarization.

Phase 4: Resting membrane potential. At rest, the cell membrane is highly permeable to K^{+}. Due to the concentration gradient, K^{+} tends to flux out of the cell through several specific types of K^{+} channels.

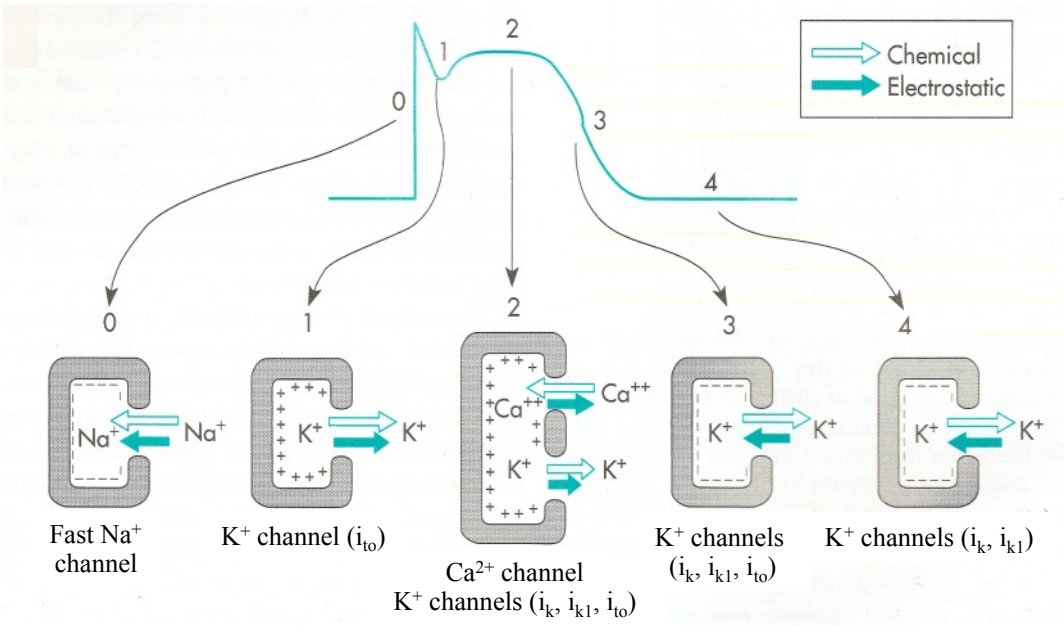

Fig. 3 A typical ventricular AP consists of five phases. Various ion fluxes contribute to different phases of AP. The direction of ions flux is determined by the net effects between chemical (concentration gradient) and electrostatic force. Modified from[18].

Unlike the ventricular APs, the upstroke of the pacemaker potential is mainly caused by the influx of Ca^{2+} current through L-type Ca^{2+} channels. Since the nodal cells have low density of Ca^{2+} channels, the conduction is much slower. The plateau phase does not sustain, thus, following the slow depolarization, APs directly proceed to repolarization (phase 3). Similar to the ventricular APs, phase 3 is primary dependent on the efflux of K^+ current (Fig. 4).

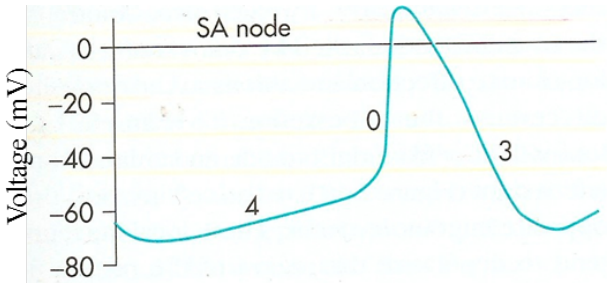

Fig. 4 Pacemaker potential. Pacemaker potential has a less negative and unstable resting potential (phase 4), less steep upstroke (phase 0), and slower repolarization (phase 3). Modified from[19].

Automaticity

Certain cardiac cells have the ability to initiate APs spontaneously and rhythmically, despite lacking innervation or stimulation. These cells are mainly found in nodal tissue (SA node and AV node) and specialized conducting fibers (Purkinji fibers). However, under normal physiological condition, the APs firing rate in SA node which is much faster than that of the AV node and Purkinje fibers, overdrives and suppresses the pacemaking activities from the other sites. Thus, SA node serves as the only pacemaker of the heart.

The pacemaker cells express special f-channels. I_f current is a mixture of Na^+ and K^+, which is the underlying mechanism of cardiac automaticity[20]. Unlike the ventricular APs, the pacemaker potential has a less negative and unstable resting potential (phase 4). This is attributed to the cell membrane being leaky to Na^+ and low K^+ permeability. Thus, the positively charged Na^+ ions spontaneously enter the cell membrane raising the resting membrane potential. At the same time, K^+ also slowly flow out of the cell. Both actions cause the slow depolarization and when the potential reaches the threshold (about -40 mV), the APs are initiated and the cells enter phase 3.

Conductivity – Cardiac functional syncytium

Instead of fusing together to form a syncytium as in skeletal muscle cells, individual cardiac cells connect to each other via intercalated discs. This unique structural component contains gap junctions and adhesion junctions (Fig. 5).

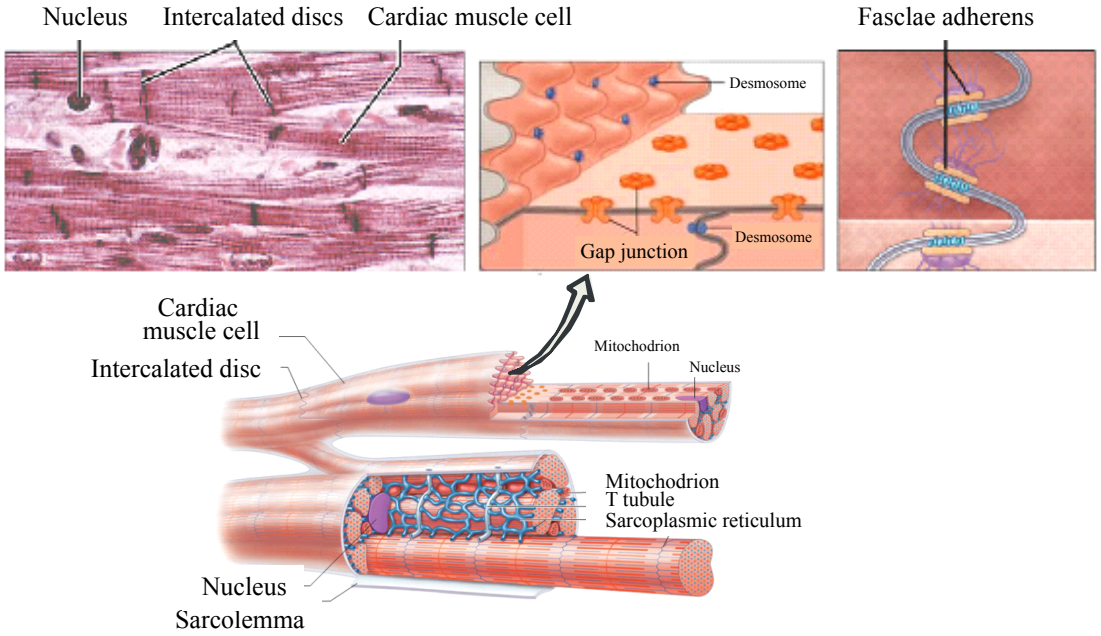

Fig. 5 Microscopic view of cardiac muscle cells. (Left) cardiac muscle cells are striated, branched, and interconnected to each other by intercalated discs. Intercalated disc contains gap junctions, desmosomes (Middle) and fasciae adherens (Right). Modified from http://antranik.org/myocardium/ and http://classes.midlandstech.edu/carterp/Courses/bio211/chap18/chap18.html

Gap junctions are intercellular channels that connect cytoplasma membrane of neighboring cells. These channels allow ions and molecules to pass through, so that cardiac cells are electrically and metabolically coupled. Thus, APs initiated from the pacemaker cells can be propagated freely to the adjacent cells, throughout the whole heart and eventually induce synchronized contractions. Adhesion junctions stabilize the sarcolemma between cells to provide support and strength so that neighboring cells can be held together tightly during contraction (sliding). As a result of both electrical and mechanical coupling, the heart function as a single contractile unit known as cardiac functional syncytium.

Contractility: E-C coupling

From a microscopic point of view, every heartbeat is associated with a membrane depolarization (AP) and a subsequent rise and decay of free intracellular calcium concentration (calcium transient or calcium cycling). This process is called excitation-contraction coupling (E-C coupling). These sequential events that AP triggers contraction of myocytes are indications of cardiac functional syncytium and critical for the heart to function normally.

The T-tubule system and sarcoplasmic reticulum (SR) play key roles in E-C coupling. In general, an AP propagated from adjacent cells causes an inward flux of extracellular calcium (I_{Ca}) through the activated L-type voltage-gated calcium channel located on T-tubules. The increase of intracellular calcium further induces a release of calcium from sarcoplasmic reticulum (SR) via calcium channels or ryanodine receptors (RyR), a process known as calcium-induced calcium release (CICR) (Fig. 6).

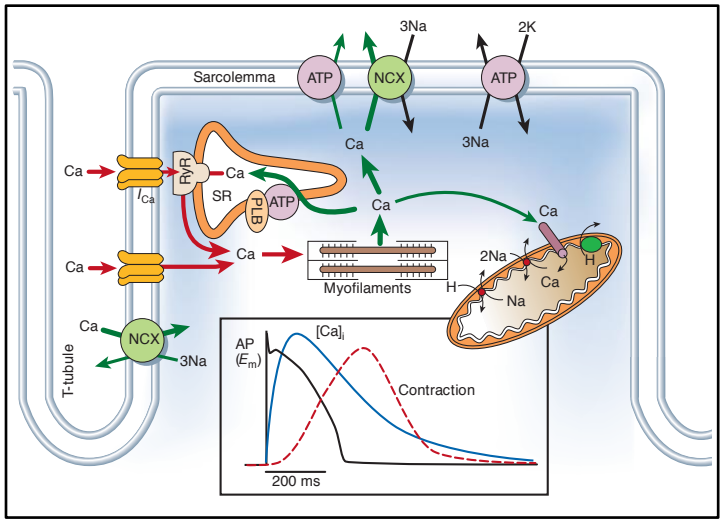

Fig. 6 Calcium-induced calcium release (CICR). Inset diagram shows the temporal relation between the cardiac action potential (black), the intracellular Ca2+ transient (blue), and the generation of contraction force (dotted red)[21].

Two types of myofilament stack up to form a bundle of myofibrils. The thin filament is composed primary of actin, tropomyosin and troponin proteins. On the other hand, the thick filament contains myosin protein (Fig. 7). The troponin complex plays pivotal roles in regulating the E-C coupling process. Free intracellular Ca^{2+} binds to the Ca^{2+} binding sites on the troponin complex (troponin-C, TnC) on the actin filament. This induces conformational changes that expose the myosin binding sites on actin monomers. Thus, the myosin heads can bind to actin monomers to form cross-bridges. This protein-protein interaction eventually transduces the Ca^{2+} signals into force development.

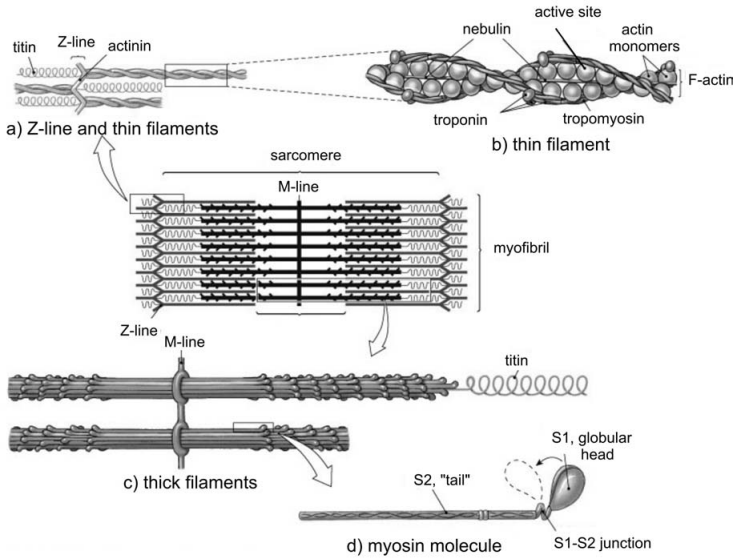

Fig. 7 Scheme of a muscle unit. Sarcomere is the functional unit of the cardiac cells. Two types of myofilament stack up to form a bundle of myofibrils. The interaction between thin and thick filament results in the contraction of the muscle[22].

The disturbances of the electrical activities in the heart

From above mentioned, the initiation and propagation of the electrical signals are important determinants for normal cardiac function. Alteration in automaticity, impaired cardiac functional syncytium, and interrupted E-C coupling under certain pathological conditions, such as ischemia, heart failure, and congenital heart disease, may disturb the electrical activities of the heart, induce arrhythmia, abnormalities in

mechanical function, and the worst case scenario, cause sudden death. Treatments of heart disease, such as medications, implantable cardiac defibrillators (ICD), stem cell therapy and cardiac tissue engineering aim to restore electrical propagation, the cardiac muscle structure, as well as the mechanical function. Thus, understandings of the electrical properties in the cardiomyocyte under normal and abnormal conditions are of considerable importance.

2.2 Investigation of cardiac electrical activities

Conventionally, the measurement of changes in membrane potential could be done by intracellular microelectrodes and extracellular multiple electrode arrays (MEA). Although it provides direct and faithful recordings of membrane potential, the impalement of intracellular microelectrodes constrains its applications in several aspects. When inserting microelectrode tips into the intracellular space, it is challenging to maintain the tips for stable recordings over longer time periods. These invasive techniques also damage the cells and cannot be applied to small cells (<3 um in diameter), subcellular organelles and in organ level[23, 24]. Recordings from more than two or three sites are not possible, thus the study of activation pattern is limited[23, 25, 26]. While MEA provide solutions for some of the above-mentioned limitations, the interpretation of the activation data[27, 28] and the determination of repolarization times remain unreliable[29, 30]. Another major concern for microelectrode based measurements, either intracellular or extracellular, is that the recordings are affected by artifacts from external electrical fields when stimulations or defibrillation are applied. This hampers their application in the studies of shock-induced arrhythmogenesis and the underlying mechanisms of whether defibrillation succeed or not[23].

To overcome these difficulties and limitations, advanced techniques by means of optical recordings were developed. The introduction of potentiometric probes made it possible to optically record dynamic change in membrane potential in axons[31, 32]. Optical imaging of action potential using voltage sensitive dyes then was first applied in the field of cardiac electrophysiology after nearly a decade[33]. Thereafter, optical imaging has drawn much attention and become a widely used method in cardiac

research. Optical mapping technique possesses several important advantages over the conventionally microelectrode methods. It can be applied in a wide range of preparations, either *in vivo* or *in vitro*, from single myocytes[34-36], cell monolayers[37-40], dissected heart tissue (i.e. ventricles[41-43], atria[44-46], conduction system[47-49]), engineered heart muscle (EHM)[50, 51], and in intact whole hearts[52-55]. The voltage sensitive dyes have rapid response to membrane potential changes within microsecond scale[25], providing high temporal resolution. In addition, the response is free of pacing and electrical shock artifacts that allow the investigation of transmembrane potential changes during stimulation and defibrillation[56, 57]. This non-invasive technique also enable stable recordings from multiple sites (few hundreds sites) simultaneously for longer time periods, giving high spatiotemporal resolution that is capable of mapping the action potential propagation, recording the repolarization map, determining the repolarization time, and calculating the conduction velocity (Fig. 8). It enables our better understandings in APs propagation, cell-cell coupling not only under normal rhythm of the heart, but also the arrhythymogenesis mechanism under pathological condition[58-61]. If proper pairs of fluorescent dyes were chosen, membrane potential and intracellular calcium could also be recorded simultaneously[52, 62-64]. Besides, by applying different parameter-sensitive dyes, optical mapping technique can also be used to measure different physiological parameters such as the cellular metabolic state, oxidative phosphorylation redox state, the oxygen content of blood and cardiac muscle, intracellular ion concentrations (Ca^{2+}, Mg^{2+}, Na^{+}), pH and more[23].

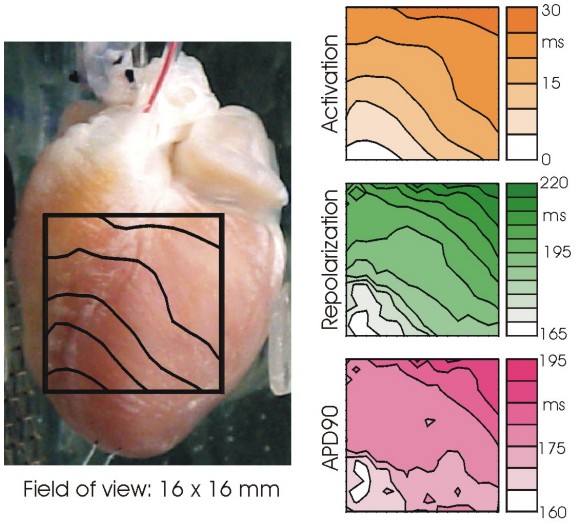

Fig. 8 An example of optical mapping of intact whole heart. (Left) Langendorff perfused rabbit heart. Inset showed the field of view from a 16x16 photodiode array and an isochronal map of APs activation. (Right) AP activation, repolarization and action potential duration at 90% repolarization (APD90) can be calculated from recorded data to show the pattern of the AP initiation and propagation. Modified from[57].

Despite the rapid response and relatively high spatiotemporal resolution, the application of fluorescent dyes in optical mapping technique to study cardiac electrophysiology also possesses certain drawbacks. While applying to mammalian systems, the most notable obstacles of this technique are the uneven distribution, non-specific binding and phototoxicity of the dyes.

Due to the complexity and multicellular structure of the heart, it is challenging to stain tissue slices or intact whole heart, either by incubation or perfusion with dye solution, homogeneously and with stable concentration. In addition, voltage-sensitive dyes bind to cell membranes of all cell types, including non-excitable cells. So, optical signals from the membranes of interest are immersed in background fluorescence from the inactive cells. This leads to poor signal-to-noise ratio (S/N). Apart from that, when exposed to fluorescent lights repeatedly, fluorescent dyes tend to react with oxygen and produce free radicals that can damage cells; hence the experiment duration is limited by phototoxicity.

Modifications of parameter-sensitive probes and better staining procedures that could result in higher sensitivity and S/N are needed. Recently, the introduction of genetically encoded fluorescent protein sensors has advanced optical mapping to a new direction.

2.3 Genetically encoded voltage sensitive fluorescent protein as a tool

With the advent of green fluorescent protein (GFP) from jellyfish *Aequorea victoria*[65] and subsequent development of its variants[66, 67], imaging of living cells became feasible[68]. The fluorescent protein (FP)-based biosensors can be targeted to specific cell types by making use of cell-specific promoters to drive their expression. By further refinements of the FP-labeling technology it has become possible to create not only stationary cell labels, but biosensors for the evaluation of cellular activities, such as the alterations of intracellular calcium[69-74], pH[75-77], reactive oxygen species (ROS)[78, 79], and PKA-activity[80]; or light-activated channelrhodopsins for the control of molecular processes[81]. These technologies can be summarized as optogenetic tools as they combine genetic engineering with *in vivo* fluorescent probes[82-84]. Of special interest to the cardiac field is the use of optogenetic tools to visualize the alterations in membrane potential with minimal invasion. This appears particularly difficult because of the necessity to target the voltage sensors to biological membranes and the challenge to detect small alterations in membrane voltage.

The original idea for designing the genetic voltage sensors was derived from the voltage-gated ion channels. In general, the subunit of a voltage-gated ion channel (sodium or potassium) consists of six transmembrane segments, in which the S1-S4 regions serve as the voltage-sensing domain (VSD) while the S5-S6 regions form the pore structure (Fig. 9)[85]. The voltage-sensing mechanism is mainly based on the movement of positively charged amino acid residues in the S4 segment. Upon depolarization, the positive charges move outward across the membrane resulting in the rotation of the S4 segment. This rotational movement then pulls the S4-S5 linker and opens the pore[86].

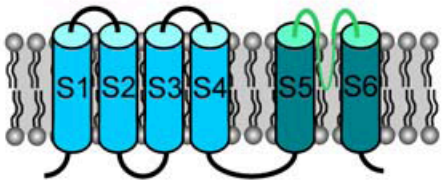

Fig. 9 The simplified membrane topology of a voltage-gated ion channel. The S1-S4 segment serves as the voltage-sensing domain (VSD), while the S5-S6 serves as the pore structure. Modified from[85].

Using GFP-based FP as the reporter and fusing it to a voltage-gated ion channel or its subunit resulted in the first generation of genetic voltage sensors. The first prototype was constructed by inserting a modified GFP into the C terminus of the *Drosophila* voltage sensitive Shaker K+ channel (FlaSh)[87] (Fig. 10A). The second prototype, sodium channel protein-based activity reporting construct (SPARC) (Fig. 10B), was created by introducing GFP into the skeletal sodium channel[88]. The third design of the voltage sensitive fluorescent protein (VSFP1) was generated by coupling a pair of cyan and yellow fluorescent protein (CFP and YFP) to the VSD of voltage-gated potassium channels (Kv2.1)[89] (Fig. 10C). In the latter case, changes in membrane potential lead to fluorescent resonance energy transfer (FRET) between CFP and YFP[90, 91].

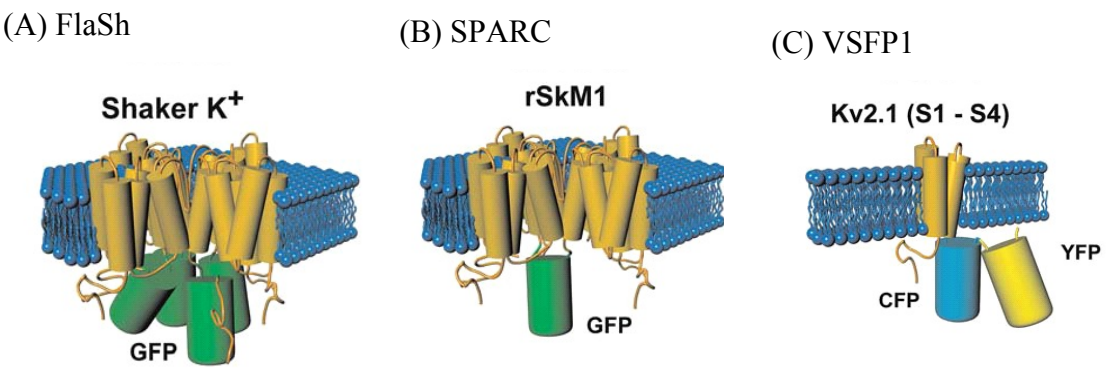

Fig. 10 Three prototypes of the first generation of genetic voltage sensor. The first generation of genetically encoded voltage sensors was based on inserting FPs into ion channel or its subunits[92].

These original ion channel-based biosensors exhibited slow kinetics, low sensitivity and lack of function or/and poor membrane targeting when expressed in mammalian cells[87, 89, 93, 94]. The possible reasons might be that the natural properties of the ion channels were compromised while inserting or attaching FPs[95].

A non-ion channel protein Ci-VSP (*Ciona intestinalis*-Voltage-Sensor-containing Phosphatase) (Fig. 11A)[85] was discovered to have a self-contained voltage sensing domain that is homologous to the VSD of the Kv channels[96]. The VSD from Ci-VSP can reside on the membrane as a monomer[96-98], which could be independent to the

interaction between other membrane proteins, thus was expected to have higher membrane targeting efficiency in mammalian cells[95]. The second generation of VSFP (VSFP2x) coupled a pair of CFP and YFP to the C-terminus of the 4th segment (S4) of the VSD from Ci-VSP[95]. By introducing a R217Q mutation in the S4 segment and optimizing the length of the linker between VSD and the FP or the FRET donor/acceptor pair, the voltage dependence of fluorescent response was shifted to a more physiological range, and both response kinetic and FRET efficiency were improved[92, 94, 95, 99]. The resulting voltage sensor is termed VSFP2.3 (Fig. 11B).

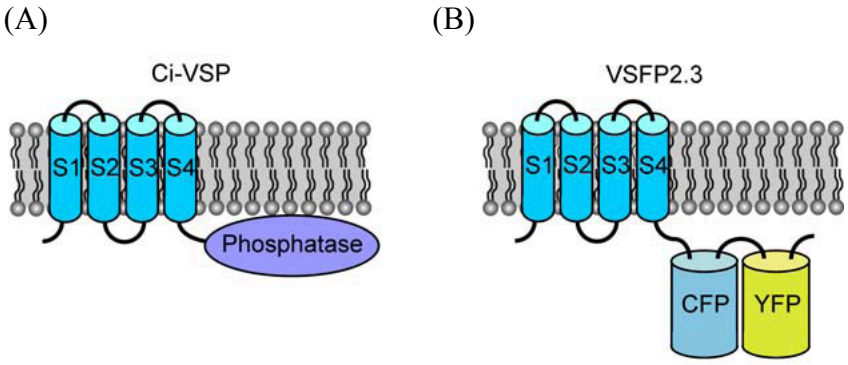

Fig. 11 Design of VSFP2.3. (A) Simplified membrane topology of Ci-VSP. Ci-VSP contains S1-S4 transmembrane segments and a cytoplasmic phosphatase. (B) By replacing the phosphatase in Ci-VSP with a pair of CFP and YFP, the second generation of voltage sensor (VSFP2.3) was formed. Modified from[85].

The voltage sensing mechanism of VSFP2.3 is mainly regulated by the S4 segment of the VSD. Upon a change in membrane potential, the movement of positive charges in the S4 segment following by a conformational transition of the protein induces the changes in the relative position between CFP (donor) and YFP (acceptor). Some energy released from the donor is transferred to the acceptor and excites the YFP emission (Fig. 12). Thus, for the FRET to occur, the emission spectrum of the donor and the excitation spectrum of the acceptor should have certain degree of overlap, and the two fluorochromes should be in the close vicinity. VSFP2.3 has been shown to have reliable function, clear membrane targeting, and relatively fast kinetics in mammalian neurons and brain slices[99-101]. Although the role of VSFP2.3 has not been

studied in heart, its biophysical properties appeared well suited for optical recordings of cardiac APs.

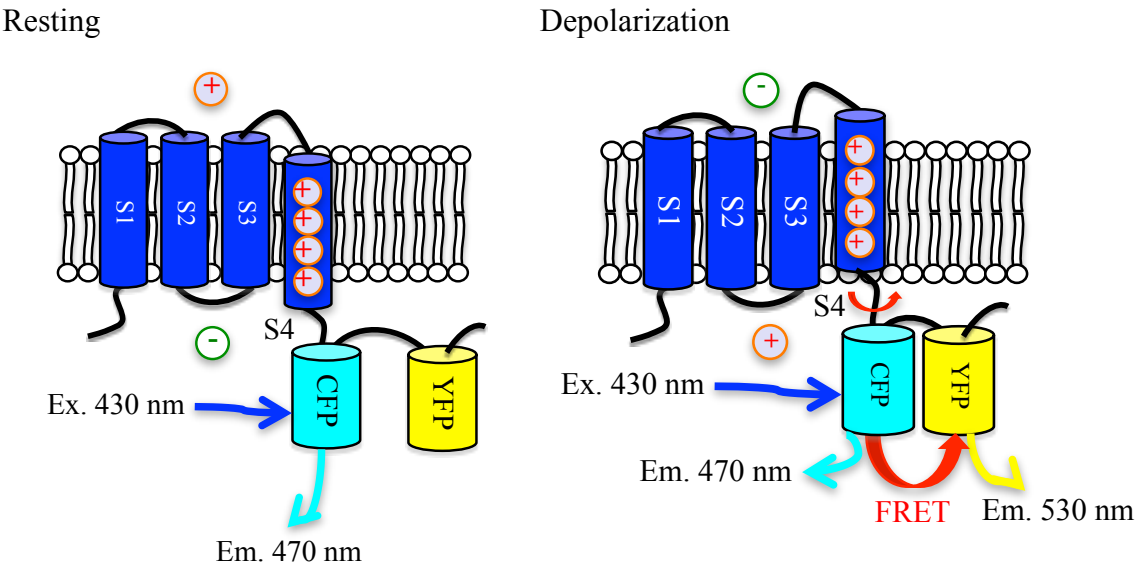

Fig. 12 The voltage sensing mechanism of VSFP2.3. (Left) At rest, cell excited by 430 nm light (CFP excitation) emits fluorescence light with wavelength 470 nm (CFP emission). (Right) Upon depolarization, charges movement in the S4 segment of the VSD and the conformational transition of the protein bring the two fluorochromes in close vicinity. Thus, FRET occurs and two emissions light, 470nm and 530 nm, can be recorded.

3. Generation and Characterization of αMHC-VSFP2.3 transgenic mouse model

To generate a transgenic mouse model expressing VSFP2.3 exclusively in the heart, a plasmid containing the VSFP2.3 transgene under the control of the cardiac specific alpha myosin heavy chain (αMHC) promoter was constructed (αMHC-VSFP2.3). Following pronuclear injection of the linearized plasmid, transgenic offspring was characterized and the function of VSFP2.3 was tested on cellular and whole heart levels.

3.1 Material and Methods

3.1.1 Cloning of the αMHC-VSFP2.3 reporter plasmid

A plasmid containing the cardiac specific αMHC promoter element (kindly provided by Prof. L. Field)[102] was used as the cloning backbone (αMHC-neo, Fig. 13). The subcloning strategy consists of the following steps (A~D), which are indicated in Fig. 13 and Fig. 14,

(A) Replacement of Xho I and Hind III cleavage sites by Pme I restriction enzyme (RE) cutting sites (GTT TAAAC): A HindIII/PmeI linker (5'-AGC TAC GTT TAA ACG T-3') was designed to have a Hind III overhang on both ends and a Pme I RE site in between. Similarly, XhoI/PmeI linker (5'-TCG AAC GTT TAA ACG T-3') was designed to have an XhoI overhang on both ends and a Pme I RE site in between. The resulting plasmid (αMHC-neo (2P)) was used for the next steps. The modification facilitated excision of the bacterial backbone with a single RE (PmeI) and created blunt ends, which reduces the propensity of self-ligation after linearization.

(B) Replacement of the neoR-polyA sequence by a well-defined intron-polyA sequence: The neoR-putative polyA fragment from αMHC-neo (2P) was replaced by a polyA sequence from pSTEC1[103] plasmid. Since there is no RE site between neoR gene and putative polyA sequence in αMHC-neo (2P), both of them were

cut out by double digestion with BamHI and NotI. Subsequently, an intron-polyA sequence from pSTEC1 was introduced. The new plasmid αMHC-PmeI-polyA was generated.

(C) Integration of a versatile multiple cloning site (MCS): A MCS was designed and integrated to simplify subsequent cloning for the integration of transgenes controlled by the αMHC promoter. Forward and reverse MCS were designed to have the same Not I overhang on both ends, and different orders of RE sites in between (Table 1). The resulting plasmid was labeled: αMHC-MCS. The final products (αMHC-MCS) were sent for sequencing to identify the forward and reverse MCS.

(D) Integration of the VSFP2.3 coding sequence into the MCS: The original VSFP2.3 encoding plasmid (VSFP2.3 cdn, Fig. 14) was kindly provided by Prof. T. Knöpfel (RIKEN, Saitama, Japan). The VSFP2.3 fragment was digested out using Nhe I/Hind III REs and inserted into the linearized αMHC-MCS plasmid. The resulting plasmid was labeled: αMHC-VSFP2.3.

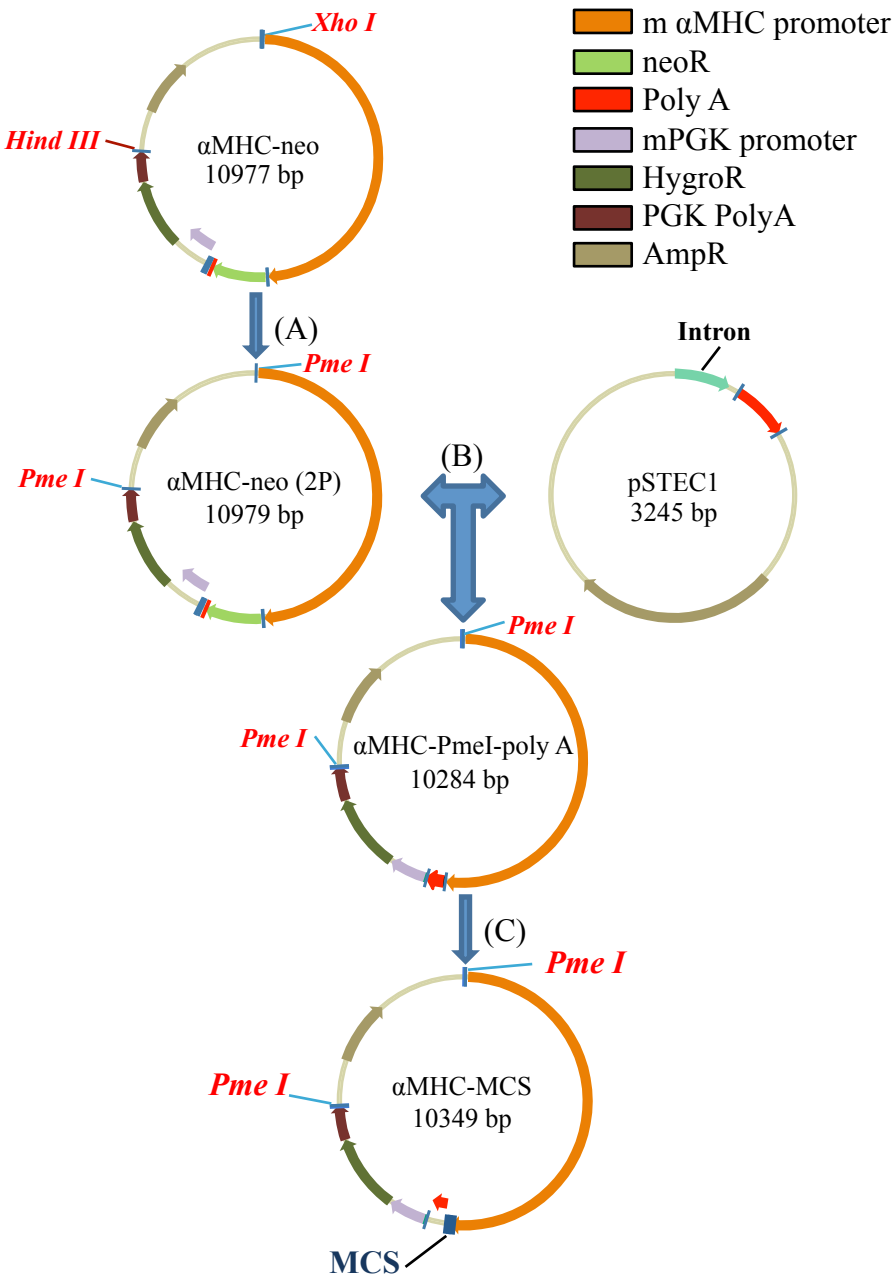

Fig. 13 Schematic overview of subcloning strategy. (A) Xho I and Hind III RE sites were replaced with PmeI. (B) neoR-polyA fragment was replaced with an intron-polyA sequence from pSTEC1. (C) A MCS was inserted between the αMHC promoter and intron-polyA sequences.

Table 1 Forward and reverse MCS linkers

Foward MCS (MCS) 65bp

NotIoh Kpn I Xho I Sal I Hind III EcoRV Not I Mlu I Nhe I Sac I

5´ - GGCC**TG**GGTACCCTCGAGGTCGACAAGCTT**C**GATATCGCGGCCGCACGCGTGCTAGCGAGCTC**CA** - 3’

3’ - **AC**CCATGGGAGCTCCAGCTGTTCGAA**G**CTATAGCGCCGGCGTGCGCACGATCGCTCGAG**GT**CCGG - 5’

Reverse MCS (rMCS) 65bp

NotIoh Sac I Nhe I Mlu I Not I EcoRV Hind III Sal I Xho I Kpn I

5´ - GGCC**TG**GAGCTCGCTAGCACGCGTGCGGCCGCGATATC**G**AAGCTTGTCGACCTCGAGGGTACC**CA** - 3’

3’ - **AC**CTCGAGCGATCGTGCGCACGCCGGCGCTATAG**C**TTCGAACAGCTGGAGCTCCCATGG**GT**CCGG - 5´

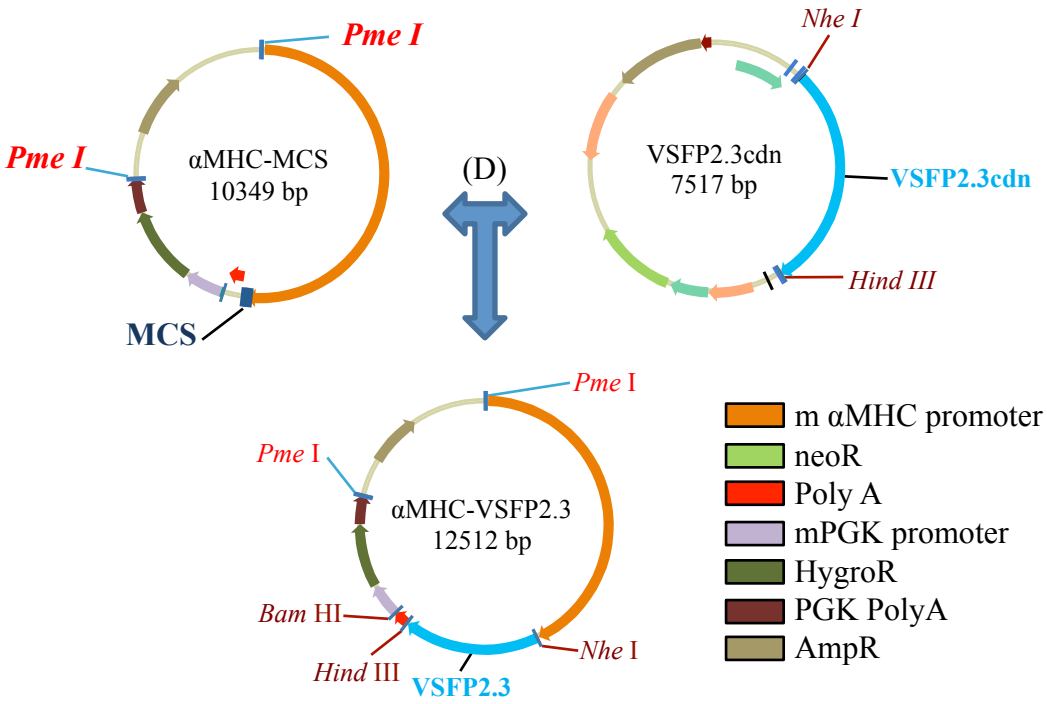

Fig. 14 Generation of αMHC-VSFP 2.3. cDNA fragment encoding for VSFP2.3 was integrated into the MCS (D).

Each subcloning step applied the molecular technologies including RE digestion, gel electrophoresis, DNA elution from gel, ligation, transformation, and plasmid DNA preparation (mini-prep). The following sections describe the individual steps in detailed.

3.1.1.1 Restriction enzyme digestion

Plasmid DNA was linearized by RE digestion as indicated below (Table 2). All reactions were performed at 37°C for 3 hours and results were confirmed by gel electrophoresis.

Table 2 Restriction enzyme digestion (A~D as indicated in Fig. 13 and 14)

Reactions for step (A)

RE	DNA (µl)	RE (µl)	Buffer (µl)	BSA (µl)	H2O (µl)	Total volume (µl)
Xho I	10	2	10	10	68	100
Hind III	10	2	10	10	68	100

Reaction for step (B)

plasmid	DNA (µl)	BamHI (µl)	Not I (µl)	Buffer (µl)	BSA (µl)	H2O (µl)	Total volume (µl)
αMHC-neo (2P)	20	2	2	10	10	56	100
pSTEC-1	15	4	2	10	10	59	100

Reaction for step (C)

plasmid	DNA (µl)	Not I (µl)	Buffer (µl)	BSA (µl)	H2O (µl)	Total volume (µl)
αMHC-PmeI -polyA	10	2	10	10	68	100

Reactions for step (D)

plasmid	DNA (µl)	Hind III (µl)	Nhe I (µl)	Buffer (µl)	BSA (µl)	H2O (µl)	Total volume (µl)
αMHC-MCS-rev	15	2	3	10	10	69	100
VSFP2.3	10	2	3	10	10	65	100

3.1.1.2 Gel electrophoresis

2.5 g of agarose was dissolved in 250 ml TAE buffer (Appendix) and boiled to obtain a 1% agarose gel solution. Following cooling of the solution, 0.2 µg/ml ethidium bromide (EtBR) was added and swirled to obtain a homogenous solution. The solution was then poured into a casting tray with appropriate combs and allowed to solidify. Samples were mixed with 6x loading dye (New England Biolabs, NEB) and loaded onto the gel. DNA fragments were separated by applying an electric field (80 V). The results were visualized under UV with GelDoc^{TM} XR+System (BioRad).

3.1.1.3 DNA elution from agarose gel

The linearized DNA fragments were eluted from the agarose gel using QIAquick gel extraction kit (QIAGEN) based on the manufacturer´s protocol. After gel electrophoresis, the appropriate DNA fragment with proper size was carefully excised from the agarose gel with a clean, sharp blade. The excised gel was weighed in a 1.5 ml reaction tube (Eppendorf) and 300 µl of Buffer QG was added per 100 mg of gel. The tubes were incubated at 50°C for 10 minutes. After the gel slice was completely dissolved, 100 µl of isopropanol was added to the tube and mixed well by vortexing. The mixture was then transferred to a QIAquick spin column with a 2 ml collection tube and spun at 13,000 x g for 1 minute. The flow-through was discarded. The column was washed with 0.5 ml Buffer QG and centrifuged at 13,000 x g for 1 minute. The flow-through was discarded and the column was washed with 0.75 ml PE Buffer. After centrifugation at 13,000 x g for 1 minute, the flow-through was discarded, and the centrifugation was repeated once to remove residual wash buffer. The column was placed into a clean 1.5 ml tube and 50 µl Buffer EB was added to the center of the column. The tube was allowed to stand at room temperature for up to 4 min and the DNA was eluted from the column by centrifugation at 13,000 x g for 1 minute. The concentration of DNA was quantified using a spectrophotometer (Nanodrop, ND-1000, Thermo Scientific).

3.1.1.4 Ligation

The purified linearized vector was ligated with inserts using T4 ligase (NEB) or Quick ligase (NEB). The mixture was incubated at 16°C overnight (Table 3). The ligation was set up based on the sizes and concentrations of the vector and insert using the following equation to obtain optimal ligation reactions,

$$Insert\ (ng) = Vector(ng) \times \frac{Insert\ (bp)}{Vector\ (bp)} \times ratio$$

Table 3 Ligation of vector and insert (A~D as indicated in Fig. 13 and 14)

Reactions for step (A)

Linearized vector	(µl)	Hind III/Pme I linker (µl)	T4 ligase (µl)	T4 ligase buffer (µl)	H2O (µl)	Total volume (µl)
αMHC-neo	6	2	1	2	9	20
		Xho I/Pme I linker (µl)	T4 ligase (µl)	T4 ligase buffer (µl)	H2O (µl)	Total volume (µl)
αMHC-neo-Pme I	6	2	1	2	9	20

Reaction for step (B)

Linearized vector	(µl)	Insert (polyA) (µl)	Quick ligase (µl)	Quick ligase buffer (2X) (µl)
αMHC-neo (2P)	3	5	1	10

Reaction for step (C)

Linearized vector	(µl)	Insert (MCS) (µl)	Quick ligase (µl)	Quick ligase buffer (2X) (µl)
αMHC-PmeI-polyA	3	7	1	10

Reaction for step (D)

Linearized vector	(µl)	Insert (VSFP2.3) (µl)	Quick ligase (µl)	Quick ligase buffer (2X) (µl)
αMHC-MCS	3	15	1.5	20

3.1.1.5 Transformation

The ligation product was transformed into competent E. coli cells (DH5α). 3 µl of ligation product was gently added into a 1.5 ml reaction tube containing 50 µl of DH5α cells. The mixture was placed on ice for 20 minutes and then heat shocked at 42°C for 30 seconds. 250 µl of SOC medium (Invitrogen) was supplemented to the mixture and incubated at 37°C with shaking at 450 rpm for one hour. The transformation mix was then plated onto an LB-agarose plate with 100 µg/ml ampicillin (Appendix) and incubated inverted at 37 °C overnight.

3.1.1.6 Plasmid DNA preparation (mini-prep)

Colonies were picked from the LB-agar plates and cultured in 50 ml reaction tubes (Falcon) containing 5 ml of LB medium (Appendix) and 100 µg/ml ampicillin. The liquid culture was incubated at 37 °C with shaking at 450 rpm for 8 to 12 hours till O.D. 0.6. Plasmid DNA was extracted and purified from DH5α cells as following: 2 ml of the liquid culture was transferred to 2 ml reaction tubes (Eppendorf). Cells were pelleted by centrifugation at maximum speed for 30 seconds. The supernatant was decanted and the pellet was resuspended with 250 µl of buffer P1 (QIAGEN, Cat#19051) by vortexing. 250 µl of buffer P2 (QIAGEN, Cat#19052) was added to the homogenous cell suspension to initiate cell lysis. The tubes were mixed well by inverting several times (without vortexing) and allowed to stand at room temperature for 5 minutes (or till the cell suspensions were clear). Lysis reaction was neutralized by the addition of 300 µl of buffer P3 (QIAGEN, Cat#19053) followed by the gentle inversion of tubes. The tubes were kept on ice for 5 minutes and centrifuged at maximum speed (20,000 x g) for 10 minutes. Supernatants containing plasmid DNA were then transferred to 1.5 ml tubes. 600 µl of isopropanol was added to each tube, mixed vigorously and kept at room temperature for 2 minutes to precipitate the plasmid DNA. The plasmid DNA was pelleted by centrifugation at maximum speed (20,000 x g) and 4°C for 20 minutes and supernatants carefully aspirated. 400 µl of 70% ethanol was added to each tube followed by gentle inversion or flicking to wash the DNA pellets. The DNA was pelleted by centrifugation at maximum speed (20,000 x g) and 4°C for 5 minutes and supernatants were carefully removed. Evaporation of

residual ethanol was performed by placing the tubes in a fume hood with the caps opened for about 30 minutes. The plasmid DNA was then dissolve with 50 µl of TE buffer (10 mM Tris-HCl, 1 mM EDTA, pH 8.0). The purified plasmid DNAs was subjected to RE digestion (section 3.1.1.1) and gel electrophoresis (section 3.1.1.2) for confirmation.

3.1.1.7 Plasmid DNA preparation (maxi-prep)

After the confirmation of purified plasmid DNAs, a maxi preparation was carried out using NucleoBond Xtra Maxi kit (Macherey-Nagel) to obtain high yield of purified plasmid DNA. 1 ml of bacterial culture was mixed with 250 ml LB medium (Appendix) containing 100 µg/ml ampicillin in a 1 L conical flask. The mixture was incubated in a shaker at 37°C overnight. The following steps were performed based on manufacturer´s protocol for low-copy plasmid purification.

250 ml of bacterial liquid culture was transferred into an ultracentrifuge tube and spun at 6,000 x g for 15 minutes at 4°C. After discarding the supernatant, the cell pellet was completely resuspended in 24 ml of Buffer RES+RNase A by pipetting the cells up and down. 24 ml of Buffer LYS was added to the suspension and mixed thoroughly by gentle invertion until a homogeneous cell lysate is obtained. The cell lysate was then incubated at room temperature for 5 minutes. During the incubation period, a NucleoBond® Xtra Column together with the inserted column filter was equilibrated with 25 ml of Buffer EQU. 24 ml of Buffer NEU was added to the suspension and the cell lysate was mixed by gently inverting the cup. The cell lysate was then loaded into the equilibrated NucleoBond® Xtra Column Filter. The column filter containing cell lysate was washed with 15 ml of Buffer EQU. The column filter was discarded and 25 ml of Buffer WASH was applied to the center of NucleoBond® Xtra Column to wash the column. The plasmid DNA was eluted by the addition of 15 ml of Buffer ELU and the eluate was collected in a 50 ml centrifuge tube. The eluted plasmid DNA was then precipitated by adding 10.5 ml of isopropanol at room temperature and mixed thoroughly using a vortex. The tube was centrifuged at 15,000 x g for 30 minutes at 4°C. After discarding the supernatant, the DNA pellet was washed with 70% ethanol at room temperature and centrifuged again at 15,000 x g for

30 minutes at 4°C. The DNA pellet was allowed to air-dry at room temperature and reconstituted with appropriate volume of buffer TE. The resulting purified plasmid DNA was quantified by a spectrophotometer (Nanodrop, ND-1000, Thermo Scientific).

3.1.1.8 DNA sequencing

To determine the order of the RE sites in the MCS, the purified plasmid DNA was prepared for sequencing. The sequencing primer (5 '-GGGAAGTGGTGGTGTAGGAA - 3') was designed to detect the sequence from the 3' end of the αMHC promoter element towards the MCS. The forward and reverse DNA fragments for sequencing were constituted in separated tubes and amplified by polymerase chain reaction (PCR) using BigDye® Terminator v3.1 Cycle Sequencing Kit (Applied Biosystems). 2.5 µl of purified plasmid DNA (>500 ng) was mixed with 3.5 µl of Read Reaction Premix, 6 µl of BigDye Sequencing buffer and 1 µl of primer (10 µM). 7 µl of H_2O was added to the mixture to the final volume of 20 µl. PCR reaction was carried out using GeneAmp® PCR System 9700 (Applied Biosystems). The PCR products were precipitated by adding 12 µl of sodium acetate and 97 µl of H_2O. After centrifugation at 1,000 x g for 25 minutes at 4°C, the supernatant was discarded and the pellet was allowed to air-dry overnight in the dark. The final products were sent to the sequencing facility in the University Medical Center Hamburg-Eppendorf. The sequencing results were aligned with MCS sequences using online analysis tool (inra alignment) to determine forward and reverse MCS.

3.1.2 Generation of αMHC-VSFP2.3 transgenic mouse

The αMHC-VSFP2.3-polyA fragment (Fig. 15) was released by BamHI/PmeI double digestion, gel purified (QIAGEN's EndoFree Maxiprep kit) according to manufacturer's protocol and microinjected into pronuclei of fertilized mouse eggs (BDF1, n=201 eggs) in the Transgenic Core Facility of the RIKEN Brain Science Institute. 6 transgenic founders were selected from 43 lines screened by PCR.

Fig. 15 αMHC-VSFP2.3-poly A fragment for pronuclei injection

Genotyping

Tail tip biopsies from 4 weeks old αMHC-VSFP2.3 mice were obtained from the animal facility. DNA was extracted using the REDExtract-N-Amp™ Tissue PCR Kit (Sigma-Aldrich) following the manufacturer´s protocol. Tissue samples were dissolved in Tissue Preparation Solution and Extraction Solution at 55°C in thermomixer (Eppendorf) at 700 rpm for 10 minutes. Samples were then deactivated at 95°C in a thermomixer at 700 rpm for 5 minutes. Neutralization Solution B was added to the mixture and the extract was used as the template for PCR.

The primers for detecting the NMDAR gene (as an internal control) and the transgene (CiVSP) are listed in Table 4. For each PCR reaction, 2 µl of tissue extracts, 5 µl of REDExtract-N-Amp PCR Reaction Mix (Sigma) and 0.4 µl of each primer (10 mM) were mixed in a total volume of 10 µl. PCR was carried out using GeneAmp® PCR System 9700 (Applied biosystems). Initially, DNA was denatured at 94°C for 5 minutes, followed by 35 cycles of 94°C for 1 minute, annealing at 55°C for 30 seconds, extension at 72°C for 45 seconds. In the end, after a single elongation step at 72°C for 10 minutes, the temperature was held at 20°C for an infinite time for the short-term storage of PCR products before proceed to gel electrophoresis.

The PCR products were mixed with 6x loading dye (Fermentas) and loaded onto 1% agrose gel containing 1% ethidium bromide. DNA bands were visualized under UV with GelDoc system (BioRad).

Table 4 Primers for the genotyping of transgenic mice

Gene	Sequences	Temp (°C)	Product size (bp)
CiVSP	For: 5'-GTCCAGTTTCGTGTCCGAGCAGTGATTG-3'	63.6	387
	Rev: 5'-TATTCTTGCTAATCGAACCACACGCAGC-3'	61.4	
NMDAR1	For: 5'- AGCCCTTCAAGTACCAGGGCCTGAC -3'	63.6	229
	Rev: 5'- AGCGGTCCAGCAGGTACAGCATCAC -3'	63.8	

3.1.3 Characterization of αMHC-VSFP2.3 transgenic mice

3.1.3.1 Fluorescence microscopy screen

After genotyping, intact whole hearts from adult transgenic mice (16-wk old, either sex) were excised and imaged under a LEICA M165 FC macroscope equipped with a LEICA DC500 digital camera with YFP epifluorescence filters.

3.1.3.2 Echocardiography

16 weeks old mice of either sex from each transgenic mouse line and wildtype mice (n=8 in each group, 4 males and 4 females) were anaesthetized in an induction chamber flooded with isoflurane and subsequently maintained under 1.5 l/minute carbogen (95% O_2/5% CO_2) with 1.5% isoflurane. Echocardiography was performed using a Vevo 2100 system (Visual Sonics Inc., Toronto, Canada) equipped with an 18-38 MHz transducer (MS400). Temperature was maintained with a heating pad at 37°C. Heart rate and electrocardiogram were monitored and recorded at the same time. Following parameters (Table 5) were either measured directly or calculated from recorded data.

Table 5 Echocardiographic parameters for the assessment of cardiac function and myocardial structure

	Parameter	Abbreviation
Functional	Heart Rate (beats/minutes)	HR
	Fractional Area Shortening (%)	FAS
	Cardiac Output (ml/minutes)	CO
Structural	Left Ventricle Inner Diameter Systole (mm)	LVIDs
	Left Ventricle Inner Diameter Diastole (mm)	LVIDd
	Anterior Wall Thickness Fraction (%)	AWThF
	Posterior Wall Thickness Fraction (%)	PWThF

$$\text{FAS (\%)} = \frac{\text{LV end diastolic area - LV end systolic area}}{\text{LV end diastolic dimension}} \times 100$$

$$\text{CO} = \frac{\text{stroke volume} \times \text{heart rate}}{1000}$$

$$\text{AWThF} = \frac{\text{LV end systolic AWTh} - \text{LV end diastolic AWTh}}{\text{LV end systolic AWTh}}$$

$$\text{PWThF} = \frac{\text{LV end systolic PWTh} - \text{LV end diastolic PWTh}}{\text{LV end systolic PWTh}}$$

Hearts, lungs and livers were harvested immediately after echocardiography. Wet weights were recorded. Tibias were also removed and tibia length was measured with a caliper. Organ weight was normalized to tibia length.

3.1.3.3 Spectral imaging of mouse hearts

Intact whole hearts were excised as previously described and cut into small pieces. Slices of heart tissue were imaged under a Nikon C1si/FN1 confocal microscope in spectral mode using a laser for fluorescence excitation (excitation filter 444 nm).

3.1.3.4 Isolation of Adult Mouse Cardiac Myocytes

Adult mouse cardiomyocytes (CMs) were isolated based on the protocol modified from previous studies[104, 105]. In brief, after the mouse was anesthetized with isoflurane, the heart was quickly excised and removed from the open chest. A cannula was inserted through the aorta and then mounted on the Langendorff perfusion system. The heart was retrograded perfused with 37ºC perfusion buffer (Appendix) at the rate of 3-4 ml/minutes. After 2 minutes, the perfusion was switched to the digestion buffer consisting of 50 ml of perfusion buffer, 2.0 mg/ml collagenase type II (Worthington, Lakewood, NJ) and 12.5 µM $CaCl_2$. The digestion was stopped when the heart became swollen and pale (usually after 8 to 10 minutes). The heart was removed from the cannula and atria were cut out. The ventricles were placed in a 6-ml culture dish containing 2.5 ml of digestion buffer. Cardiomyocytes were dissociated mechanically with fine scissors and gentle trituration. Digestion was terminated by adding 5 ml of stopping buffer consisting of 45 ml of perfusion buffer, 10% fetal bovine serum (FBS, Gibco) and 12.5 µM $CaCl_2$.

Cell suspensions were transferred to 15 ml tubes (Falcon) and left to separate by precipitation for 10 minutes. Supernatant was removed and the cell pellet was resuspended with 10 ml of stopping buffer. Calcium was re-introduced to the concentration of 1 mM in three steps by the addition of 8.75 µl, 40 µl and 50 µl of 100 mM $CaCl_2$ respectively, with 5 minutes interval. Cells were allowed to precipitate and then resuspended with 10 ml of stopping buffer containing 1.2 mM $CaCl_2$. Cells were plated on laminin (20 mg/ml, Invitrogen) coated coverslips for immunostaining.

3.1.3.5 Immunostaining of isolated adult cardiomyocytes

Isolated CMs on coverslips were fixed with acid free (pH 7), phosphate-buffered formaldehyde (4%) solution (Histofix, Roth) for 10 minutes at room temperature followed by washing with DPBS 3 times for 5 minutes/each. The cells were permeabilized and the unspecific binding sites were saturated by incubating with blocking buffer containing 5% FBS (Gibco), 1% bovine serum albumin (BSA, Sigma) and 0.5% TritonX-100 (AppliCehm) in DPBS for 2 hours at room

temperature. The cells were incubated with primary antibody against the ryanodine receptor (mouse anti-RyR2, Therma Scientific, MA3-925, 1:500) for 60 minutes at room temperature. Subsequently incubation with secondary antibody conjugated with fluorescent dye (anti-mouse Alexa Fluor® 546, Molecular Probe®) at 1:800 dilutions in blocking buffer was performed for 60 minutes at room temperature. Nuclei were counterstained with 4', 6'-diamidino-2-phenylindole (DAPI) (1 µg/ml, 1:1000, Sigma). Samples were washed thoroughly with blocking buffer 3 times for 5 minutes with a final wash with only DPBS for 5 minutes. A drop of mounting medium (Fluoromount-G, SoutherBiotech) was put on the slide and the coverslip containing the CMs was inverted over the medium carefully to prevent the trapping of air pockets within the sample. The slides were allowed to dry and then imaged. Fluorescent images were acquired using laser scanning confocal microscope (LSM710, Zeiss, Germany).

3.1.3.6 Synchronized optical imaging under voltage clamp

The voltage-dependent of fluorescence changes at steady-state was assessed by whole-cell voltage clamp and the measurements of fluorescent intensities. Experiment setup is shown in Fig. 16. Adult CMs were placed in the temperature controlled recording chamber (RC-24E, Warner Instrument) mounted on an inverted microscope (Olympus IX-71) and perfused with bath solution (Appendix). The temperature was maintained at 32-35 ºC during the experiment. Voltage-clamp was performed under whole-cell configuration using EPC 10 USB Patch Clamp Amplifiers (HEKA). Thin wall glass electrodes (TW150F, WPI) with resistance of 3-5 MΩ were pulled on micropipette puller (P-97, Shutter Instrument Co.). Pipette solution (Appendix) was injected into the glass electrodes and membrane potentials were held at -80 mV followed by 1,200 ms voltage clamp steps from -140 mV to +140 mV in 40 mV increments.

A fluorescent image system (Till Photonics) was synchronized with the patch clamp amplifier and each image acquisition was triggered by a stimulation command sent by the amplifier. Cells were illuminated by a computer-controlled monochromator (Polychrome V, TillVision). Excitation light (430 nm) passed a double band filter

(420/505 DB) and were reflected by the excitation dichroic (455 nm LP) onto the cells. The emitted light was directed by a beam splitter (DC 505 nm) and emission filters (HQ 535/30, D465/30 nm) to an EM-CCD camera (Andor iXon 885, ANDOR^{TM}) under dual-imaging mode (DV2, Photometrics). CFP and YFP intensities were recorded simultaneously.

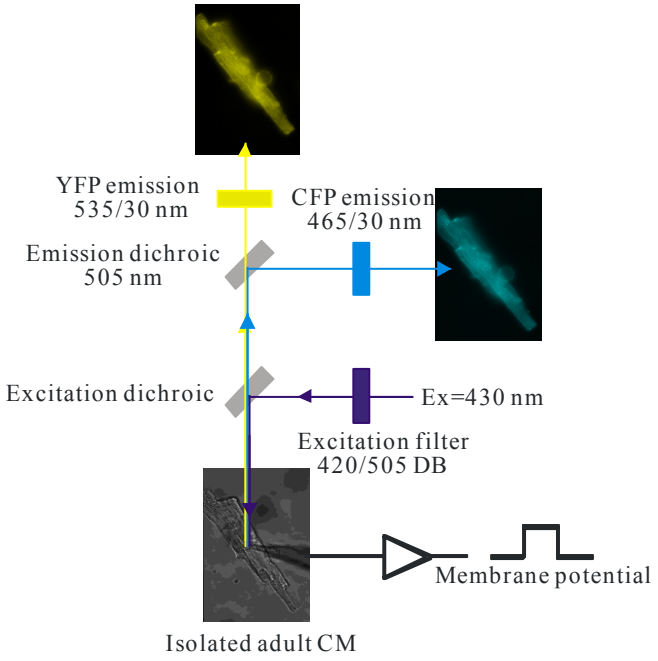

Fig. 16 Configuration of the patch-clamp and FRET imaging experiment

3.1.3.7 High speed VSFP2.3 signal recordings via photomultiplier tubes (PMTs)

Isolated adult CMs were plated onto laminin coated recording chambers (made in-house) containing Tyrode's solution at room temperature. CMs were stimulated by field stimulator (MyoPacer EP, IonOptix) at different frequencies ranging from 0.5 to 4 Hz. Simultaneously, light from a Xenon arc lamp (HyperSwitch light source, IonOptix) passed a filter (436/20 nm) and reflected by the excitation dichroic (455 nm LP) onto the cells. The emitted light with shorter wavelength (< 585 nm) was deflected by a dichroic mirror (585 nm) and then directed by another beam splitter (510 nm LPXR) to two emission filters (ET 480/40 nm [CFP], ET 535/30 nm [YFP]). CFP and YFP signals were recorded by two photomultiplier tubes (PMTs) (Fig. 17).

The CFP, YFP signals were analyzed by self-designed program based on Matlab (MathWorks). Action potentials were represented by YFP-to-CFP ratio and action potential durations (APDs) were calculated.

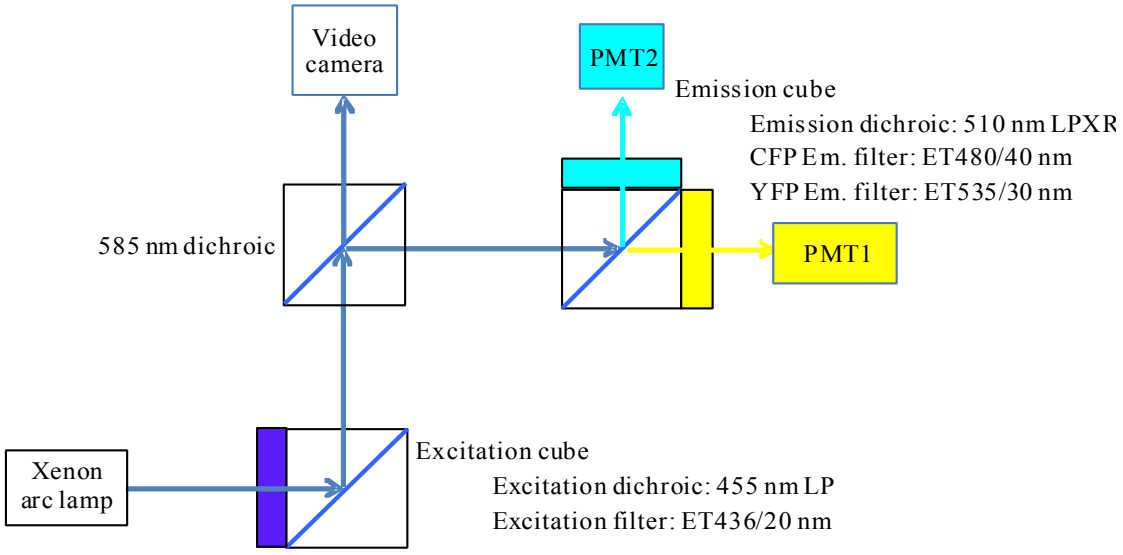

Fig. 17 Schematic of optical AP measurement from isolated CMs

3.1.3.8 Simultaneous high speed PMT and patch clamp recordings

To compare the APs recorded from optical signals and conventional patch clamp method, another similar PMTs system attached to a patch clamp amplifer (Axopatch 200B, Molecular Devices) was used (in collaboration with Dr. Teun de Boer at the Department of Medical Physiology at University Medical Center Utrecht). Data acquired from both PMTs and patch clamp was controlled by pClamp 9.0 software (Molecular Devices), signals were recorded at 4 kHz.

Isolated adult CMs were placed in a custom made recording chamber mounted on an inverted microscope (Nikon TE-2000) fitted with a 40x/1.3 NA oil immersion objective and superfused with bath solution at 37ºC. Experiments were performed under whole-cell configuration using Axoclamp amplifier. APs were triggered by injecting 2 nA/2 ms currents at 1 Hz. Cells were illuminated by a computer-controlled monochromator (Optoscan, Cairn Research). Excitation light (437/20 nm) was

reflected by a dichroic mirror (458 nm). The Emitted light was first split by a 514 nm dichroic mirror. The reflected light (<514 nm) was filtered by a cyan emission filter (483/32 nm BP). The transmitted light (>514 nm) was then separated by the second dichroic (600 nm). The reflected light (<600 nm) was filtered by a yellow emission filter (514 nm LP). Light with wavelength longer than 600 nm was imaged using a camera for observation of the cell during experiment (Fig. 18).

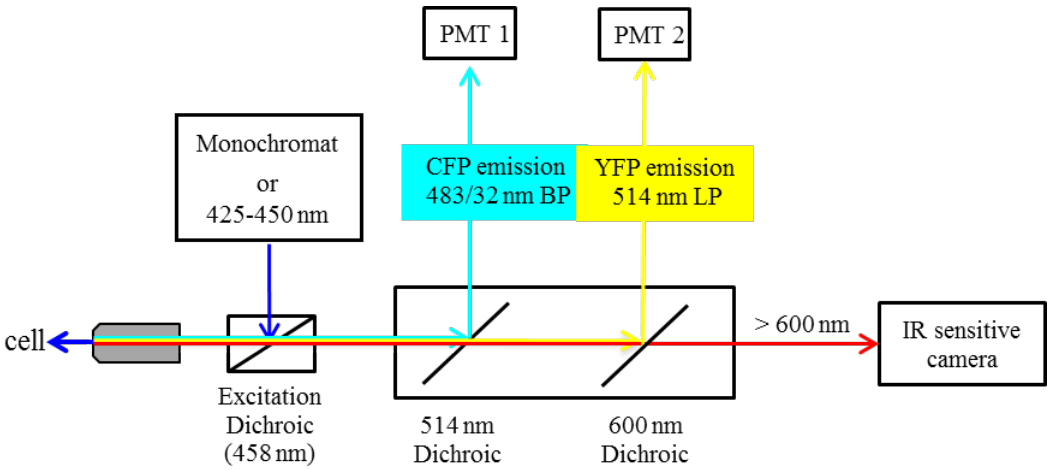

Fig. 18 Simultaneously recording of optical and electrical APs from isolated CMs

APs were analyzed using conventional approaches, resulting in APD_{50} and APD_{90} values. Fluorescence signals were analyzed by calculating the ratio of cyan and yellow fluorescence, filtering the ratio signal using the total variation denoising algorithm (TVDIP, $\lambda = 0.01$) by Little and Jones[106], and analyzed using the same approach as used for the electrical APs. APD values obtained for both APs and FRET responses were tested for correlation by calculating Pearson's correlation coefficient.

3.1.3.9 Optical mapping of spread of excitation in Langendorff perfused hearts

Optical recordings of electrical activity on intact whole heart were done on adult mice of either sex aged between 12 and 16-week-old (in collaboration with N. Raad, Prof. S. Lehnart and Prof. S. Luther; University Medical Center Göttingen and Max-

Planck-Institute for Dynamic and Self-Organization). Mice were heparinized through intraperitoneal injection before the experiments. Mice were sacrificed by cervical dislocation in isoflurane (Floren, Abbot-Germany) anesthesia. The hearts were excised quickly, cannulated via the aorta and then Langendorff perfused with oxygenated (95% O_2, 5% CO_2) modified Tyrode´s solution (Appendix) at a flow rate of 4 ml/min. Mechanical contraction was suppressed by the excitation-contraction uncoupler (blebbstatin [5 μM], Sigma). Temperature was maintained at 38 °C during experiment. A bipolar pacing electrode (50-100 kΩ, FHC, USA) was placed in the center of the anterior ventricular wall and the heart was paced at basic cycle lengths (BCL) of 100 ms (amplitude 2.5x diastolic threshold, duration 2 ms). Self-terminated ventricular tachycardia episodes were induced by sending a 200-pulse train at a BCL of 80 ms. An electrocardiogram (vECG) was monitored throughout the experiment using custom-made Ag-AgCl ECG electrodes placed horizontally and parallel to the septum, at a distance of 1 mm from the epicardial surface.

The illumination was provided by a 100 W short-arc mercury lamp (HBO103W/2, Olympus, Germany) and fluorescence collected using an upright macro-zoom microscope (MVX10, Olympus). The excitation light was reflected by a dichroic mirror (480 nm), passed through a 438±24nm BP filter (CFP excitation, Semrock) directly on the heart. The fluorescent emission from the heart passed through a 542±27 nm filter (YFP emission, Semrock, Inc.) and collected by a 100x100 pixel CMOS camera (Ultima-L; SciMedia USA Ltd.). Imaging of YFP signals was carried out using a 0.63x objective (MVPLAPO 0.63x, NA0.15, Olympus) at a zoom of 4x and recorded at a frame rate of 500 Hz under spontaneous and paced conditions.

The data collected from the camera were frame-selected using a custom-made software written in Java, and was further analyzed with custom-made software written in Matlab (the Mathworks).

3.1.3.10 *In vivo* optical APs recordings using fiber optics

An imaging system using optic fibers was built up (Fig. 19) to establish the minimal invasive means for recording optical APs in living mice (in collaboration with Dr. C.

Richter, Dr. B. Unsoeld, and Prof. S. Luther; University Medical Center Göttingen and Max-Planck-Institute for Dynamic and Self-Organization). Light was delivered from a metal halide lamp (Photofluor II, 200 W) guided through the optic fiber bundle containing three PMMA fibers each with 1 mm in diameter, and passed through the excitation filter cube **(**excitation filter: ET 436/20 nm, excitation dichroic: 455 nm LF) to shine the heart. The emission light was collected by the same optic fiber bundle, passed through the emission filter cube **(**emission dichroic: 510 nm LPXR, CFP em. filter: ET 480/40 nm**,** YFP em. filter: ET 535/30 nm) and directed to two EMCCD cameras (Cascade 128+, Photometrics®) for recordings of CFP and YFP signals.

(A)

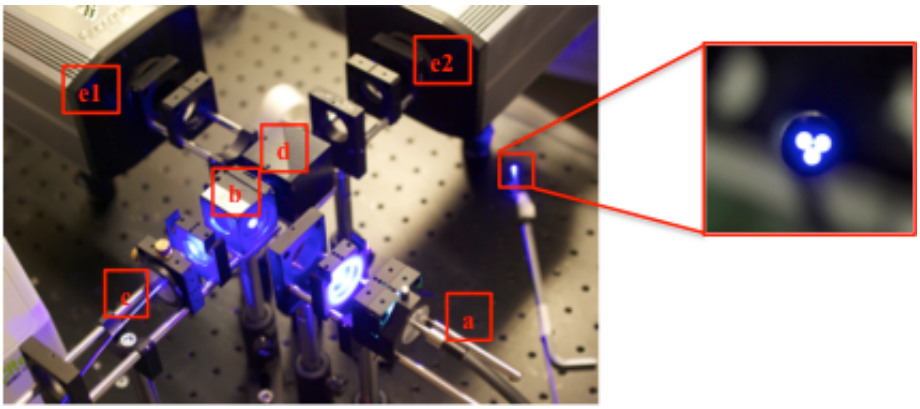

(B)

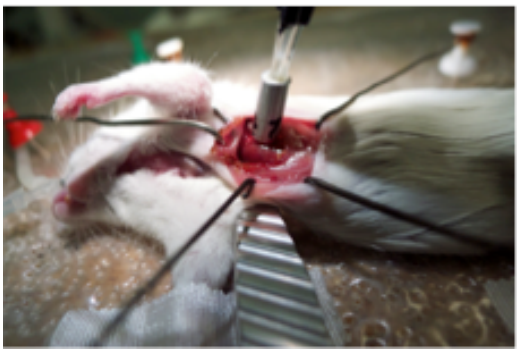

Fig. 19 Optic fiber system for AP measurement of intact whole heart and *in vivo* experiment. (A) The arrangement of the imaging setup: (a) light source; (b, d) excitation and emission filter cubes; (c) optic fiber bundle; (e1, e2) EMCCD cameras. Enlarged picture show the tip of optic fiber bundle. (B) The tip of optic fiber bundle was placed on the heart of an open chest mouse.

3.2 Results

3.2.1 Cloning of αMHC-MCS

Colonies were picked after transformation and overnight culture under ampicillin selection. The extracted and purified plasmid DNAs were checked by RE digestion. Based on the size of the fragments from RE digestion, clone 1, 2, 3, 5, 6, 7, and 8 were confirmed to be positive clones. Sequencing results showed successful cloning for αMHC-MCS plasmids (Fig. 20).

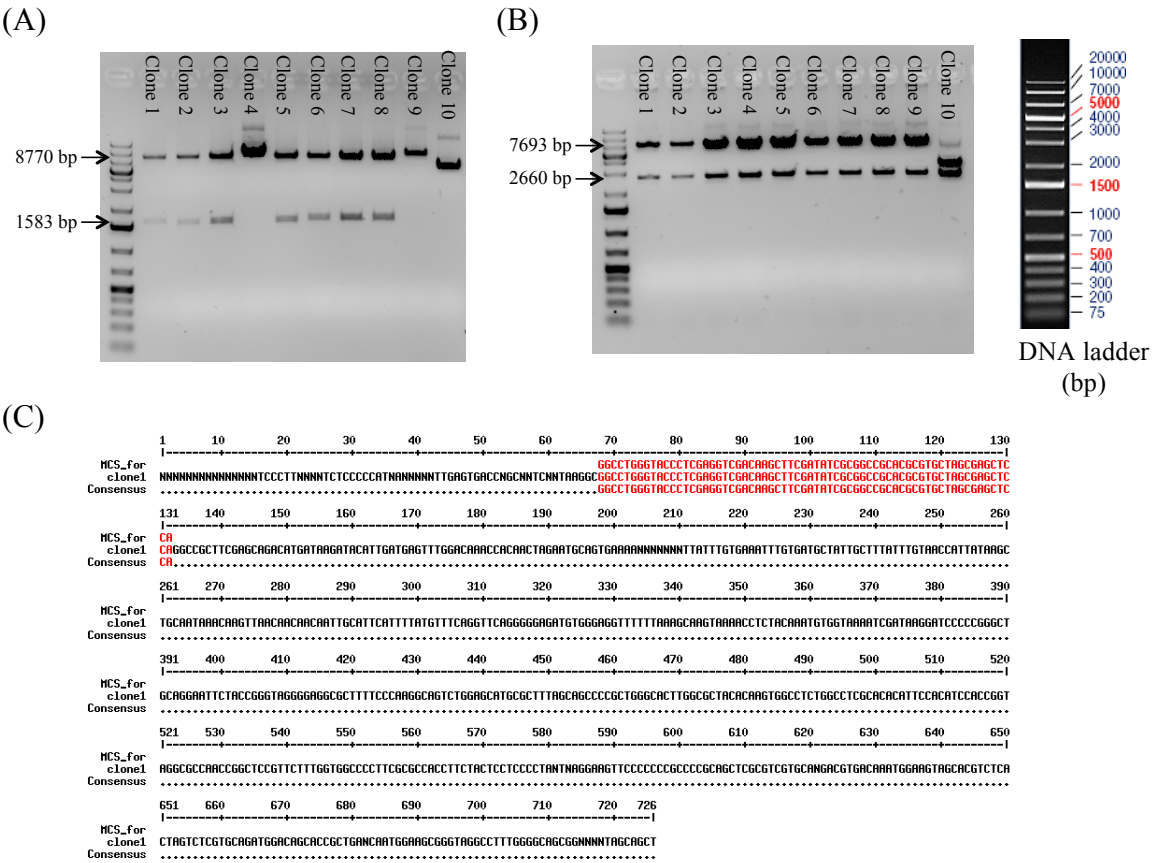

Fig. 20 Screen of the αMHC-MCS colonies by RE digestion. Restriction digestion with Sac I and Xho I (A) as well as Pme I (B). SacI/XhoI double digest of αMHC-MCS yielded two fragments (8770 bp and 1583 bp). Pme1 digest yielded two fragments with 7693 bp and 2660 bp. (C) Representative sequencing DNA integrity of the multiple cloning site (clone 1, MCS; red). DNA ladder: 1 kb plus (Fermentas).

The coding sequence for VSFP2.3 was then inserted into αMHC-MCS (reverse MCS). The resulting vector (αMHC-VSFP2.3) was confirmed by digesting with different RE (Fig. 21).

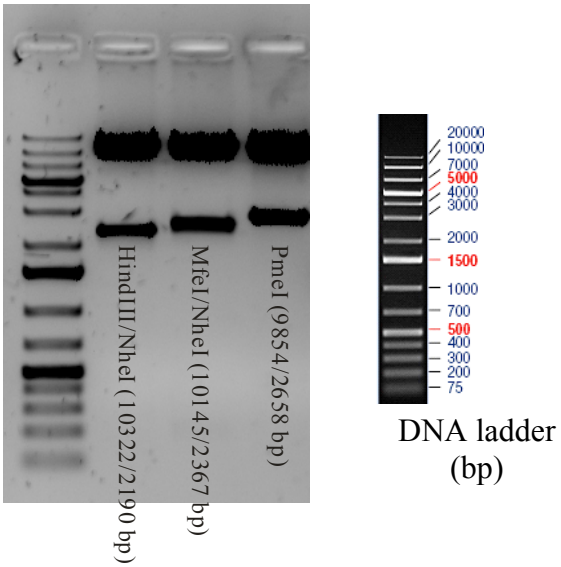

Fig. 21 Confirmation of αMHC-VSFP2.3 vector by RE digestion. DNA was digested with the indicated REs. Fragment sizes correspond to the anticipated DNA sequences. DNA ladder: 1 kb plus (Fermentas).

3.2.2 Characterization of the αMHC-VSFP2.3 transgenic mice

3.2.2.1 Genotyping of the αMHC-VSFP2.3 transgenic mice

43 founders were born and screened by PCR for αMHC-VSFP2.3 integration (Fig. 22) and 6 transgenic founders were selected for further analyses.

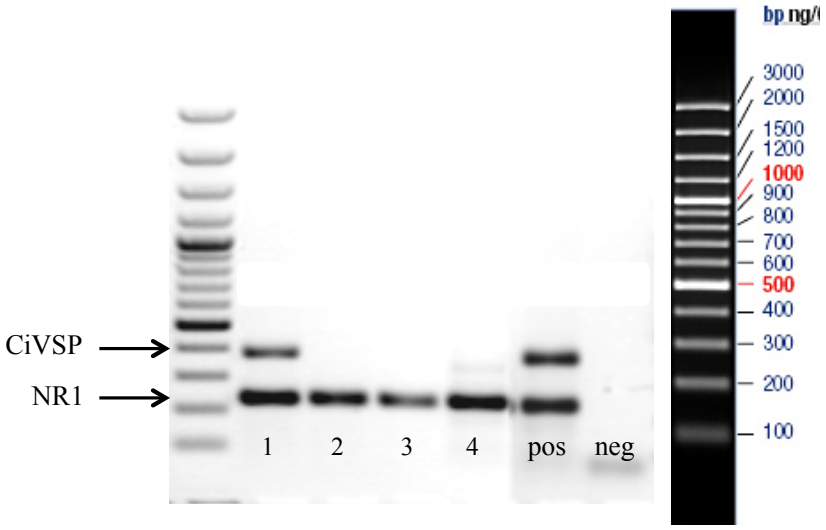

Fig. 22 Representative genotyping of αMHC-VSFP2.3 founder mice. DNA isolated from mouse tail tips was subjected to multiplex PCR for the CiVSP sequence and NR1 (mouse NMDA receptor 229 bp – served as internal control). Transgenic mice displayed a 359 bp band corresponding to CiVSP (Lane 1 is from founder #123). DNA ladder: 100 bp plus (Fermentas); VSFP2.3 plasmid was used as positive control and water as negative control.

3.2.2.2 Detection of the YFP reporter by fluorescence microcopy

The first macroscopic screen for YFP demonstrated that 4 out of the 6 PCR-confirmed αMHC-VSFP2.3 founders showed clear myocardial YFP expression (Fig. 23). Strongest and homogeneous YFP signals were recorded from the #123 line.

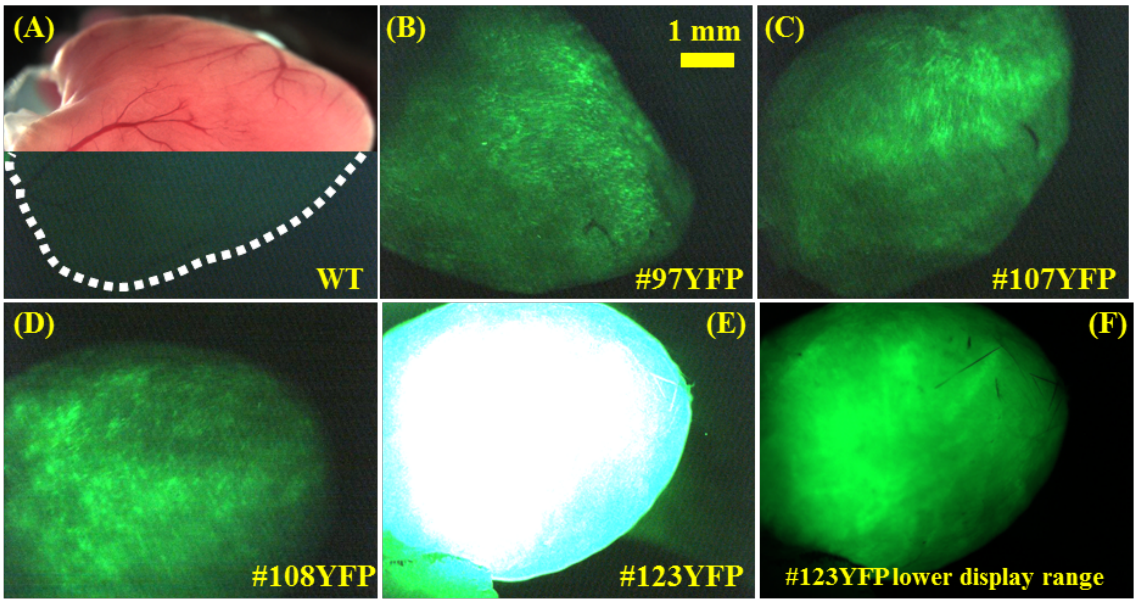

Fig. 23 Epifluorescent whole heart images from four established mouse lines. (A) Wildtype mouse heart under standard illumination and fluorescent excitation (with YFP filter). (B-F) fluorescent excitation (with YFP filter) only. (A-E) image displayed range: 0-50. (F) Image displayed with a limited display range: 0-40 (Image-Pro). All images are displayed at 2x magnification and were captured at 1 second exposure time.

3.2.2.3 Detection of CFP and YFP signals in a transgenic mouse heart

A heart sample from #123 was subjected to illumination at 440 nm. Emission spectrum analyses confirmed two emission peaks at 475 nm and 530 nm at the anticipated wavelengths confirming the presence of CFP and YFP (Fig. 24).

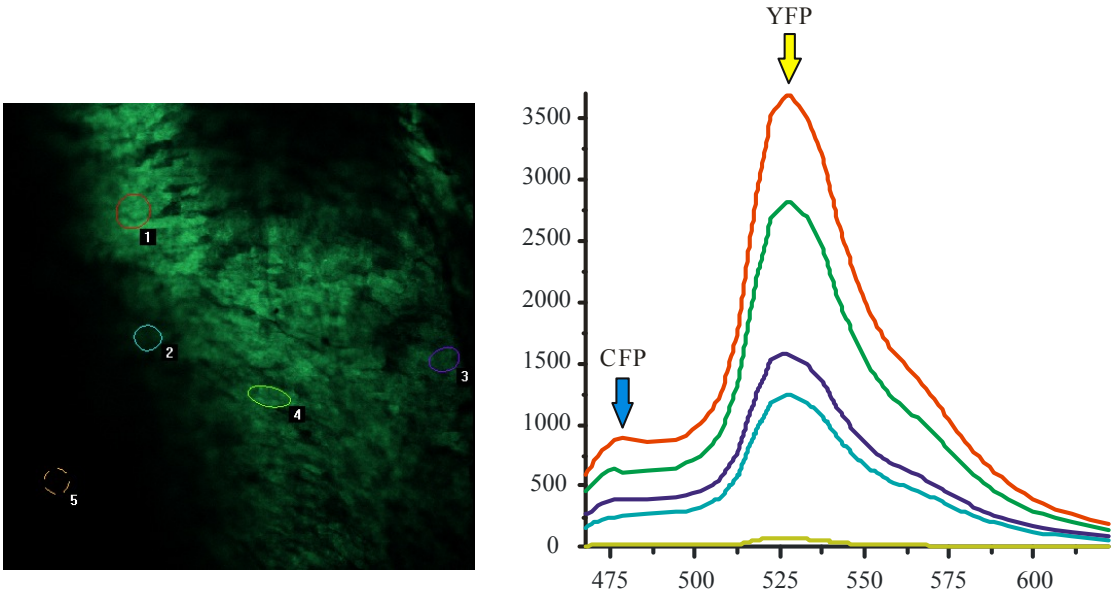

Fig. 24 Emission spectrum recordings in αMHC-VSFP2.3 heart tissue under 440 nm illumination. 5 regions of interest (ROI) (marked in the left panel) were specifically analyzed. The right graph displays the fluorescent signal intensities (ordinate) at the scanned wavelength range between 467 and 622 nm (abscissa). The color coded ROIs in the left panel match with the similarly colored emission spectra in the right graph.

3.2.2.4 Localization of the VSFP2.3 in cardiomyocytes from aMHC-VSFP2.3 mice

Cardiomyocytes were isolated from transgenic mouse line #123 using Langendorff perfusion. Epifluorescence imaging demonstrated homogeneous, but differential levels of expression of the reporters restricted to cardiomyocytes. Confocal laser scanning microscopy revealed sarcolemmal membrane targeting suggesting the translocation of the VSFP2.3 sensor namely to the t-tubular system (Fig. 25A). Co-localization with the cardiomyocyte specific sarcomeric calcium release channel (Ryanodin Receptor 2; RyR2) supported the observation. This was further confirmed by the analysis of fluorescence intensity plots recorded in the long axis of the cardiomyocytes (Fig. 25C). Another observation was that VSFP2.3 seemed to be highly concentrated at cardiomyocyte ends, which typically constitute the intercalated disc (Fig. 25A, white arrows).

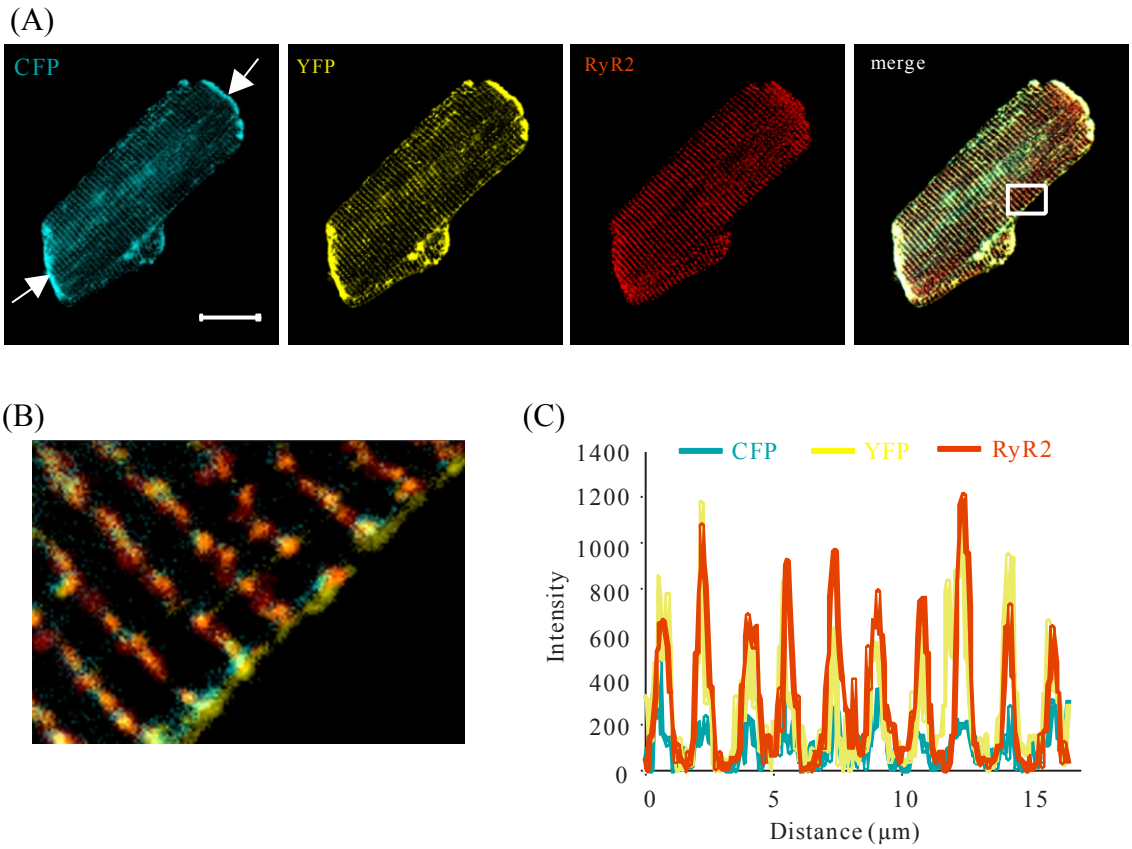

Fig. 25 Confocal images of adult CMs isolated from αMHC-VSFP2.3 transgenic mouse heart. (A) Detection of CFP and YFP fluorescence as well as fluorescent labeled RyR2; channels are superimposed in the far right panel (scale bar: 20 µm). (B) Magnification of the marked area in the merged image in (A). (C) Fluorescence intensity plot confirmed colocalization of VSFP2.3 with RyR2.

3.2.2.5 Echocardiographic assessment of αMHC-VSFP2.3 mouse lines

Echocardiography did not reveal any differences in heart morphology and function in αMHC-VSFP2.3 lines (#97, #107, #108, #123) (Table S-1, Appendix). Despite apparently different levels of transgene expression (Fig. 23), cardiac function (FAS, HR, and CO) and myocardial structure (LVIDd, LVIDs, AWThF and PWThF) remained intact (Fig. 26). The enlargement of liver and the increase of lung weight are the indications of right side heart failure, and left ventricular failure. Additional analyses of heart, liver and lung weight normalized to body weight and tibia length were in agreement with the finding of uncompromised heart function (Fig. 27).

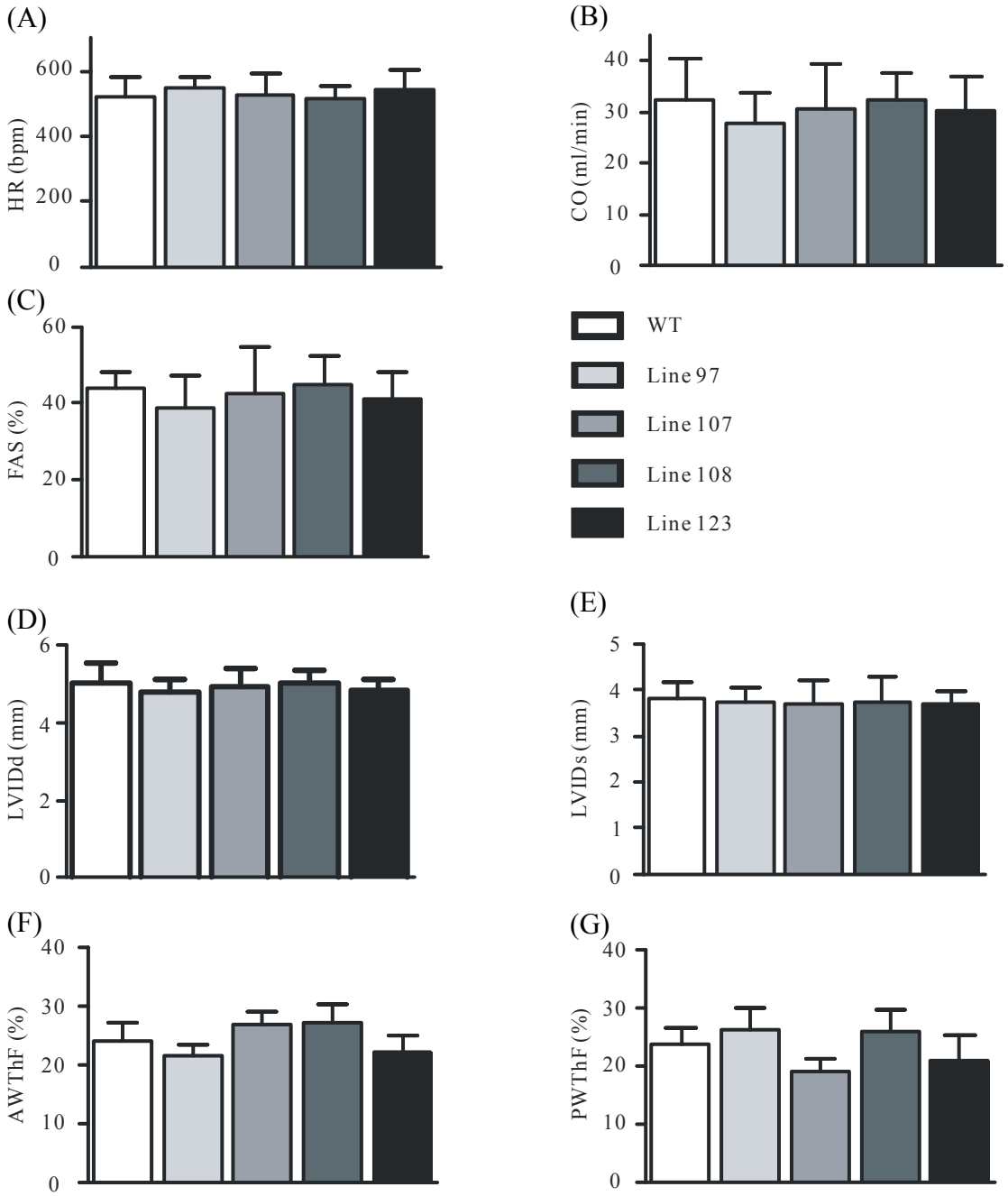

Fig. 26 Echocardiography in wildtype and αMHC-VSFP2.3 transgenic mice. Panels display a select set of echocardiography data (A) heart rate (HR); (B) cardiac output (CO); (C) fractional area shortening (FAS), (D) left ventricular inner diameter in diastole (LVIDd), (E) left ventricular inner diameter in systole (LVIDs), (F) anterior wall thickening fraction (AWThF), and (G) posterior wall thickening fraction (PWThF). ANOVA did not detect any differences between groups ($p < 0.05$). WT: wildtype.

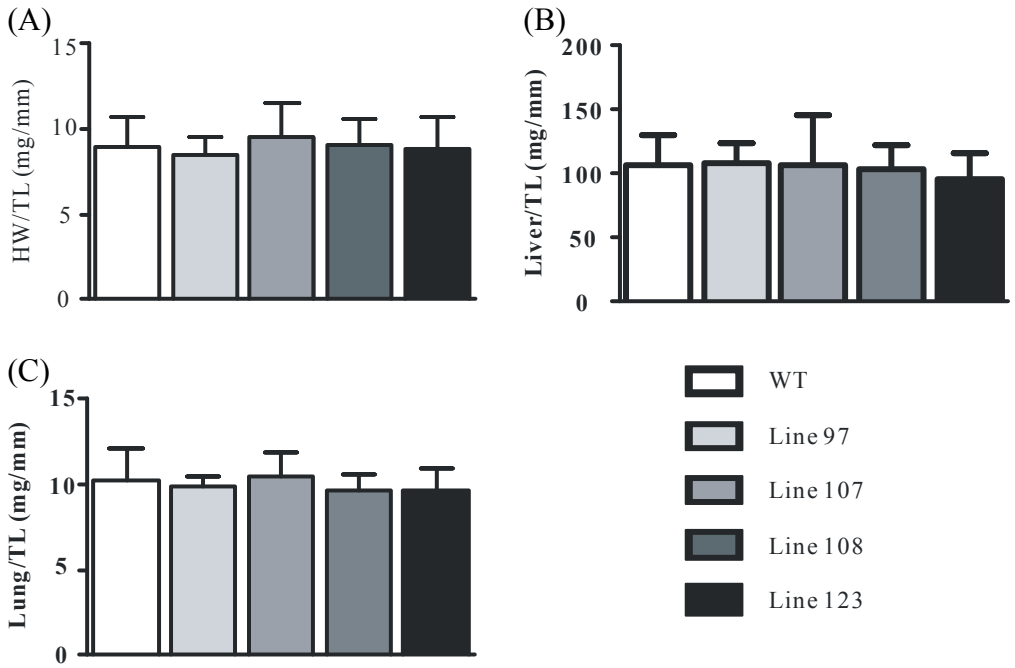

Fig. 27 Organ mass normalized to tibia length. (A) Heart weight to tibia length ratio. (B) Liver weight to tibia length ratio. (C) Lung weight to tibia length ratio. WT: wildtype mice (n=8/group, ANOVA: no sitgnificant differences between groups, $p < 0.05$).

3.2.2.6 Voltage dependence of fluorescence changes

Isolated adult CMs were held at a holding potential of -80 mV under whole-cell voltage clamp configuration (Fig. 28A bottom trace). The CFP and YFP fluorescence signals were recorded simultaneously (Fig. 28A top and second traces). Upon depolarization, the CFP intensities decreased while YFP intensities increased. The percentage of fluorescent change ($\Delta F/F_0$) of CFP and YFP are about 3% and 2%, respectively. The YFP/CFP ratios were derived from the recorded signals. Ratiometric analyses ($\Delta R/R_0$) showed an enhanced change of 6%. The mean values of YFP/CFP ratios plotted against membrane potentials follow a typical Boltzmann function with a half maximal response of -41±5 mV (Fig. 28B). This value falls within the physiological range (-80 to +20 mV) suggesting that VSFP2.3 can be used to monitor membrane potentials.

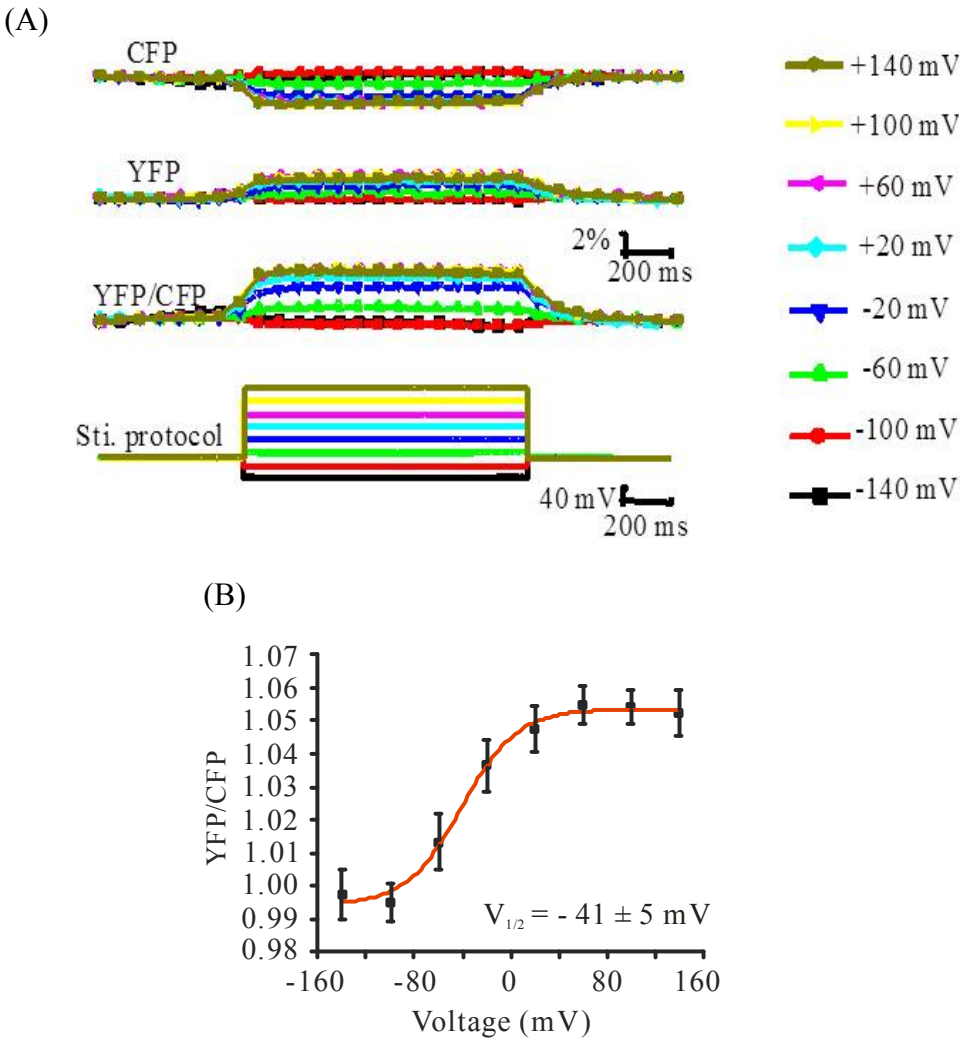

Fig. 28 Changes in VSFP2.3 fluorescent signals under under different membrane holding potential. (A) Representative CFP, YFP signals and YFP/CFP ratios at indicated voltages. (B) Plot of the steady state YFP/CFP ratio (ordinate) versus membrane potential (abscissa). n=6 per time-point. Boltzmann curve fit.

3.2.2.7 Optical action potential from isolated adult cardiomyocytes

After confirmation of the principal functionality of the VSFP2.3 sensor in cardiomyocytes, it was necessary to study the utility of VSFP2.3 in analyzing voltage changes in single beating cardiomyocytes. For this, isolated adult mouse cardiomyocytes were paced under field stimulation at different frequencies ranging from 0.5 to 4 Hz. CFP and YFP signals were recorded simultaneously via two synchronized photomultipliers at a sampling rate of 1 kHz and optical APs were presented as YFP/CFP ratio. The percentage changes in fluorescence intensities

($\Delta F/F_0$) were 2.5% and 1.5% for CFP and YFP, respectively, resulting in YFP/CFP change ($\Delta R/R0$) of 4% (Fig. 29A). The optical APs responded properly to different stimulation frequencies (Fig. 29B). Action potential durations at 20, 50 and 90 percent of repolarization (APD_{20}, APD_{50}, and APD_{90}) were reverse proportional to the stimulation frequency (Fig. 29C).

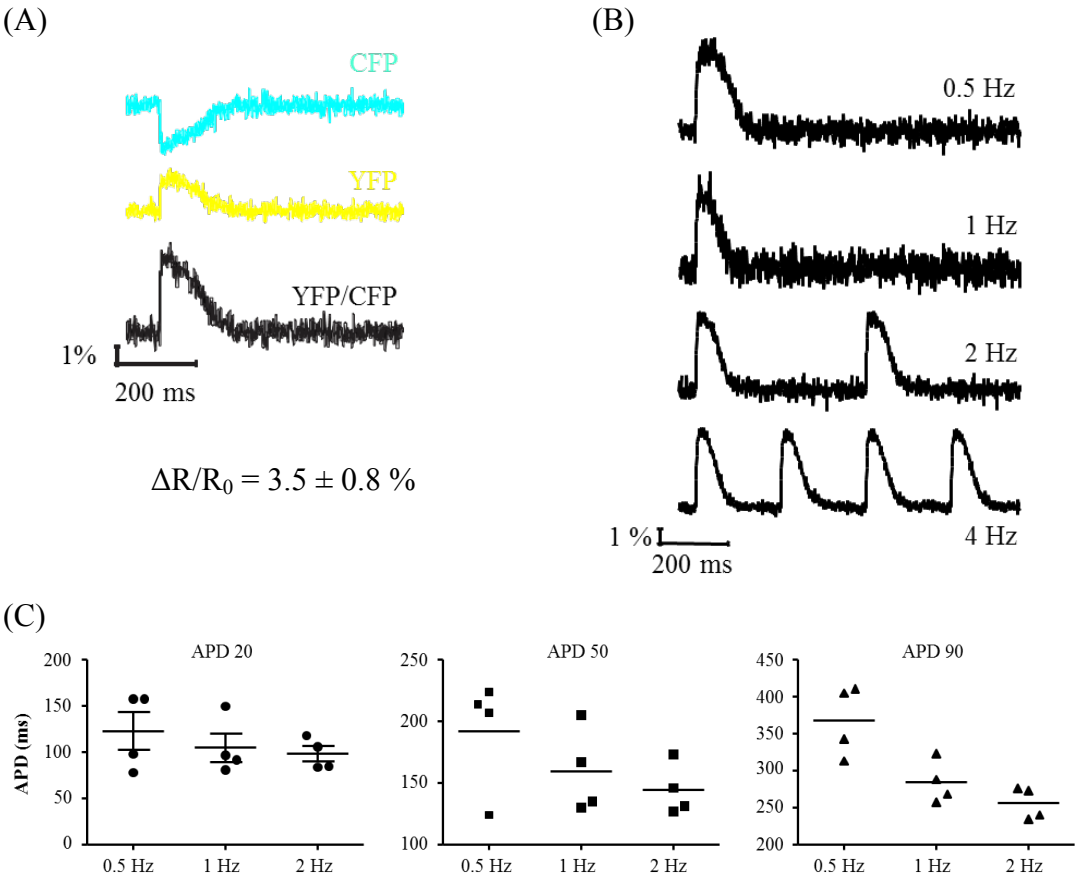

Fig. 29 Optical action AP recordings from adult αMHC-VSFP2.3 CMs. (A) CFP, YFP signals were recorded in cardiomyocytes at 1 Hz field stimulation. The YFP/CFP ratio is displayed in black as optical AP. (B) Optical APs recorded at different stimulation frequencies. (C) Display of action potential duration (APD) at different frequencies (mean±SEM, n=4)

3.2.2.8 Optical and electrical action potential recordings in isolated adult cardiomyocytes

AP kinetics under field stimulation appeared to be unphysiologically long (e.g. APD_{50} at 2 Hz: 144 ± 21 ms) and previous reports argued for the necessity to directly inject currents into cardiomyocytes to faithfully record action potentials patch clamping. Hence, we performed whole-cell current clamp experiments combined with CFP and YFP detection via synchronized photomultipliers to record electrical and optical APs simultaneously. The time points of maximal depolarization velocity (t_{max}) of both electrical APs and optical APs (YFP/CFP ratio) were determined (Fig. 30A). The average difference in t_{max} derived from optical and electrical APs was 0.46±0.06 ms (287 APs were analyzed) indicating the fast "on" kinetics.

In contrast to the fast on kinetics, the off kinetics were significantly prolonged in the optical APs (Fig. 30A, and Table 6). Moreover, the correlation between APD_{90} between electrical and optical APs was modest. In contrast, a strong correlation between electrical APD_{90} and optical APD_{50} (R^2=0.88; Fig. 30B) was observed.

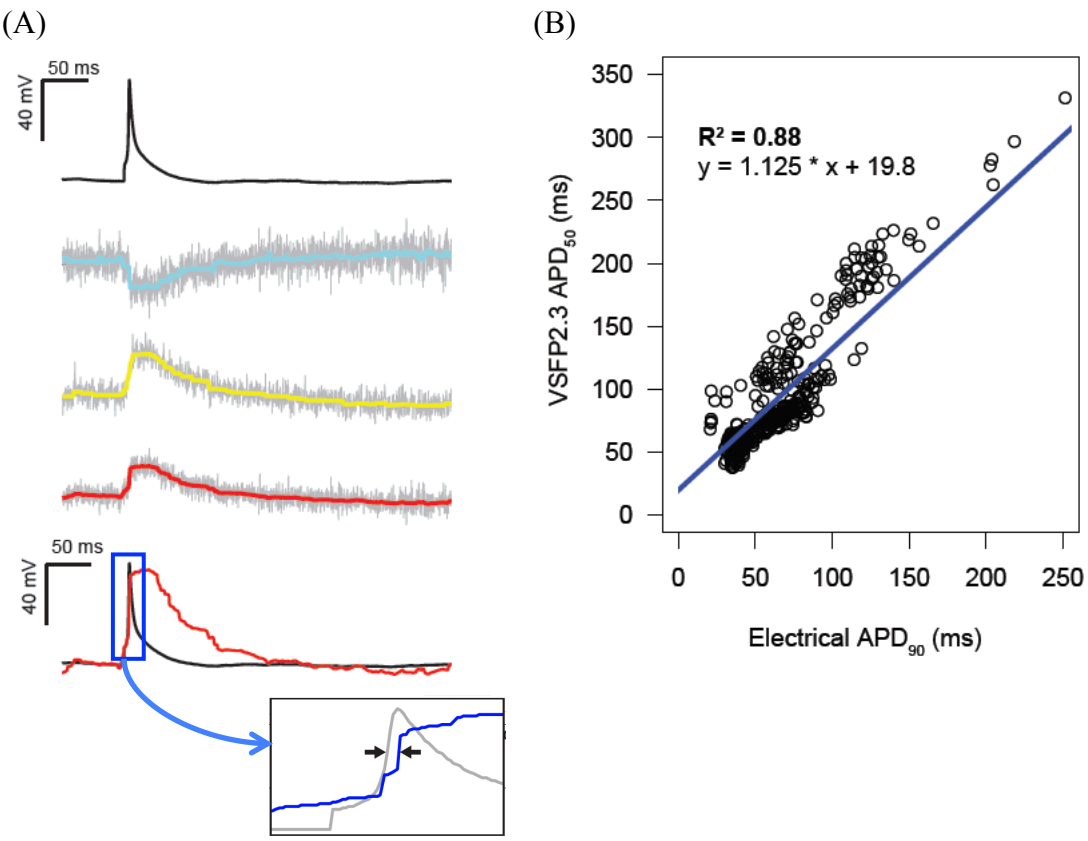

Fig. 30 Electrical and optical APs recorded from adult αMHC-VSFP2.3 CMs. (A) Electrical APs measured by patch clamp electrode (black trace). CFP and YFP signals were recorded by two PMTs (cyan and yellow traces) and synchronized with the electrical signal. Optical APs was derived by YFP/CFP ratio (red trace). Inset denotes the upstroke time difference between electrical and optical APs (0.46±0.06 ms, n = 287). (B) Evidence for a linear correlation between optical APD_{50} and electrical APD_{90} (N [cells] = 7, n [recorded APs] = 358) was provided.

Table 6 Action potential characteristics

	APD_{50} (ms)	APD_{90} (ms)	Resting membrane potential (mV)
Electrical AP	12.8 ± 2.4	70.9 ± 3.0	-77.2 ± 3.4
VSFP2.3 response	99.5 ± 3.6	180.5 ± 4.9	Not available

Average values ± standard error of the mean. (N [cells] = 7, n [recorded APs] = 358)

3.2.2.9 Optical action potential recordings from Langendorff perfused αMHC-VSFP2.3 hearts

For technical reasons (synchronization of dual imaging not fully established) optical APs were first derived from the fractional change of only the YFP signals (ΔF/F) from the VSFP2.3 sensor. Heart rate was monitored and volumetric ECG (vECG) recordings were obtained steadily from two electrodes place on the left and right ventricle throughout the experiment. The fractional change in YFP signals was 1.2-1.5% in these experiments. For optimization of S/N, signals from 10 pixels were averaged. This allowed for robust 1:1 recordings of optical APs corresponding to the vECG signal at sinus rhythm (Fig. 31A). For visual display of epicardial wave front propagation, 10x10 binning was exploited (Fig. 31A, lower right). Electrical pacing at 10 Hz confirmed that the optical APs responded properly to the initiation of electrical pulses (black arrows in Fig. 31B). Subsequently, we asked whether ventricular tachyarrhythmia could be visualized in the VSFP2.3 model. For this periods of self-terminating ventricular tachycardia were induced. Optical recordings of irregular depolarization pattern could be clearly visualized (Fig. 31C).

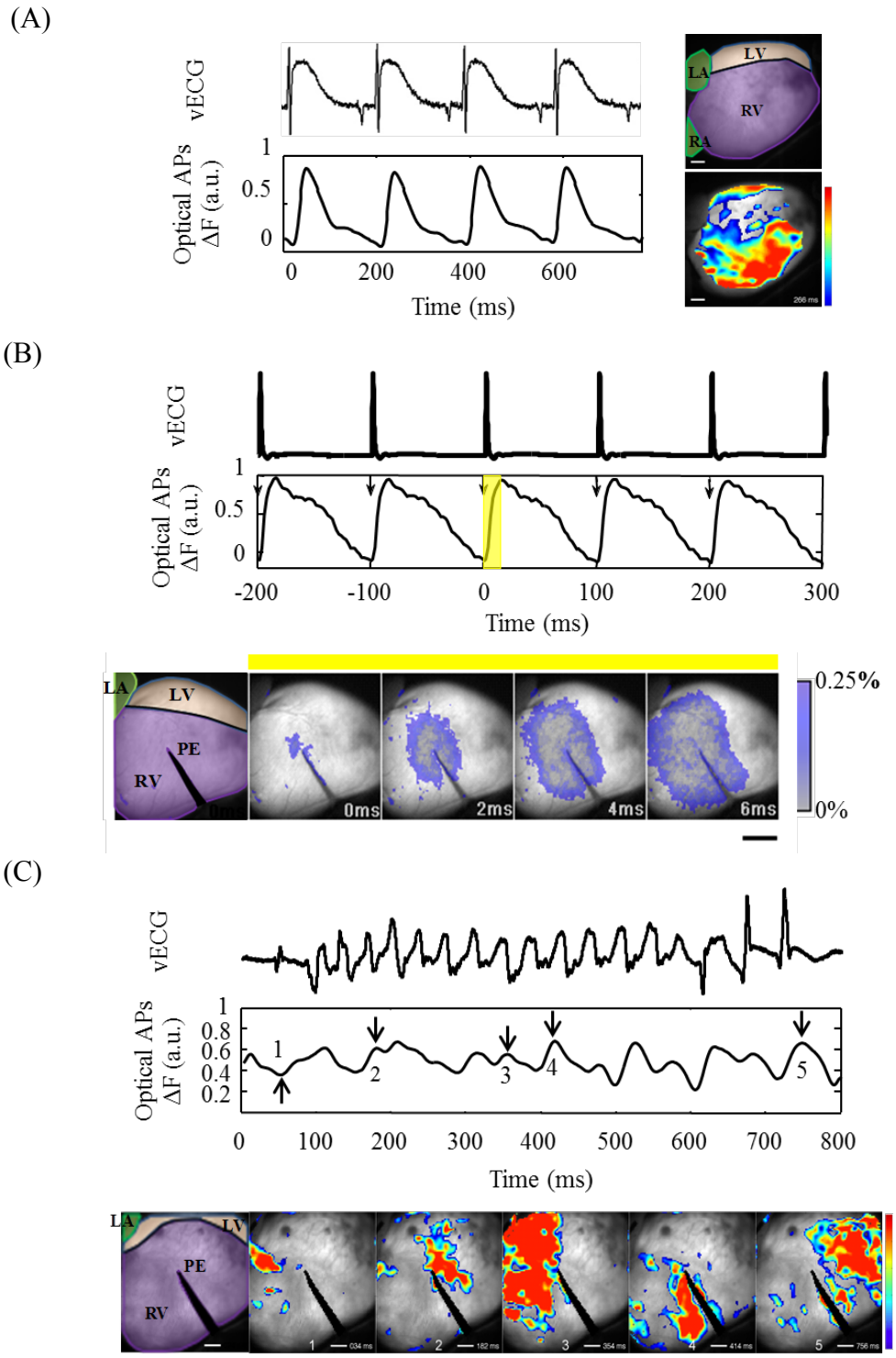

Fig. 31 Optical mapping of VSFP2.3 transgenic hearts under Langendorff perfusion. Hearts were either beating spontaneously at sinus rhythm (A) or under electrical stimulation at 10 Hz (B). Ventricular arrhythmia was induced after a 200-pulse train at a BCL of 80 ms (C). Scale bar in (A) and (C): 1mm, in (B): 2mm. LA: left atrium; RA: right atrium; LV: left ventricle; RA: right ventricle. PE: pacing electrode

3.2.2.10 Fiber optics FRET recordings from beating hearts

Fiber optic imaging system for *in vivo* APs measurement was first optimized *in vitro* on Langendorff perfused hearts. Data showed the signals from each bundle could be recorded and the noise could be cancelled out by taking YFP-to-CFP ratio (Fig. 32B and 32C). With the optic fiber bundle placing closely against the heart, the motion artifact could be minimized while recorded without applying the E-C uncoupler (blebbstatin) (Fig. 32B). The signal quality was comparable to the recordings while the E-C uncoupler was applied (Fig. 32C). We also tested the applicability on living mice with open chest. The preliminary data were plausible (Fig. 33). Although some technical issues remain to be solved, we anticipate the chronic measurement *in vivo* would be achievable.

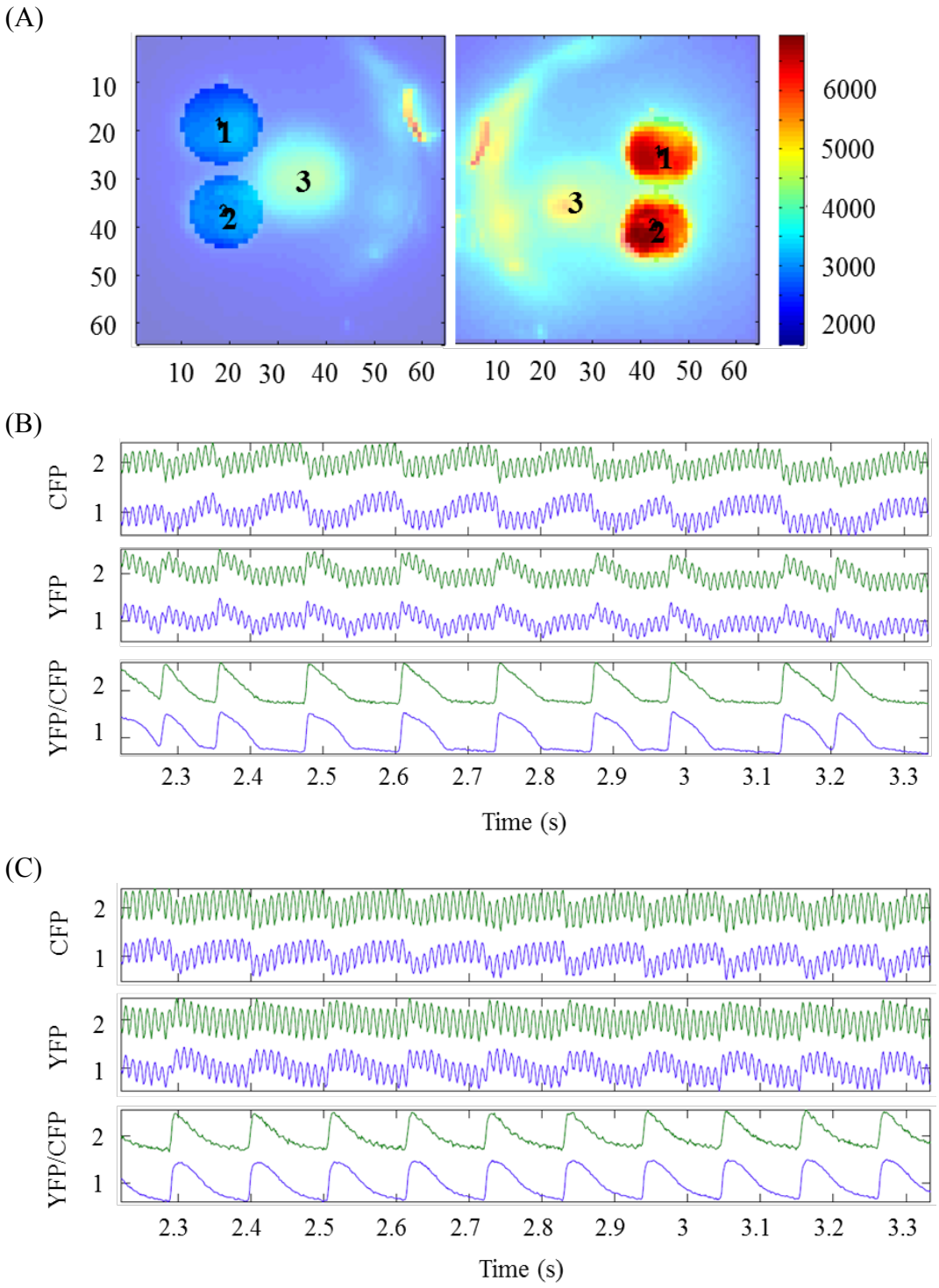

Fig. 32 Optical APs recorded by optic fiber on a Langendorff perfused heart. (A) Arrangement of fiber bundle during analysis. Numbers indicate the AP traces shown in the y-axis in (B) and (C). Representative CFP, YFP recordings and optical AP traces during spontaneous beating without the addition of blebbistatin (B) and with blebbistatin (C).

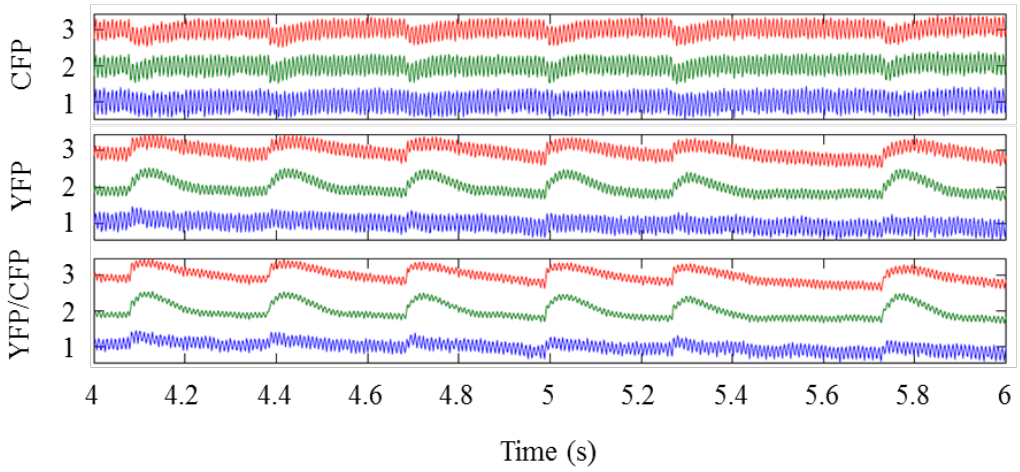

Fig. 33 *In vivo* optical APs recorded by optic fiber bundle. Representative CFP, YFP recordings and optical AP traces during spontaneous beating. Numbers in the y-axis corresponds to the arrangement of optic fiber shown in Fig. 32A. Note that signals were recorded at sever bradycardia (most likely junctional rhythym).

3.3 Discussion

3.3.1 Transgenic mouse model

Use of a cell type specific promoter element, such as the αMHC promoter[107], allows for cardiomyocyte specific labeling. A caveat with this model is that FP expression can cause myocardial damage under some circumstances[71, 72, 108, 109]. In a parallel line of experiments, we confirmed that cardiomyocyte restricted GCaMP2 overexpression would lead to severe myocardial hypertrophy, heart failure, and death (own data). In the αMHC-VSFP2.3 transgenic mouse model we did not observe any obvious transgene toxicity. Even in high expression, cardiac function was unimpaired compared to low expression and non-transgenic littermates (Fig. 26). Importantly, VSFP2.3 was clearly localized at the sarcolemma including the intracellular t-tubular system. Because of the highest signal in the transgenic line #123 without signs of transgene toxicity we decided to use this mouse line for a more in-depth characterization of the VSFP2.3 sensor as an optogenic tool to study cardiac membrane potential changes in isolated cardiomyocyte and whole hearts.

3.3.2 VSFP2.3 in cardiac electrophysiology

The QT interval in electrocardiomgrams (ECG) can be presented as the action potential durations (APDs) in cellular level[110]. Thus, APDs can be an important parameter for describing physiological situation and pathophysiological questions. Since neonatal and adult CMs behave completely different to pharmacological interventions, adult CMs remain the more useful model for the investigation of APs in adult situation[36]. With genetically encoded voltage sensor VSFP2.3 expressed in CMs, APD can be monitored easily by making use of optical (non-invasive) tool.

The voltage sensing mechanism in VSFP2.3 consists of two components. The fast component links to the charge movement in the fourth transmembrane segment of the VSD, while the slow component correlates to the conformational change of the VSD[111]. Previous studies in neurons showed that VSFP2.3 exhibits fast “on” kinetics (activation upon depolarization) and relatively slow “off” kinetics (repolarization) (1.9±0.9 and 78.4±0.5, respectively)[99]. The fast “on” would be sufficient to follow

sodium (Na^+) channel opening in phase 0. The "off" kinetics is too slow and will lead to a pseudo-elongation of APD by approximately 80 ms (Fig. 30).

The rapid upstroke in optical APs was comparable to that of electrical APs indicating VSFP2.3 can be useful for the studies of the initiation and propagation of electrical impulse *in vivo*. As expected, the delayed repolarization (by 80 ms) resulted in prolonged optical APDs. However, the strong correlation between electrical APD_{90} and optical APD_{50} suggested it might be possible to use a mathematical model to translate the optical recordings into corresponding electrical signals.

In addition to the current clamp experiments, we performed field potential excitation of isolated cardiomyocyte and observed markedly prolonged APDs (Fig. 29). This discrepancy could be due to the underlying mechanisms that trigger the action potential are different between field stimulation and point stimulation by current clamp[112], especially for the rod-shape adult cardiomyocytes. The changes in transmembrane potential of single cardiac cells exhibit spatial heterogeneity during field stimulation[113-115]. The complex responses may be affected by the amplitude, orientation of the electric field that could result in depolarization on one end of the cells and hyperpolarization on the other end. This might led to the prolongation in optical APDs while taking the fluorescence changes from the whole cells. Thus, cautions should be taken while comparing under different experiment condition.

Optical mapping of Langendorff perfused heart using voltage sensitive dyes is a commonly used technique to investigate the initiation and propagation of APs. E-C uncouplers such as 2,3-Butanedione 2-Monoxime (BDM), cytochalasin D (CytoD) and blebbstatin are used to suppress mechanical contraction[57, 116-119]. However, these uncouplers are toxic and have shown to alter bona fide APs[116, 120, 121].

In this study, we have demonstrated an alternative technique to record APs at normal sinus rhythm, under pacing and during an arrhythmic episode (Fig. 31) in transgenic mice hearts expressing VSFP2.3. Importantly, the design of the FRET sensor allows for ratiometric imaging and thus correction for motion artifacts without the application of chemical uncouplers. However, our first experiments did not take advantage of this for technical reasons (the imaging set-up was equipped with a single camera for YFP detection only after CFP excitation). Fiber optics system equipped

with two EMCCD cameras provides a potential solution. Preliminary data from fiber optics recordings demonstrated that FRET imaging is feasible even under spontaneous sinus rhythm in Langendorff perfused hearts (Fig. 32). With the optic fiber bundle placing closely against the heart, the motion artifact could be minimized while recorded without applying the E-C uncoupler (blebbstatin) (Fig. 32B). Although technically challenging, the first *in vivo* optical measurements suggested that measuring APs over multiple time points is feasible.

4. Generation of double transgenic induced pluripotent stem cell lines (αMHC-VSFP2.3 / αMHC-neoR)

4.1 Materials and Methods

4.1.1 Generation of double transgenic mice (αMHC-VSFP2.3 / αMHC-neoR)

In order to be able to select for pure cardiomyocytes during *in vitro* cardiac differentiation, the transgenic mouse that carried the neoR gene under the control of αMHC promoter (αMHC-neoR) were mated with αMHC-VSFP2.3 mice. Tail biopsies from the offspring were obtained at age of 4 weeks. The extraction of genomic DNA and genotyping were done as described in section 3.1.2. The primers for detecting the VSFP2.3 transgene (CiVSP) were listed in Table 4 in section 3.1.2 and the primers for detecting the neoR gene are listed in Table 7. Following the confirmation of the double transgenic mice via genotyping, tail tip fibroblasts (TTFs) were generated from a 6 weeks old mouse.

Table 7 Primers for the genotyping of the neomycin resistant gene

Gene	Sequences	Tm (°C)	Product size (bp)
Neomycin resistance	For: 5'-TCCTGCCGAGAAAGTATCCATCATGGCTGA-3'	63	383
	Rev: 5'-ATTCGCCGCCAAGCTCTTCAGCAATATCAC-3'	63	

4.1.2 Generation of fibroblasts from adult double transgenic mouse tail

TTFs were isolated from one of the double transgenic mice at age of 6 weeks based on the modified protocol described by Salmon et al.[122]. Briefly, the mouse tail was cut off with approximately 2 cm in length and incubated in ice-cold mouse embryonic fibroblasts (MEF) medium for one hour. After incubation, the tail was washed with ice-cold DPBS (Ca^{2+}/Mg^{2+} free, Gibco) containing 2X penicillin/streptomycin (P/S, 10,000 IU/l, 10,000 µg/l, 100x, Gibco) followed by a 70% ethanol wash and another ice-cold DPBS wash. The tail was chopped into small pieces and digested in MEFs

medium (Appendix) containing 400 units/ml collagenase II (Worthington, Lakewood, NJ) overnight at 37°C in a humidified incubator with 5% CO_2. The cells were further dissociated by trituration several times. Cell suspension was filtered using 70 μm cell strainer (BD Falcon™) and collected in a 50 ml tube (Falcon). Cells were pelleted by spinning at 200 x g for 5 minutes and the collagenase solution was aspirated. The cell pellet was resuspended with MEF medium, plated onto a 60-mm dish and incubated at 37°C in a humidified incubator with 5% CO_2 (passage 1). When the density reached around 80-90% confluence, cell number was counted and cells were split and frozen for further experiment. All experiments were done within three passages to avoid replicative senescence[123].

4.1.3 Viral transduction

Viral transduction was performed in collaboration with Dr. Kaomei Guan and Dr. Katrin Streckfuss-Boemeke (Department of Cardiology and Pulmonology, German Center for Cardiovascular Research, University Medical Center Goettingen). Two days before viral transduction, TTFs were plated onto a 12 well plate coated with 0.1% gelatin with different densities. To induce the reprogramming, we applied two different lentivirus systems. The STEMCCA system contains a humanized excisable lentivirus system containing all four reprogramming factors Oct4, Klf4, Sox2 and c-Myc in a single "stem cell cassette" (pHAGE2-EF1aFull-hOct4-F2A-hKlf4-IRES-hSox2-P2A-hcMyc-W-loxP, OKSM)[124]. The pE4-OKSM system contains a humanized excisable retroviral vector encoding for four reprogramming factors Oct4, Sox2, Klf4 and c-Myc linked by picornaviral 2A peptides[125].

For different cell types, the transduction efficiency varies. Thus, to optimize the results, different multiplicity of infection (MOIs) were applied to different wells. On the day of viral transduction, TTFs from one of the 12 wells were collected and cell number was counted. The number of cells in each well was then calculated proportionally based on the new cell count. MOIs were derived based on the following equation:

MOI = the volume of the virus used (ml) x virus titer (U/ml) / cell number

The condition for viral transduction (number of cells, virus used, and MOI) within the 12 well plate was summarized in Table 8. On the day of viral transduction, medium in each well was replaced with 500 µl of feeder layer medium (FLm) (Appendix) containing 5 µg/ml polybrene (Sigma), 2x P/S (Gibco). Then 300 µl of virus mixtures with predefined MOI was added to each well. The 12 well plate was kept at 37°C in a humidified incubator with 5% CO_2. One the next day, the virus-containing medium was replaced by rinsing the wells twice with FLm containing 2x P/S (Gibco), and the plate was kept in the incubator for two days. The cells were cultured in FLm till ESC-like colonies were observed. The medium was changed every other day. Once colonies formed, they were picked individually using pipette tips and transferred to a well of the 12-well plate containing MEFs. Each candidate clone was then expanded a 6-well, 6-cm dish and eventually to a 10 cm MEFs dish.

Table 8 Conditions of viral transduction in each well

0.36 x 10^5 cells Retro, MOI 2.5	0.36 x 10^5 cells StemCCa V3, MOI 2.5	0.36 x 10^5 cells StemCCa V4, MOI 1	0.36 x 10^5 cells StemCCa V4, MOI 2.5
0.43 x 10^5 cells Retro, MOI 1	0.43 x 10^5 cells StemCCa V3, MOI 1	Negative control	For cell counting
0.51 x 10^5 cells Retro, MOI 0.5	0.51 x 10^5 cells StemCCa V3, MOI 0.5	0.51 x 10^5 cells StemCCa V4, MOI 0.1	0.51 x 10^5 cells Retro, MOI 5

4.1.4 Culturing of iPSC clones

ESC-like colonies were cultured on feeder layer cells (MEFs). The MEFs were treated with 10 µg/ml Mitomycin-c (MMC, *Sigma*) or γ-irradiation (30 Gray) to inhibit the proliferation. At least one day before plating the ESC-like colonies, 10 cm culture dishes (Nunclon™Δ) were coated with 0.1% gelatin and incubated at 37°C in a humidified incubator with 5% CO_2 for 10 minutes. Around one million inactive MEFs were plated and cultured with MEF medium. Medium was changed after 24 hours. The MEFs plates were kept at 37°C in a humidified incubator with 5% CO_2 one week before use.

ESC-like cells were suspended in mES medium (Appendix). 1 x 10^6 cells were plated on the MEFs dishes, and cells were evenly distributed by swirling the dishes gently. Medium was changed daily. The cells were passaged every one or two day at 1:3 or 1:6 ratio depending on the colony size and density. When the cell density reached 80% confluence, cells were split into fresh MEFs dishes. Medium was aspirated and cells were washed with DPBS once. 3 ml of 0.25% Trypsin-EDTA (1x) (Invitrogen) was added to the 10-cm dish and incubated at 37°C in a humidified incubator with 5% CO_2 for 3 minutes. Trypsin was inactivated by adding 7 ml of mES medium. Single cell suspension was obtained by trituration several times. The single cell suspension was then transferred to a 50 ml tube and pelleted at 300xg for 5 minutes. Supernatant was removed and pellet was resuspended with 10 ml fresh mES medium. Cell number was counted and proper number of cells (1~2 million) was plated onto 10 cm fresh MEF dishes.

4.1.5 Cryopreservation of iPSCs

For cryostorage, cells were collected after trypsinization and counted as described above. After centrifugation (300 x g, 4°C, 5 minutes), the pellet was resuspended with freezing medium containing 40% FBS (PAA), 10% DMSO (Sigma) and 50% mES medium. 1 ml of cell suspension was transferred to cryovials. The cryovials were placed in the isopropanol freezing container and stored in -80°C freezer. The isopropanol freezing container allows the temperature to drop 1°C per minute.

Thawing of cells was done quickly. The cryovial was removed from -80°C freezer and put in 37°C water-bath. After thawing, the cell suspension was transferred to a 50 ml tube containing 9 ml of mES medium and mixed well by pipetting up and down several times. The cell suspension was then transferred to a 10 cm dish pre-cultured with inactive MEFs.

4.1.6 Characterization of double transgenic induced pluripotent stem cell lines

4.1.6.1 PCR-Genotyping

DNA was extracted from cultured cells using DNeasy Blood & Tissue Kit (QIAGEN) following the manufacture´s protocol. In brief, 1-2x10^6 cells were collected and pelleted at 300 x g for 5 minutes. The cell pellet was resuspended with DPBS and cells were lysed with Buffer AL containing proteinase K. After incubating at 56°C for 10 minutes, DNA was precipitated by adding 96-100% ethanol and mixing thoroughly. Samples were transferred into DNeasy Mini spin columns and spun at 8000 rpm for 1 minute to allow DNA to bind to the membrane of the columns. The columns were washed with Buffer AW1 and AW2 in sequence. Finally, DNA was eluted from the columns by adding Buffer AE.

PCR reactions were carried out using GeneAmp® PCR System 9700 (Applied biosystems) and Extaq DNA polymerase (TaKaRa Bio. Inc.). Each reaction mixture contains 1.6 µl dNTP, 2 µl 10x buffer, 0.2 µl of each primer (10mM), 0.1 µl Extaq and 2µl DNA. Distilled water was added to fill up to a final volume of 20 µl. The primer sequences for detecting the transgene CiVSP and neoR are listed in Table 4 and Table 7. PCR conditions are described in Table 9. PCR products were separated by electrophoresis in 1% agarose gels as described above (section 3.1.1.2.).

Table 9 PCR condition for the genotyping of neoRVSFP iPSC lines

94°C	30 sec	
98 °C	10 sec	32 cycles
*55/61°C	30 sec	
72°C	30 sec	
72°C	5 min	
4°C	∞	
*55°C for CiVSP, 61°C for neoR		

4.1.6.2 RNA extraction

Total RNA was isolated from cultured cells using Trizol® Reagent (Invitrogen). Medium was first removed from the culture dishes and cells were washed once with

DPBS. 1 ml of Trizol was added to the culture dish and cells were scratched off the dish using cell scrapers. The resulting suspensions were collected in 1.5 ml eppendorf tubes and incubated at room temperature for 5 minutes. 0.2 ml of chloroform was added and mixed thoroughly using a vortex. After incubation at room temperature for 3 minutes, phase-separation was facilitated by centrifugation at 12,000 x g and 4°C for 15 minutes. The upper aqueous phase containing the RNA was transferred to a clean eppendorf tube. RNA was precipitated by adding 500 µl of 100% isopropranol, incubation at room temperature for 10 minutes, and subsequent centrifugation at 12,000 x g and 4°C for 10 minutes. The supernatant was removed and a gel-like DNA pellet became visible on the bottom of the tube. The pellet was washed with 1 ml of 75% ethanol in DEPC-treated water, and centrifuged again at 7,500 x g for 5 minutes at 4°C. After removing the supernatant, the pellet was air-dried for 5 to 10 minutes. Then pellet was then resuspended with DEPC water and RNA concentration was measured with a spectrophotometer (Nanodrop, ND-1000, ThermoScientific) at a wavelength of 260 nm.

To remove potential contamination of genomic DNA, the RNA samples were treated with DNase I (Roche). 1 µg of RNA was mixed with 1 µl of DNase buffer and 0.2 µl of DNase I (10 U/ µl) to have a total reaction volume of 10 µl and incubated at 37°C for 20 minutes. 1 µl of 40 mM EDTA was added into the reaction and incubated at 75°C for 10 minutes to inactivate the DNase I. The resulting products were proceeded to complementary DNA (cDNA) synthesis.

4.1.6.3 Reverse transcription and PCR

cDNA was reverse transcribed (RT) using High Capacity cDNA Reverse Transcription Kit (Applied Biosystems) with Oligo dT primer. Negative control from each clone was included to examine for genomic DNA contamination. The constitution of each RT reaction and PCR condition is listed in Table 10. The cDNAs were processed to semi-quantify the expression of the pluripotent genes by RT-PCR. The RT-PCR condition and primer sequences are listed in Table 11 and Table 12.

Table 10 RT reaction and the condition of thermal cycling

	µl
DNase I treated RNA (1µg)	11
1x RT buffer	2
25x dNTP mix (100 mM)	0.8
10x RT oligo dT	2
MultiScribe™ Reverse Transcriptase	1
RNase Inhibitor	1
Nuclease free H_2O	2.2
Total	20

Temp (°C)	Time
25	10 min
37	120 min
85	5 sec
4	∞

Table 11 RT-PCR reaction and the condition of thermal cycling

	µl
cDNA	2.5
Primer_for (10 µM)	0.25
Primer_rev (10 µM)	0.25
10x buffer	2.5
Extaq (5 unit/µl)	0.125
H_2O	17.375
Total	25

Temp (°C)	Time	# of cycles
94	2 min	
94	30 sec	35
55	30 sec	
72	1 min	
72	1 min	
4	∞	

Table 12 Primer sequences used in RT-PCR

Gene	Sequences	Tm (°C)	Product size (bp)
Oct 3/4	Forward: 5'-GCCCCAATGCCGTGAAG- 3'	57.6	101 bp
	Reverse: 5'-CAGCAGCTTGGCAAACTGTTC- 3'	59.8	
Nanog	Forward: 5'-TGCTACTGAGATGCTCTGCACA- 3'	60.3	71 bp
	Reverse: 5'-TGCCTTGAAGAGGCAGGTCT- 3'	59.4	
Sox2	Forward: 5'-GGCAGCTACAGCATGATGCAGGAGC- 3'	60	131 bp
	Reverse: 5'-CCTGCAGTACAACTCCATGACCAG- 3'	60	
Rex1	Forward: 5'-GGCCAGTCCAGAATACCAGA- 3'	59	232 bp
	Reverse: 5'- GAACTCGCTTCCAGAACCTG - 3'	59	
GAPDH*	Forward: 5'-ATGTTCCAGTATGACTCCACTCACG- 3'	63	171 bp
	Reverse: 5'- TGTCGTGGAGTCTACTGGTGTCTTC -3'	65	

* Housekeeping gene

4.1.6.4 Cardiac differentiation efficiency

To evaluate the efficiency of cardiac differentiation, each cell line was differentiated *in vitro* by inducing the formation of embryoid bodies (EBs) in hanging drops. For this, cell colonies were dissociated into single cell suspensions by trypsinization as described before. The feeder layer cells (MEFs) were removed by preplating the cell suspension for 30 minutes. After preplating, the supernatant was collected in 50 ml tubes and the number of cells was counted as described before. After cell counting, cell suspension was diluted to 500 cells per 20 µl of differentiation medium (Appendix). 20 µl drops were placed on the lids of 15 cm culture dishes using a multichannel pipette and carefully inverted to cover the dishes. Each dish contained 15 ml DPBS to prevent the drops from drying out. The 15 cm dishes were incubated at 37°C in a humidified incubator with 5% CO_2 for 3 days. After 3 days, EBs were collected by rinsing the lids with 10 ml differentiation medium and transferred to 10 cm petri dishes for suspension culture for 3 more days. After suspension culture, EBs were plated onto 10 cm cell culture dishes coated with 0.1% gelatin for adhesion culture. On day 11 (11 days after the initiation of hanging drops), 200 µg/ml of neomycin (G-418, PAA) was added into the differentiation medium to select for pure cardiomyocyte population. The differentiation was terminated on day 16. The morphology of the EBs and beating activities were observed daily throughout the period of differentiation. The line with highest beating activities was chosen for further experiments.

4.1.6.5 Immunofluorescence staining of pluripotent markers

Undifferentiated iPS cells were cultured on inactive MEFs on coverslips coated with 0.1% gelatin. Once 70-80% confluence was reached, cells were fixed with 4% Histofix (Roti®, Roth) at room temperature for 10 minutes followed by three washes with DPBS (5 minutes each time). The staining was done as described in section 3.1.3.5 with minor modification. Since the iPSC colonies are compact and dense, the incubation of primary antibodies was done at 4°C overnight. Primary antibodies for detecting the pluripotent markers were diluted to working concentration in blocking buffer: Oct4 (abcam, ab19857, 1:500), Nanog (abcam, ab80892, 1:500), Sox2

(abcam, ab97959, 1:500), SSEA1 (abcam, ab16285, 1:50). Secondary antibodies used were Alexa Fluor® 488 and Alexa Fluor® 546 (1:800, Molecular Probe®) and nuclei were stained with DAPI (Sigma, 1:1000). Fluorescent images were taken using laser scanning confocal microscope (LSM 710, Zeiss, Germany).

4.1.6.6 Alkaline Phosphatase staining

Alkaline phosphatase (ALP) is highly expressed in undifferentiated pluripotent stem cells. ALP staining was performed on undifferentiated iPS cells cultured on inactive MEFs in a 6-well plate based on manufacture´s protocol (86R-1KT, Sigma). In brief, equal amount (200 µl) of Sodium Nitrite Solution and FRV-Alkaline Solution were mixed thoroughly by gentle inversion and allowed to stand at room temperature. After 2 minutes, 9 ml of deionized water was added to the mixture to form diazonium salt solution. The diazonium salt solution was diluted with 200 µl of Naphthol AS-Bl Alkaline Solution and this alkaline-dye mixture was kept from light. Cells were fixed with warm (18-26 ºC) Citrate-Acetone-Formaldehyde Fixative Solution for 30 seconds followed by rinsing with deionized water for 45 seconds gently. The alkaline-dye mixture was added to the fixed cells and incubated at room temperature for 15 minutes in dark. Cells were rinsed in deionized water for 2 minutes, and counterstained with Hematoxylin Solution for 2 minutes. Finally, cells were rinsed thoroughly in tap water, air dried, and proceed to microscopic evaluation.

4.1.6.7 Spinner flask culture

To enhance the culture process, spinner flask cultures were implemented. iPSCs were cultured and passaged as described before. Before initiating differentiation, cells should be passaged at least two times. iPSC colonies were dissociated into single cells by trypsinization as described before. After preplating for 30 minutes to reduce the MEF content, cell suspensions were collected in 50 ml tubes and cell number was counted. Ten million cells were transfer to another 50 ml tube and pelleted by centrifugation at 300 x g and 4°C for 5 minutes. After centrifugation, the supernatant was removed and the pellet was resuspended with 25 ml differentiation medium. The

cell suspension was then transferred into a 125 ml culture vessel (Techne, F7988) containing 25 ml of differentiation medium. The stirring speed was set to 60 rpm (day 0). On the next day (day 1), 50 ml of differentiation medium was added into the culture vessel. Half of the medium was replaced every other day.

4.1.6.8 Quantitative PCR

The selected iPSC line was differentiated *in vitro* using modified spinner flask method as described in section 4.1.6.7. EBs were collected on day 5 and plated in 12-well plates coated with 0.1% gelatin. Total RNA was isolated from undifferentiated cells (day 0) and EBs harvested on culture days 5, 7, 11 and 20 from the wells. cDNA was synthesized as described above in section 4.1.6.3. Quantitative PCR was performed in triplicates using Fast SYBR® Green Master Mix (Applied Biosystems) on ABI PRISM 7900HT Fast Real-Time PCR system (Applied Biosystems). For each reaction, 1 µl of cDNA was mixed with 5 µl of 2X Fast SYBR® Green Master Mix, 0.25 µl of forward and reverse primer mix (final concentration: 50 nM), and 3.75 µl of nuclease-free water. Primers used for quantitive PCR were listed in Table 13. Each PCR run included water controls (no cDNA) and dilution curves from cDNA pools to ensure linearity of PCR amplification. The PCR conditions were as follows: after heat up to 50ºC for 2 minutes, initiation of polymerase activation was run at 95ºC for 10 minutes, followed by 40 cycles of denaturation at 95ºC for 15 seconds, annealing and extension at 60ºC for 1 minute. A final dissociation stage was performed at 95ºC for 15 seconds, 60ºC for 15 seconds and 95ºC for 15 seconds.

Comparative quantification was carried out using the ΔΔCt method to determine the levels of gene expression at different time points. The differences in Ct values ($\Delta C_{t,\ sample}$) for each sample were derived by normalizing the Ct values of each time point ($C_{t,\ GOI}{}^{S}$) to those of the housekeeping gene (GAPDH) ($C_{t,\ norm}{}^{S}$). The Ct value from differentiation day 20 was used as the calibrator ($\Delta C_{t,\ calibrator}$). The differences in Ct values for each time point were then normalized again to the difference in control group. The fold change in expression levels was presented as $R = 2^{-\Delta\Delta C_t}$, and the values were plotted against differentiation time points.

$$\Delta C_{t,sample} = C_{t,GOI^s} - C_{t,norm^s}$$

$$\Delta C_{t,\ calibrator} = C_{t,GOI^c} - C_{t,norm^c}$$

$$\Delta\Delta C_t = \Delta C_{t,\ sample} - \Delta C_{t,\ calibrator}$$

$$R = 2^{-\Delta\Delta C_t}$$

Table 13 Primer sequences used in real-time PCR

Gene	Sequences	Tm (°C)	Product size (bp)
Nkx2.5	Forward: 5'- CAAGTGCTCTCCTGCTTTCC - 3'	60	134
	Reverse: 5'- CTTTGTCCAGCTCCACTGC - 3'	61	
YFP	Forward: 5'- TACCTGAGCACCCAGTCCAA- 3'	59.4	110
	Reverse: 5'- CCCTTGCTCACCATGAGAGT- 3'	59.4	
αMHC	Forward: 5'- GCTGACAGATCGGGAGAATCAG - 3'	57	113
	Reverse: 5'- CCCCTATGGCTGCAATGC - 3'	53	
GAPDH*	Forward: 5'- ATGTTCCAGTATGACTCCACTCACG - 3'	63	171
	Reverse: 5'- TGTCGTGGAGTCTACTGGTGTCTTC -3'	65	

* Housekeeping gene

4.1.7 Engineered heart muscles from αMHC-VSFP2.3/neoR iPSCs

To enable cardiac muscle engineering, cardiomyocyte yield from differentiating iPSC-cultures were further optimized in spinner flask cultures.

4.1.7.1 Scale up of cardiac differentiation in spinner flask cultures

The initiation of cardiac differentiation was as described above in section 4.1.6.7. However, instead of plating the EBs on day 5, spinner flask culture was extended for the whole cardiac differentiation and selection phase. Half of the medium was

replaced every other day. On day 11, 200 µg/ml of neomycin (G-418, PAA) was added to the medium for the selection of cardiomyocytes. After 5 days of selection, EBs were harvested and digested into single cardiomyocytes for further experiment.

4.1.7.2 Digestion of embryoid bodies into single cardiomyocytes

EBs were collected from the culture vessel and transferred into two 50 ml tubes. The tubes were placed upright for 15 minutes to allow EBs to precipitate. The supernatant was aspirated and EBs were resuspended with 6 ml of collagenase I (Sigma) containing 20 µl/ml DNase I (Calbiochem). The tubes were incubated at 37°C for 1 hour in a water bath with shaking. 20 ml of DPBS (w/o Ca/Mg) was added and single cells were obtained by triturating with 10 ml pipette few times. The cells were pelleted by centrifuge at 200 x g for 5 minutes at room temperature. For further digestion, the pellet was resuspended with 5 ml 0.25% trypsin-EDTA and incubated at room temperature for 10 minutes on a shaker. The trypsin suspension was triturated with 5 ml pipette to yield single cell solutions. The enzyme digestion was neutralized with 20 ml differentiation medium containing 20 µl/ml DNase and then triturated further using 10 ml pipette. The cells were pelleted by centrifuge at 200 x g for 5 minutes at 4°C. After resuspended with 10 ml differentiation medium, the number of cells was counted.

4.1.7.3 Generation of engineered heart muscle

Self-made glass culture dishes consisting of 4 ring-shape molds (Fig. 34A) (inner diameter 4 mm, outer diameter 10.6 mm) were used for casting the EHMs. The volume inside each mold is 450 µl. All the pipetting steps were carried out on ice to prevent premature polymerization of the EHM reconstitution mixture. 1.5 million of cells containing 70% of iPSC-derived cardiomyocytes and 30% non-cardiomyocytes (inactive MEFs) were mixed and resuspended with appropriate volume of differentiation medium. Equal amount of 2X DMEM was added to collagen type I (DM6, Devro Medical) and the yellow/orange color indicated the acidity of the mixture. The pH was adjusted (~7.4) with 0.1 N NaOH. Finally, the proper amount of

cell suspension was supplemented into the mixture. A standard pipette scheme for generating four EHMs is listed in Table 14. The homogeneity of mixture was achieved by triturating with pre-cooled 2 ml pipette several times. 450 µl of mixture was cast into each mold and incubated at 37°C in a humidified incubator with 5% CO_2 for one hour. After initial condensation, 6 ml of differentiation medium was added into each glass culture dish.

The EHMs were incubated at 37°C in a humidified incubator with 5% CO_2 for three days. On day 3, EHMs were transferred to static stretchers (Fig. 34B) and kept in culture for 10 more days. Medium was changed every other day during the whole period of culturing.

Table 14 Standard pipette scheme for generating 4 EHMs

1. Collagen type I (0.4 mg/EHM)	306 µl
2. 2x DMEM	306 µl
3. NaOH (0.1N)	60 µl
4. Cell suspension	1428 µl

* pipetting should be carried out in the order indicated by number

2x DMEM

FCS (PAA-102)	40 %
10x DMEM	20 %
P/S	2 %
Sterile H_2O	

4.1.7.4 Contractility measurements

On day 10~13, EHMs were suspended between retaining hooks and force transducers inside organ baths containing physiological Tyrode´s solution (Appendix) (Fig. 34C). The temperature in the organ baths was maintained at 37°C and the pH were adjusted to 7.4 with carbogen (95% O_2, 5% CO_2 gas mixture). After 15 minutes of equilibration, EHMs were electrically stimulated at 4 Hz with pulse duration of 5 ms

and 200 mA current. EHMs were pre-stretched under 1.8 mM [Ca^{2+}] till the force reached a stable level (Lmax). The solution inside the organ baths was replaced with fresh Tyrode´s solution containing 0.2 mM [Ca^{2+}]. Contraction forces were initially measured under 0.2 mM [Ca^{2+}] subsequently under different calcium concentration from 0.4 mM to 2.8 mM with a 0.4 increment. Each force measurement should be done at least 5 minutes after the addition of calcium. The maximum and minimum forces were measured by PC-based acquisition software (BMON, Engineering firm G. Jaeckel, Hanau). Force of contraction (FOC) was calculated by the difference between maximum and minimum forces.

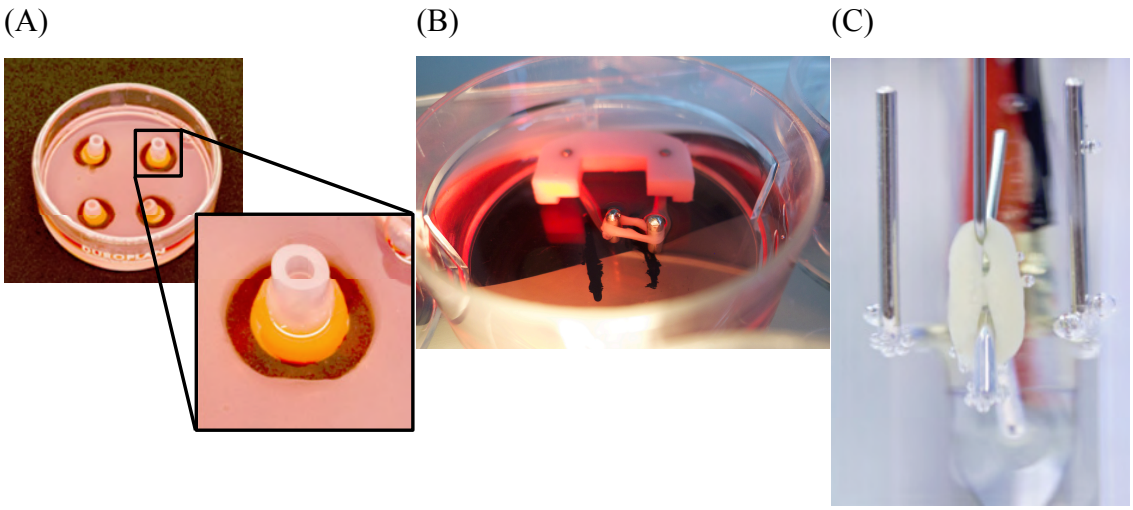

Fig. 34 Generation of neoRVSFP iPSC EHMs. (A) Casting molds for mouse EHMs. (B) EHM on static stretcher. (C) EHM in the organ bath during force measurement (A and C were provided from Dr. Peter Christalla[126])

4.1.8 Statistics

All values are presented as means with standard error of the mean (SEM). Pairwise comparisons were done by two-tailed Student's t-test (paired or unpaired as appropriate; Gaussian distribution was assumed). For comparisons of concentration response curves two-way ANOVA was utilized. Groups were considered significantly different if a p-value small than 0.05 was reached. Sample number (n), statistical test

and p-value are presented with each data set. Data analysis was performed with Microsoft Excel and GraphPad Prism (GraphPad Software Inc., San Diego).

4.2 Results

4.2.1 Genotyping of αMHC-neoR x αMHC-VSFP2.3 double transgenic mice

Mating of αMHC-neoR (kindly provided by Prof. L. Field, Indianapolis) and αMHC-VSFP2.3 transgenic mice gave birth to twelve offspring. PCR-genotyping identified four out of the twelve offspring as being positive for the neomycin resistance (neoR) and VSFP2.3 (Fig. 35).

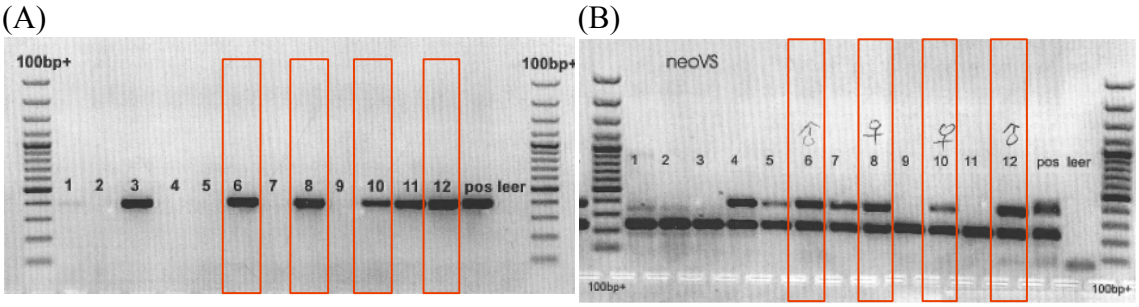

Fig. 35 PCR-Genotyping of neoR/VSFP2.3 double transgenic mice. Electrophoretic separation of PCR amplified DNA fragments specific for the neoR (383 bp; A) and the CiVSP (359 bp; B). NR1 (229 bp) was amplified as internal control to ensure proper DNA loading. DNA ladder: 100 bp plus (Fermentas).

4.2.2 Genotyping of αMHC-neoR x αMHC-VSFP2.3 double transgenic fibroblasts

DNA was extracted from tail tip fibroblasts (TTFs) outgrowths at passage 1 (Fig. 36A) and subjected to PCR for neoR and VSFP2.3 (Fig. 36B an 36C).

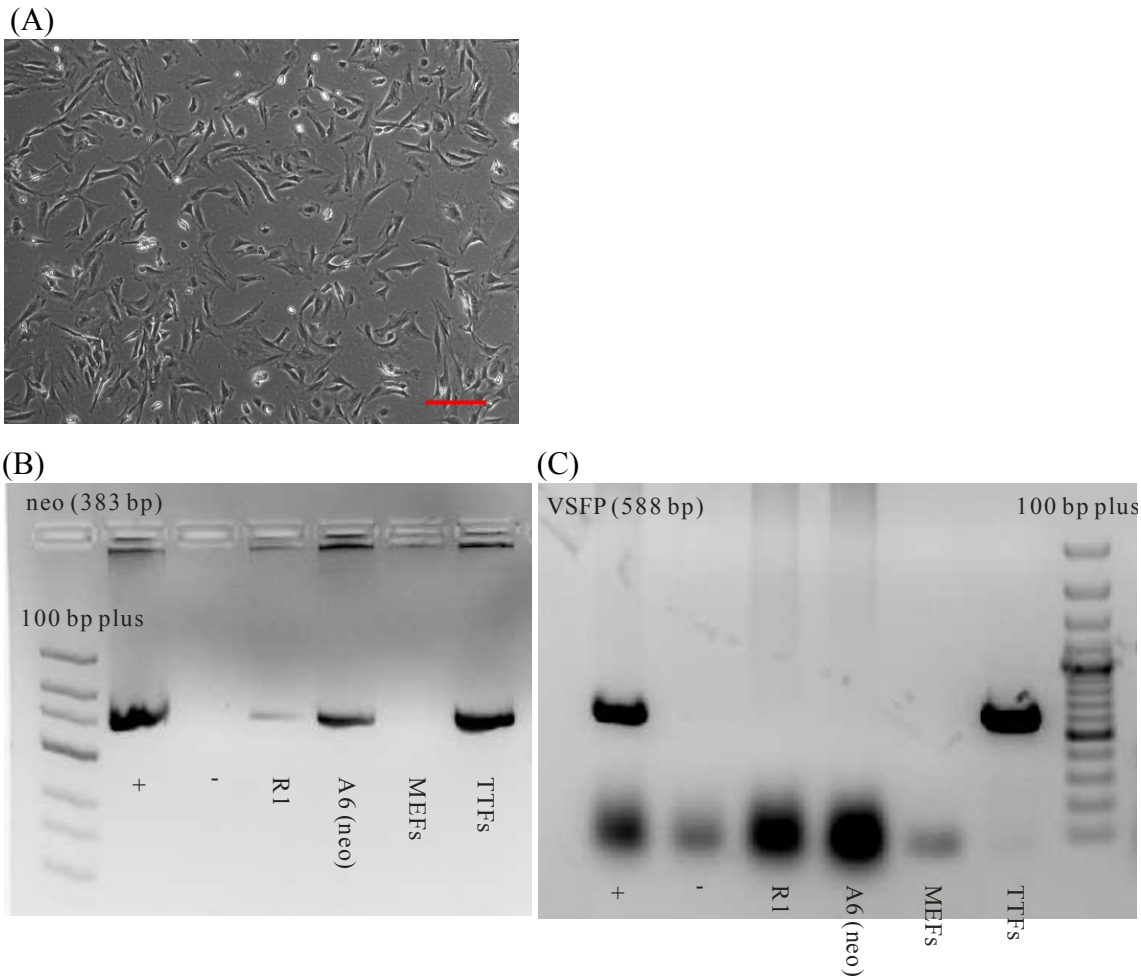

Fig. 36 αMHC-neoR x αMHC-VSFP2.3 double transgenic fibroblasts. (A) Morphology of TTFs (passage 1) generated from a 6-week-old double transgenic mouse (#6) used for reprogramming. Scale bar: 200 µm. (B) and (C) PCR for detecting neomycin resistant gene and VSFP2.3 gene. (+) positive control using αMHC-neoR vector in (B) and αMHC-VSFP2.3 vector in (C). (-) negative control without DNA. R1: DNA from the R1 wildtype mouse ESC line (mESC). A6 (neoR): DNA from transgenic mESC with neomycin resistance. MEFs: DNA from wildtype mouse embryonic fibroblasts. TTFs: DNA from double transgenic tail tip fibroblasts. DNA ladder: 100 bp plus (Fermentas).

4.2.3 Generation of αMHC-neoR x αMHC-VSFP2.3 iPSCs

Following viral transduction of the double transgenic TTFs, compact colonies with smooth edges resembling ESC morphology were first observed in some of the STEMCCA transduced wells six days after lentiviral transduction (Fig. 37B). TTFs transfected with pE4-OSKM gave rise to cell aggregations (Fig. 37C, left), but do not

form ESC-like colonies after subsequent cell culture (Fig. 37C, middle and right), which might indicate the reprogramming was not fully complete.

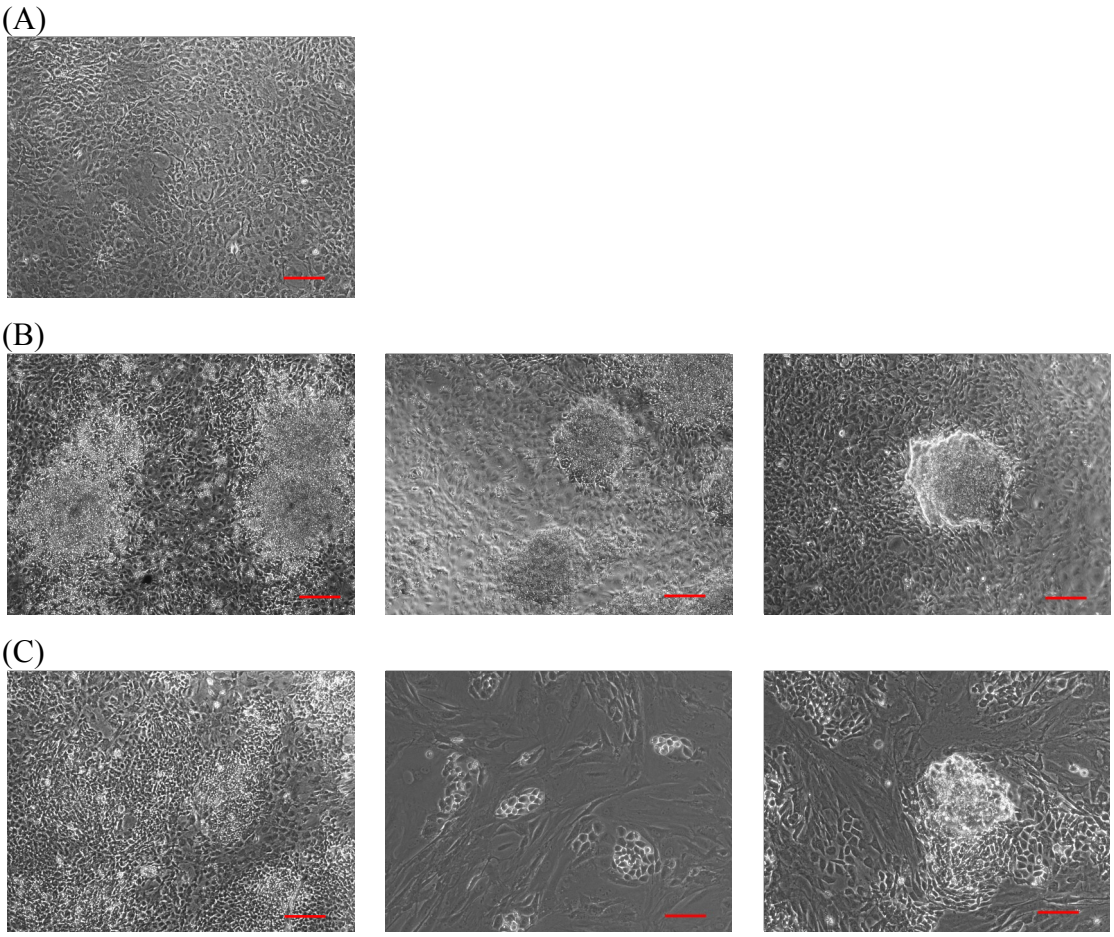

Fig. 37 Morphology of the cells after viral transduction. (A) Negative control: TTFs without viral transduction after six days in culture. Scale bar: 200 µm. (B) Six days after transduction in the STEMCCA group: (left) MOI 2.5; (middle) MOI 1; (right) MOI 0.1. Scale bar: 200 µm. (C) Six days after transduction with pE4-OSKM: (left) day 6, MOI 5; (middle) day 8, MOI 5; (right) day 10, MOI 5. Scale bars: (left) 200µm; (middle, right) 100 µm.

These ESC-like colonies from the STEMCCA group were picked from the 12-well plate and transferred to a well and expanded in a new 12-well plate containing inactive MEFs. After 12 passages, cells still retain as ESC-like morphology (Fig. 38). Initially, 6 clones (#2, 3, 5, 6, 7, 8) were randomly chosen for further characterization. All these clones were from the STEMCCA group.

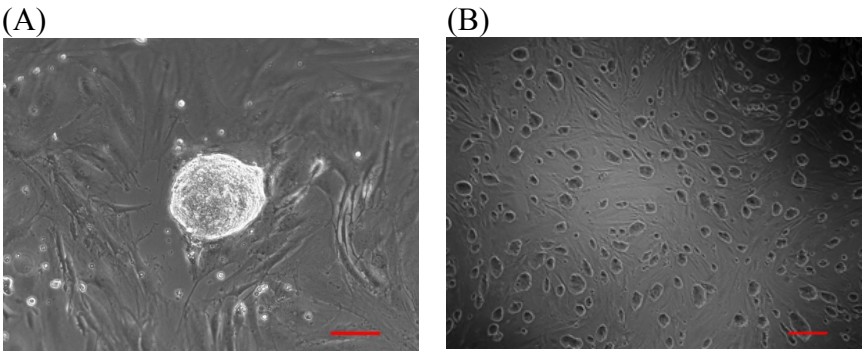

Fig. 38 Morphology of αMHC-neoR x αMHCVSFP2.3 iPSC. (A) A compact colony with smooth edge at passage 2 (scale bar: 100µm). (B) iPSC clone #6 at passage 12 (Scale bar: 200 µm).

4.2.4 Characterization of the new αMHC-VSFP2.3 / αMHC-neoR iPSC lines

4.2.4.1 PCR-genotyping of the αMHC-neoR x αMHCVSFP2.3 iPSC lines

DNA isolated from iPSC line 2, 3, 5, 6, 7, and 8 revealed that five out of six clones were positively PCR amplified for the neoR and VFP2.3 genes (Fig. 39). However, Clone 8 did not show any PCR bands could but could be differentiated into cardiomyocytes and selected under G418 supplementation, suggesting a false negative PCR.

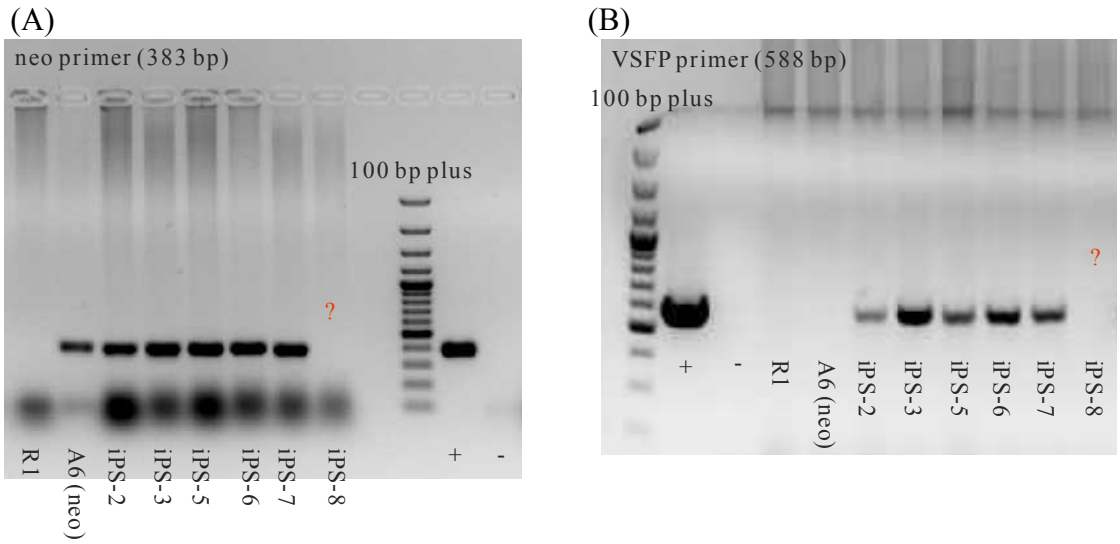

Fig. 39 Genotyping of neoRVSFP iPSC lines. R1: wildtype mESC. A6 (neoR): transgenic mESC line with neomysin resistant gene. (+): positive control using αMHC-neo vector in (A) and αMHC-VSFP2.3 vector in (B). (-): negative control without DNA.

4.2.4.2 Pluripotency and cardiac differentiation of αMHC-VSFP2.3 / αMHC-neoR iPSC lines

Semi-quantitative reverse transcription (RT)-PCR performed on RNA extracted from undifferentiated cells revealed that all six iPSCs clones expressed the pluripotent markers including Oct 3/4, Nanog, Sox 2 and Rex 1. (Fig. 40). The mouse ESC line (A6-neoR) and TTFs served as positive and negative controls, respectively.

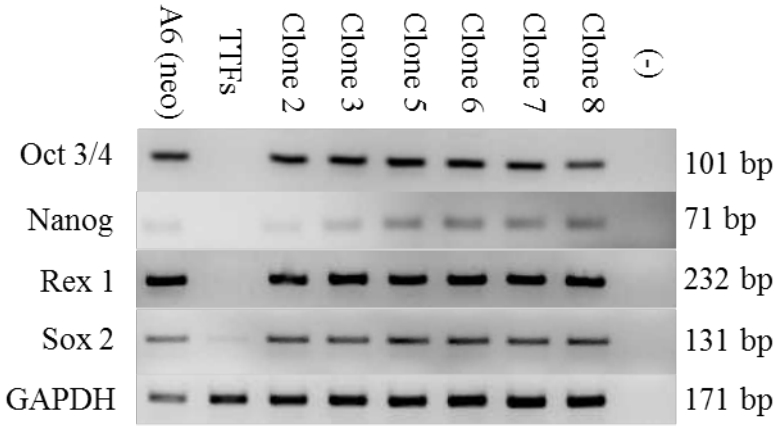

Fig. 40 RT-PCR for the pluripotent marker genes. 6 lines were tested for the expression of classical stemness markers (Oct3/4, Nanog, Rex1, Sox2). GAPDH was amplified as an internal control. A6 (neoR) – control ESC line. (-) RT-minus control.

All iPSC lines could be differentiated *in vitro* into beating cardiomyocytes via the hanging drop method. These beating cardiomyocytes survived G418 selection and demonstrated fluorescent signals characteristic of the VSFP2.3 transgene. Clone 7 was randomly selected for cardiac differentiation and denoted as neoRVSFP iPSC-7.

neoRVSFP iPSC-7 could be maintained at undifferentiated state for several passages, and showed positive staining for alkaline phosphatase (Fig. 41), Oct4, Nanog, Sox 2 and the SSEA-1 (Fig. 42), confirming the pluripotency of iPSC-7.

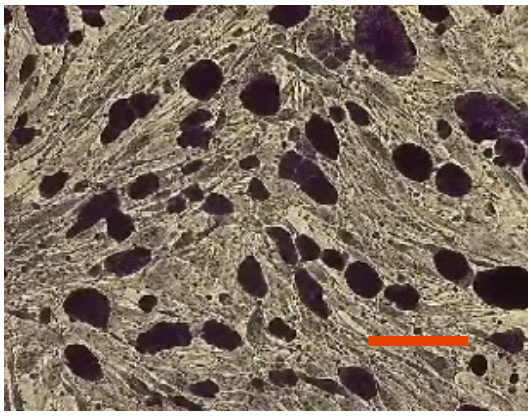

Fig. 41 Alkakine phosphatase activity in neoRVSFP iPSC-7. The dark purple stain in the iPSC colonies indicates presence of alkaline phosphatase. Scale bar: 200μm.

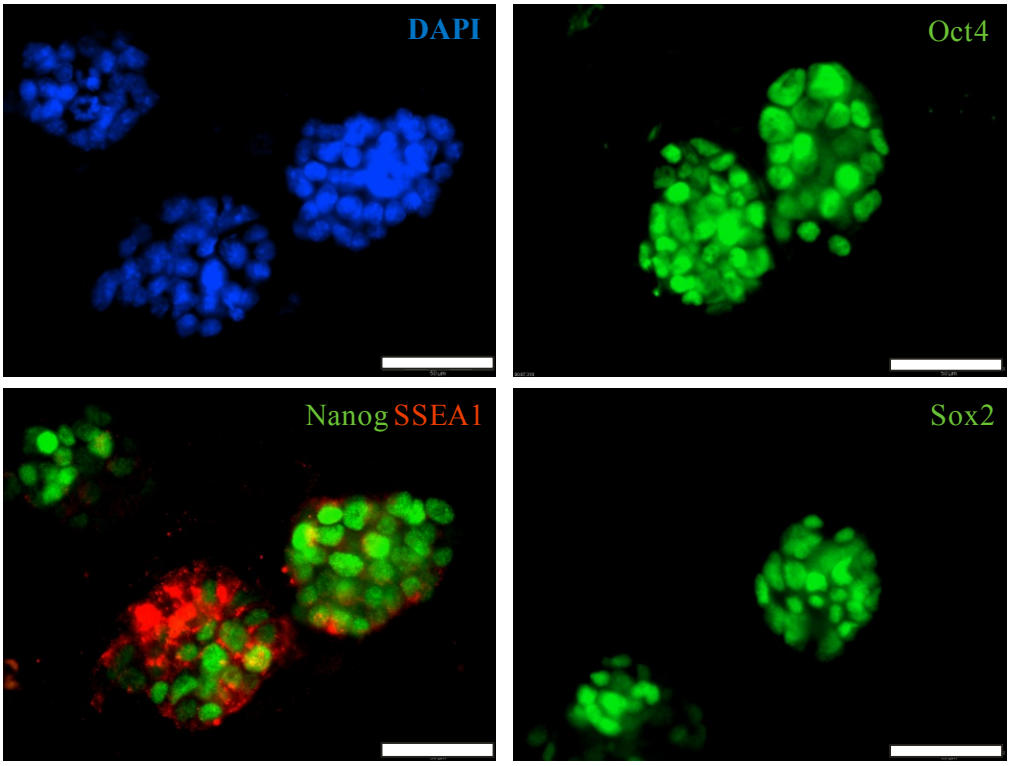

Fig. 42 Immunofluorescent staining of neoRVSFP iPSC-7 for the pluripotent markers. Colonies were fixed in the presence of formaldehyde and immune-labeled for Oct4 (nuclear), Nanog (nuclear), SSEA1 (cell surface) and Sox2 (nuclear) as indicated. Scale bars: 50µm

4.2.4.3 Bioreactor derivation of neoRVSFP iPSC cardiomyocytes

Scaling up cardiac differentiation was initiated in spinning flasks (bioreactor). EBs collected from bioreactor started to show spontaneously beating activities at culture day 6. Total mRNA extracted from EBs at different time points showed upregulation of cardiac specific gene (α-MHC) from culture day 5 onwards. YFP expression levels are also correlated with the highest expression on day 11. The expression level of the early cardiac marker Nkx 2.5 was observed to peak at day 5 and subsequently reduced over extended culture (Fig. 43).

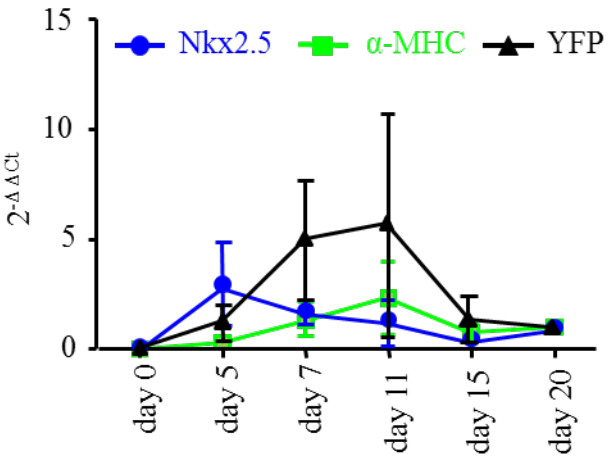

Fig. 43 Assessment of cardiomyocyte surrogate transcripts, including YFP from VSFP2.3, by quantitative PCR. RNA from indicated culture days (abscissa) was amplified and quantified by qPCR. The ordinate indicates fold changes from day 0. YFP is expressed under αMHC-promoter control and appears to correlate well with the endogenous αMHC transcript. n = 4/time point.

4.2.4.4 Functional VSFP2.3 expression in neoRVSFP iPSC cardiomyocytes

neoRVSFP iPSC-7-derived CMs showed YFP fluorescence under 488 nm excitation (Fig. 44A). A simultaneously detected decrease in CFP and increase in YFP fluorescence (Fig. 44B, red dotted lines) indicated the VSFP2.3 sensor was functional in iPSC-derived cardiomyocytes. From this data, optical APs (YFP/CFP ratio) could be derived. Further studies are necessary to determine the AP properties in detail.

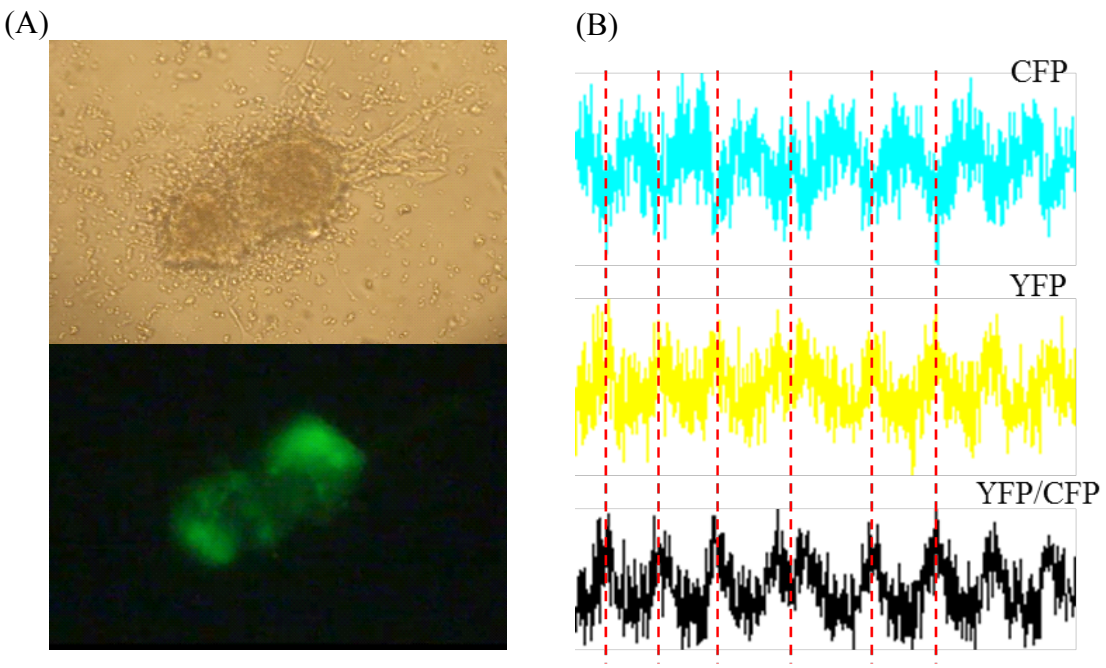

Fig. 44 neoRVSFP iPSC-derived beating EB. (A) Bright field image of a beating EB and fluorescence signals from the same EB under 488 nm excitation. (B) Changes in CFP and YFP signals were recorded, and YFP/CFP ratios were derived (right).

4.2.5 Construction of Engineered Heart Muscle from neoRVSFP iPSC

EHMs were generated from neoRVSFP iPSC-derived cardiomyocytes supplemented with 30% inactive MEFs. EHMs showed spontaneous contracting at culture day 4 (one day after transferring to stretchers). Isometric force measurements at culture day 13 demonstrated positive inotropic response of increasing extracellular calcium concentrations with maximal contractile force (0.23±0.04 mN) at 2.0±0.4 mM extracellular calcium (n=8) (Fig. 45B).

(A) (B)

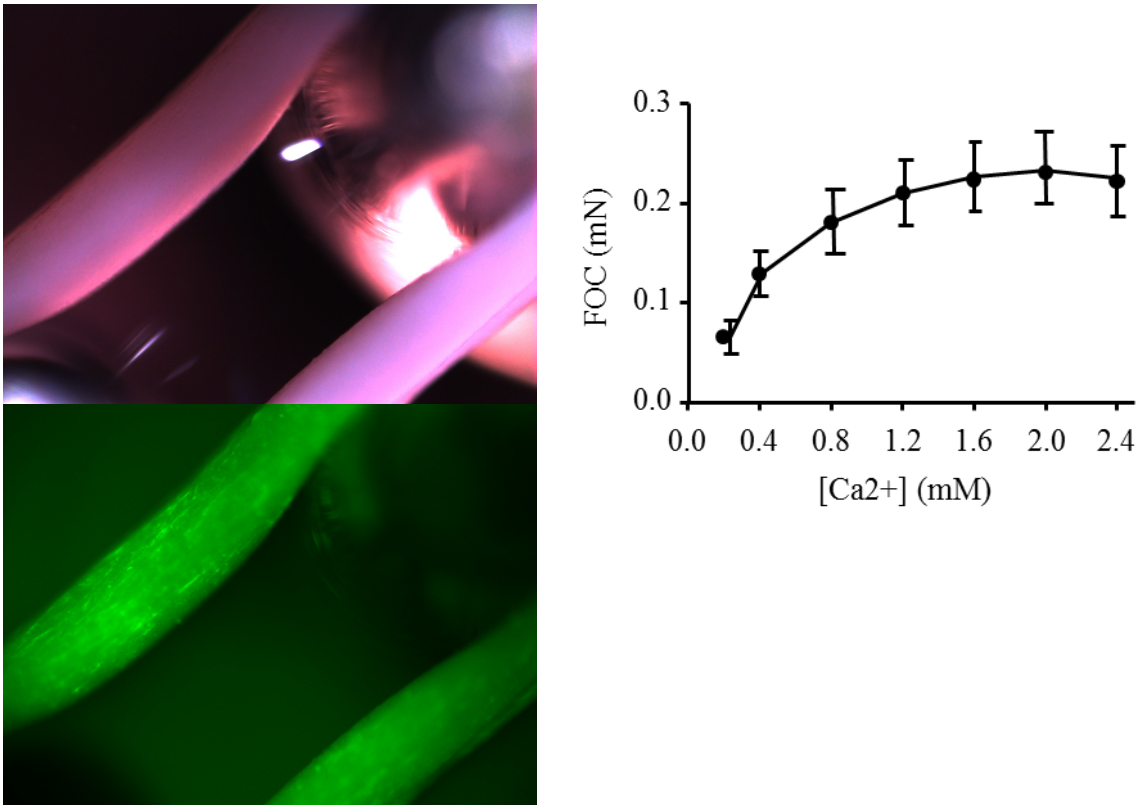

Fig. 45 neoRVSFP iPSC-CM derived EHMs. (A) neoRVSFP iPSC-derived EHM under bright filed (upper) and 488 nm illumination (lower). (B) EHMs (n=8) were subjected to isometric force measurements; the ordinate indicates force of contraction (FOC) in mN; the abscissa indicates the extracellular calcium concentration. Contraction experiments were performed at 37 °C and under 4 Hz filed stimulation in Tyrode's solution.

4.3 Discussion

VSFP2.3 in regenerative medicine and cardiac tissue engineering

Another application of VSFP2.3 is in functional labeling of cardiomyocyte derived from pluripotent stem cells for subsequent studies of electrophysiological maturation and in case of intramyocardial applications as well as electrical integration. To generate pluripotent stem cells carrying the VSFP2.3 transgenes and an additional transgene for cardiomyocyte selection we crossed αMHC-VSFP2.3 line 123 with αMHC-neoR mice[127]. Double transgenic mice were selected as fibroblast donors that were subsequently subjected to reprogramming according to the Yamanaka protocol[3]. The resulting induced pluripotent stem cells (iPSCs) possessed properties of embryonic stem cells (ESCs), i.e. unlimited self-renewal and differentiation into multiple lineages (ectoderm, mesoderm, and endoderm). From the several iPSC lines, one was selected randomly for further characterization including embryoid body culture and bioreactor culture for cardiomyocyte derivation. First optical imaging experiments confirmed that the derived cardiomyocytes harbor a functional VSFP2.3 transgene. Future studies will exploit these properties to define how pharmacological and biophysical stimuli can impact on cardiomyocyte diversification (e.g. nodal vs. working myocardium) and maturation. Data from our own group supports the notion that tissue engineering may push cardiomyocyte maturation in vitro towards a postnatal phenotype[128]. Accordingly, first attempts to engineer heart muscle from iPSC-derived cardiomyocytes expressing VSFP2.3 were performed providing first proof-of-concept for a VSFP2.3 cardiac muscle engineering approach. In addition, VSFP2.3 engineered heart muscle (EHM) may be useful to study the time course of electrical integration of EHM after in engraftment in vivo.

Advancing the VSFP2.3 model to human pluripotent stem cells would also in this respect be highly desirable. In this study, first human ESC lines were generated with stably integrated VSFP2.3 sensor (based on genomic PCR). Additional validation experiments will be necessary to assess stability of the transgene and utility also for optical imaging of human APs in pluripotent stem cell-derived cardiomyocytes. In human cells the slow signal decay may not be as limiting as in the mouse because of the physiologically slower AP kinetics as compared to rodents.

5. Summary

Optogenetics has evolved rapidly in the past two decades[129]. The combination of optical and genetic techniques makes real-time and chronic imaging within certain cell populations, tissues and organs feasible. Genetically encoded fluorescent protein (FP) sensors have advanced the studies associated with diverse aspects of living cells and organisms[68, 101]. FP-labeling provides structural information, visualization and quantification of molecular activities, physiological events, and interaction of biomolecules in living cells, tissues or whole organisms. Moreover, molecular processes can be controlled by fluorescent light[130].

Probes for monitoring of membrane potential require membrane targeting, strong signal emission, low noise, and fast kinetics. These features make the design of voltage sensors more challenging. Voltage-gated ion channel based FPs sensors[87-89] failed to fulfill these requirements while expressed in mammalian cells due to the destruction of the integrity of natural voltage-gated ion channel structure. A self-contained voltage-sensing domain (VSD) from *Ciona intestinalis* voltage sensor-containing phosphatase (Ci-VSP) was recently discovered[96] and demonstrated membrane targeting as a monomer[97]. The first Ci-VSP based voltage sensor utilized the tandem FRET pair (CFP/YFP) attached to the C-terminal of the fourth transmembrane segment of Ci-VSP[95]. With the modification of linker length between VSD and FPs pair (VSFP2A-D), fine tuning by site mutation (VSFP2.1) and optimization of amino acids composition, the resulting sensor, VSFP2.3, has been shown to exhibit defined expression on plasma membrane, fast response to membrane potential within physiological range in PC12 cells[85].

Several VSFP2-based variants were further introduced by using different FP pairs (VSFP2x)[85, 99, 101, 131, 132] or monochromic FPs (VSF3x)[85, 133]. The different variants are summarized in Table 15. The use of near-red or red-shifted FPs such as mOrange, mKate2, TagRFP, provides better spectral separation from green tissue autofluorescence and also enables signal detection from deeper inside the target tissue. However, the red shifted variants also exhibited low quantum yield and high bleaching rate[132, 133]. In addition, the plasma membrane targeting efficiency of some far-red FPs and coral-derived FPs (Mermaid) is suboptimal and intracellular aggregates were often observed during long-term expression[99, 101, 131, 132]. On the other

hand, although monochromic FPs-based VSFP3x covered a broad range of color spectrum and displayed fast response, the sensitivity to electrical signals was less and signal amplitudes were smaller than VSFP2x[133].

All the above-mentioned VSFPs have been investigated intensively in neuron cells, brain slice, and *in vivo* recordings of brain[99-101]. However, none of them has been exploited in the field of cardiac electrophysiology. Each VSFP has its own pros and cons with regard to different experiment systems. Many efforts have been made in producing new version of voltage sensors and the advancement is still progressing. We chose VSFP2.3 for the cardiac research since it remains one of the best-validated VSFP variants, and holds some promising features. Firstly, the plasma membrane targeting is more specific and responsiveness to electrical signals is more reliable as compared to other FP sensors. Secondly, this FRET-based sensor provides ratiometric measurement that minimizes the motion artifacts caused by heartbeat and breathing in *in vivo* experiment.

In this study, we presented the first proof of concept that extends the application of VSFP2.3 in the field of cardiac research. The following main results have been obtained:

1. The first transgenic mouse model with stable expression of VSFP2.3 in the heart was established and characterized.
2. Transgenic mouse iPSC lines with cardiomyocyte restricted VSFP2.3 for optical action potential measurement and cardiomyocyte selection were established.

Table 15 Ci-VSP based VSFP2 variants

sensor	FP(s)/peak emission wavelength(s) (nm)	Expression system for functional characterization	sensitivity (at xx mV)	Response time constant (ms)		Ref.
				on	off	
VSFP2.1	CFP/477 YFP/529	PC12 cells, neuron	ΔR/R: 6.8%/100 mV (at -70mV)	15	75	95
VSFP3.1	CFP/475	PC12 cells	ΔF/F: 2.2% (at -43 mV)	1.8	105	85, 133
VSFP2.3	CFP/477 YFP/529	PC12 cells, neurons, mouse	ΔR/R: 22%/100 mV (at -50 mV)	30, ~2	~80	85, 132
VSFP2-Mermaid	mUKG/490 mKOk/560	Xenopus oocytes, NT cells	ΔR/R: 21%/100 mV (at -43 mV)	30, ~2	~80	131, 132
VSFP2.4	mCitrine/529 mKate1.3/633	PC12 cells	ΔR/R: 20.5%/100 mV (at -54 mV)	30, ~2	~80	132
VSFP3x	mCitrine/529 mOrange/562 TagRFP/584 mKate2/633	neurons	ΔF/F: 2.5~5%/100 mV	2-100	~100	133
VSFP2.42	mCitrine/529 mKate2/633	neurons, brain slices and *in vivo*	ΔR/R: 20.5% (at -50 mV)	80, 2	~80	101
VSFP2-Butterfly1.2	mCitrine/529 mKate2/633	neurons, brain slices and *in vivo*	ΔR/R: 22.2% (at -79 mV)	10, 2	~80	134

Adapted from[135]

6. Outlook

With the VSFP2.3 transgenic mouse model and an induced pluripotent stem cell lines, we anticipate to gain insight into the following questions:

1. Factors, such as mechanical stimulation, electrical stimulation or chemical stimulation (growth factor, small molecular...etc.), that enhance cardiac differentiation, the maturation of cardiomyocytes, and tissue formation in EHMs
2. To visualize the formation of a functional syncytium during cardiogenesis in 2D culture, EHMs, and the integration of implanted cells and EHMs with native myocardium
3. To study certain disease models, myocardium healing/regeneration process.

Alternative fluorochromes providing better spectral separation and tissue penetration can be beneficial to in vivo studies and need to be further investigated.

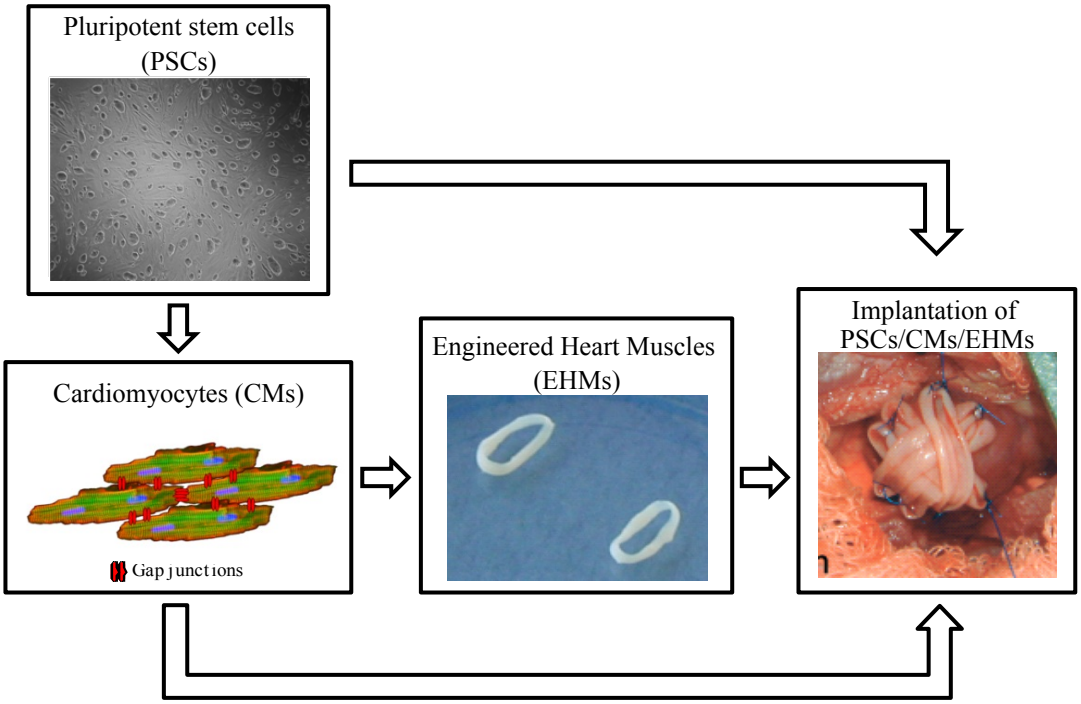

In Vitro	*In Vitro*	*In Vivo*[16]
• PSCs-derived CMs	• Mechanical properties • Electrical properties	• Integration into native myocardium

Fig. 46 Schematic of the application of αMHC-VSFP2.3

7. Bibliography

1. Cao, F. et al. Spatial and temporal kinetics of teratoma formation from murine embryonic stem cell transplantation. *Stem Cells Dev* **16**, 883-891 (2007).
2. Hentze, H. et al. Teratoma formation by human embryonic stem cells: evaluation of essential parameters for future safety studies. *Stem cell research* **2**, 198-210 (2009).
3. Takahashi, K. & Yamanaka, S. Induction of pluripotent stem cells from mouse embryonic and adult fibroblast cultures by defined factors. *Cell* **126**, 663-676 (2006).
4. Hanley, J., Rastegarlari, G. & Nathwani, A.C. An introduction to induced pluripotent stem cells. *British Journal of Haematology* **151**, 16-24 (2010).
5. Shimizu, T. et al. Fabrication of pulsatile cardiac tissue grafts using a novel 3-dimensional cell sheet manipulation technique and temperature-responsive cell culture surfaces. *Circulation Research* **90**, e40 (2002).
6. Hata, H. et al. Engineering a novel three-dimensional contractile myocardial patch with cell sheets and decellularised matrix. *European journal of cardio-thoracic surgery : official journal of the European Association for Cardio-thoracic Surgery* **38**, 450-455 (2010).
7. Bel, A. et al. Composite cell sheets: a further step toward safe and effective myocardial regeneration by cardiac progenitors derived from embryonic stem cells. *Circulation* **122**, S118-123 (2010).
8. Ott, H.C. et al. Perfusion-decellularized matrix: using nature's platform to engineer a bioartificial heart. *Nature medicine* **14**, 213-221 (2008).
9. Radisic, M. et al. Biomimetic approach to cardiac tissue engineering: oxygen carriers and channeled scaffolds. *Tissue engineering* **12**, 2077-2091 (2006).
10. Radisic, M. From the Cover: Functional assembly of engineered myocardium by electrical stimulation of cardiac myocytes cultured on scaffolds. *Proceedings of the National Academy of Sciences* **101**, 18129-18134 (2004).
11. Zimmermann, W. et al. Tissue engineering of a differentiated cardiac muscle construct. *Circulation Research* **90**, 223-230 (2002).
12. Martens, T.P. et al. Percutaneous cell delivery into the heart using hydrogels polymerizing in situ. *Cell transplantation* **18**, 297-304 (2009).
13. Huang, G., Pashmforoush, M., Chung, B. & Saxon, L.A. The role of cardiac electrophysiology in myocardial regenerative stem cell therapy. *J Cardiovasc Transl Res* **4**, 61-65 (2011).
14. Radisic, M. et al. Functional assembly of engineered myocardium by electrical stimulation of cardiac myocytes cultured on scaffolds. *Proceedings of the*

National Academy of Sciences of the United States of America **101**, 18129-18134 (2004).

15. Vunjak-Novakovic, G., Lui, K.O., Tandon, N. & Chien, K.R. Bioengineering heart muscle: a paradigm for regenerative medicine. *Annu Rev Biomed Eng* **13**, 245-267 (2011).
16. Zimmermann, W.-H. et al. Engineered heart tissue grafts improve systolic and diastolic function in infarcted rat hearts. *Nature Medicine* **12**, 452-458 (2006).
17. Wang, Y. & Hill, J.A. Electrophysiological remodeling in heart failure. *J Mol Cell Cardiol* **48**, 619-632 (2010).
18. Berne, R.M. & Levy, M.N. in Cardiovascular Physiology, Edn. 8th 7-53 (Mosby, Inc., United States of America; 2001).
19. Sperelakis, N. in Cell Physiology Sourcebook - A Molecular Approach, Edn. 3rd. (ed. N. Sperelakis) (Academic Press, USA; 2001).
20. Mangoni, M.E. & Nargeot, J. Genesis and regulation of the heart automaticity. *Physiol Rev* **88**, 919-982 (2008).
21. Bers, D.M. Cardiac excitation-contraction coupling. *Nature* **415**, 198-205 (2002).
22. Koubassova, N.A. & Tsaturyan, A.K. Molecular mechanism of actin-myosin motor in muscle. *Biochemistry (Mosc)* **76**, 1484-1506 (2011).
23. Efimov, I.R., Nikolski, V.P. & Salama, G. Optical imaging of the heart. *Circ Res* **95**, 21-33 (2004).
24. Salama, G. in Optical Mapping of Cardiac Excitation and Arrhythmias. (eds. D.S. Rosenbaum & J. Jalife) (Futura Publishing Co., Inc., Armonk, NY; 2001).
25. Efimov, I.R. & Cheng, Y. in Quantitative Cardiac Electrophysiology. (ed. R.D. Cabo C) (Dekker, New York; 2002).
26. Rosenbaum, D.S. & Jalife, J. in (Futura Publishing, Armonk, NY; 2001).
27. Sih, H. & Berbari, E. in Cardiac Mapping, Edn. 2. (eds. M. Shenasa, M. Borggrefe & G. Breithardt) (Blackwell Publishing, Inc./Futura Division, Elmsford, NY; 2003).
28. Biermann, M. et al. in Cardiac Mapping, Edn. 2. (eds. M. Shenasa, M. Borggrefe & G. Breithardt) 11 (Blackwell Publishing, Inc./Futura Division, Elmsford, NY; 2003).
29. Scacchi, S., Franzone, P.C., Pavarino, L.F. & Taccardi, B. A reliability analysis of cardiac repolarization time markers. *Math Biosci* **219**, 113-128 (2009).

30. Steinhaus, B.M. Estimating cardiac transmembrane activation and recovery times from unipolar and bipolar extracellular electrograms: a simulation study. *Circ Res* **64**, 449-462 (1989).

31. Davila, H.V., Salzberg, B.M., Cohen, L.B. & Waggoner, A.S. A large change in axon fluorescence that provides a promising method for measuring membrane potential. *Nat New Biol* **241**, 159-160 (1973).

32. Cohen, L.B., Keynes, R.D. & Hille, B. Light scattering and birefringence changes during nerve activity. *Nature* **218**, 438-441 (1968).

33. Salama, G. & Morad, M. Merocyanine 540 as an optical probe of transmembrane electrical activity in the heart. *Science* **191**, 485-487 (1976).

34. Bu, G. & Berbari, E.J. Optical recording of single cardiomyocyte transmembrane potential in Langendorff-perfused mouse hearts. *Computers in Cardiology*, 357-360 (2007).

35. Bu, G., Adams, H., Berbari, E.J. & Rubart, M. Uniform Action Potential Repolarization within the Sarcolemma of In Situ Ventricular Cardiomyocytes. *Biophysj* **96**, 2532-2546 (2009).

36. Tian, Q. et al. Optical action potential screening on adult ventricular myocytes as an alternative QT-screen. *Cellular physiology and biochemistry : international journal of experimental cellular physiology, biochemistry, and pharmacology* **27**, 281-290 (2011).

37. Tung, L. & Zhang, Y. Optical imaging of arrhythmias in tissue culture. *Journal of Electrocardiology* **39**, S2-S6 (2006).

38. Enticheva, E. & Bien, H. Macroscopic optical mapping of excitation in cardiac cell networks with ultra-high spatiotemporal resolution. *Progress in Biophysics and Molecular Biology* **92**, 232-257 (2006).

39. Lan, D., Pollard, A., Knisley, S. & Fast, V. Optical mapping of Vm and Cai2+ in a model of arrhythmias induced by local catecholamine application in patterned cell cultures. *Pflügers Archiv European Journal of Physiology* **453**, 871-877 (2007).

40. Hong, J.H., Choi, J.H., Kim, T.Y. & Lee, K.J. Spiral reentry waves in confluent layer of HL-1 cardiomyocyte cell lines. *Biochem Biophys Res Commun* **377**, 1269-1273 (2008).

41. Glukhov, A.V. et al. Transmural dispersion of repolarization in failing and nonfailing human ventricle. *Circ Res* **106**, 981-991 (2010).

42. Seo, K. et al. Structural heterogeneity in the ventricular wall plays a significant role in the initiation of stretch-induced arrhythmias in perfused rabbit right ventricular tissues and whole heart preparations. *Circ Res* **106**, 176-184 (2010).

43. Strom, M., Wan, X., Poelzing, S., Ficker, E. & Rosenbaum, D.S. Gap junction heterogeneity as mechanism for electrophysiologically distinct properties across the ventricular wall. *Am J Physiol Heart Circ Physiol* **298**, H787-794 (2010).

44. Koura, T. et al. Anisotropic conduction properties in canine atria analyzed by high-resolution optical mapping: preferential direction of conduction block changes from longitudinal to transverse with increasing age. *Circulation* **105**, 2092-2098 (2002).

45. Sakai, T. Optical mapping of the spread of excitation in the isolated rat atrium during tachycardia-like excitation. *Pflugers Archiv : European journal of physiology* **447**, 280-288 (2003).

46. Sakai, T. Optical mapping analysis of the spatiotemporal pattern of experimental tachyarrhythmia in improved isolated rat atrium preparation. *The journal of physiological sciences : JPS* **58**, 87-97 (2008).

47. Rentschler, S. et al. Visualization and functional characterization of the developing murine cardiac conduction system. *Development (Cambridge, England)* **128**, 1785-1792 (2001).

48. Wu, J., Wu, J., Olgin, J., Miller, J.M. & Zipes, D.P. Mechanisms Underlying the Reentrant Circuit of Atrioventricular Nodal Reentrant Tachycardia in Isolated Canine Atrioventricular Nodal Preparation Using Optical Mapping. *Circulation Research* **88**, 1189-1195 (2001).

49. Hucker, W.J., Fedorov, V.V., Foyil, K.V., Moazami, N. & Efimov, I.R. Optical Mapping of the Human Atrioventricular Junction. *Circulation* **117**, 1474-1477 (2008).

50. Radisic, M. et al. Optical mapping of impulse propagation in engineered cardiac tissue. *Tissue engineering. Part A* **15**, 851-860 (2009).

51. Katare, R.G., Ando, M., Kakinuma, Y. & Sato, T. Engineered heart tissue: a novel tool to study the ischemic changes of the heart in vitro. *PLoS ONE* **5**, e9275 (2010).

52. Lang, D., Sulkin, M., Lou, Q. & Efimov, I.R. Optical mapping of action potentials and calcium transients in the mouse heart. *Journal of Visualized Experiments* (2011).

53. Salama, G. & Choi, B.R. Images of Action Potential Propagation in Heart. *News in physiological sciences : an international journal of physiology produced jointly by the International Union of Physiological Sciences and the American Physiological Society* **15**, 33-41 (2000).

54. Matiukas, A. et al. Near-infrared voltage-sensitive fluorescent dyes optimized for optical mapping in blood-perfused myocardium. *Heart Rhythm* **4**, 1441-1451 (2007).

55. Lee, P. et al. Single-sensor system for spatially resolved, continuous, and multiparametric optical mapping of cardiac tissue. *Heart Rhythm* **8**, 1482-1491 (2011).

56. Sharma, V., Qu, F., Nikolski, V.P., DeGroot, P. & Efimov, I.R. Direct measurements of membrane time constant during defibrillation strength shocks. *Heart Rhythm* **4**, 478-486 (2007).

57. Cheng, Y., Mowrey, K.A., Nikolski, V., Tchou, P.J. & Efimov, I.R. Mechanisms of shock-induced arrhythmogenesis during acute global ischemia. *Am J Physiol Heart Circ Physiol* **282**, H2141-2151 (2002).

58. Chang, M.G. et al. Spiral waves and reentry dynamics in an in vitro model of the healed infarct border zone. *Circ Res* **105**, 1062-1071 (2009).

59. Arora, R., Das, M.K., Zipes, D.P. & Wu, J. Optical mapping of cardiac arrhythmias. *Indian pacing and electrophysiology journal* **3**, 187-196 (2003).

60. Chen, P.S. et al. Imaging arrhythmogenic calcium signaling in intact hearts. *Pediatric cardiology* **33**, 968-974 (2012).

61. Ding, C. et al. High-resolution optical mapping of ventricular tachycardia in rats with chronic myocardial infarction. *Pacing and clinical electrophysiology : PACE* **33**, 687-695 (2010).

62. Fast, V.G. Simultaneous optical imaging of membrane potential and intracellular calcium. *J Electrocardiol* **38**, 107-112 (2005).

63. Salama, G. & Hwang, S.M. Simultaneous optical mapping of intracellular free calcium and action potentials from Langendorff perfused hearts. *Curr Protoc Cytom* **Chapter 12**, Unit 12 17 (2009).

64. Saba, S. et al. Dual-Dye Optical Mapping after Myocardial Infarction: Does the Site of Ventricular Stimulation Alter the Properties of Electrical Propagation? *Journal of Cardiovascular Electrophysiology* **19**, 197-202 (2008).

65. Prasher, D.C., Eckenrode, V.K., Ward, W.W., Prendergast, F.G. & Cormier, M.J. Primary structure of the Aequorea victoria green-fluorescent protein. *Gene* **111**, 229-233 (1992).

66. Heim, R. & Prasher, D.C. Wavelength mutations and posttranslational autoxidation of green fluorescent protein. *Proc. Natl. Acad. Sci.* **91**, 12501-12504 (1994).

67. Tsien, R.Y. The green fluorescent protein. *Annu. Rev. Biochem.* **67**, 509-544 (1998).

68. Chudakov, D.M., Matz, M.V., Lukyanov, S. & Lukyanov, K.A. Fluorescent Proteins and Their Applications in Imaging Living Cells and Tissues. *Physiological Reviews* **90**, 1103-1163 (2010).

69. Nakai, J. & Ohkura, M. A high signal-to-noise Ca2+ probe composed of a single green fluorescent protein. *Nature Biotechnology* **19**, 137-141 (2001).

70. Lee, M.Y. et al. Local subplasma membrane Ca2+ signals detected by a tethered Ca2+ sensor. *Proceedings of the National Academy of Sciences of the United States of America* **103**, 13232-13237 (2006).

71. Kotlikoff, M.I. Genetically encoded Ca2+ indicators: using genetics and molecular design to understand complex physiology. *The Journal of Physiology* **578**, 55-67 (2006).

72. Tallini, Y.N. et al. Imaging cellular signals in the heart in vivo: Cardiac expression of the high-signal Ca2+ indicator GCaMP2. *Proceedings of the National Academy of Sciences of the United States of America* **103**, 4753-4758 (2006).

73. Mao, T., O'Connor, D.H., Scheuss, V., Nakai, J. & Svoboda, K. Characterization and subcellular targeting of GCaMP-type genetically-encoded calcium indicators. *PloS one* **3**, e1796 (2008).

74. Díez-García, J. et al. Activation of cerebellar parallel fibers monitored in transgenic mice expressing a fluorescent Ca2+ indicator protein. *European Journal of Neuroscience* **22**, 627-635 (2005).

75. Urra, J. et al. A genetically encoded ratiometric sensor to measure extracellular pH in microdomains bounded by basolateral membranes of epithelial cells. *Pflügers Archiv - European Journal of Physiology* **457**, 233-242 (2008).

76. Bizzarri, R., Serresi, M., Luin, S. & Beltram, F. Green fluorescent protein based pH indicators for in vivo use: a review. *Analytical and Bioanalytical Chemistry* **393**, 1107-1122 (2008).

77. Tantama, M., Hung, Y.P. & Yellen, G. Imaging Intracellular pH in Live Cells with a Genetically Encoded Red Fluorescent Protein Sensor. *J. Am. Chem. Soc.* **133**, 10034-10037 (2011).

78. Liu, Z., Celotto, A.M., Romero, G., Wipf, P. & Palladino, M.J. Genetically encoded redox sensor identifies the role of ROS in degenerative and mitochondrial disease pathogenesis. *Neurobiology of Disease* **45**, 362-368 (2012).

79. Hanson, G.T. et al. Investigating Mitochondrial Redox Potential with Redox-sensitive Green Fluorescent Protein Indicators. *Journal of Biological Chemistry* **279**, 13044-13053 (2004).

80. Zhang, J. Genetically encoded reporters of protein kinase A activity reveal impact of substrate tethering. *Proceedings of the National Academy of Sciences* **98**, 14997-15002 (2001).

81. Arrenberg, A.B., Stainier, D.Y.R., Baier, H. & Huisken, J. Optogenetic Control of Cardiac Function. *Science* **330**, 971-974 (2010).

82. Kasparov, S. The many facets of optogenetics. *Experimental Physiology* **96**, 1-3 (2010).

83. Knoepfel, T. et al. Toward the second generation of optogenetic tools. *Journal of Neuroscience* **30**, 14998-15004 (2010).

84. Mutoh, H., Perron, A., AKEMANN, W., Iwamoto, Y. & KNOPFEL, T. Optogenetic monitoring of membrane potentials. *Experimental Physiology* **96**, 13-18 (2010).

85. Lundby, A., Mutoh, H., Dimitrov, D., Akemann, W. & KnOpfel, T. Engineering of a Genetically Encodable Fluorescent Voltage Sensor Exploiting Fast Ci-VSP Voltage-Sensing Movements. *PLoS ONE* **3**, e2514 (2008).

86. Catterall, W.A. Ion channel voltage sensors: structure, function, and pathophysiology. *Neuron* **67**, 915-928 (2010).

87. Siegel, M.S. & Isacoff, E.Y. A genetically encoded optical probe of membrane voltage. *Neuron* **19**, 735-741 (1997).

88. Ataka, K. & Pieribone, V.A. A Genetically Targetable Fluorescent Probe of Channel Gating with Rapid Kinetics. *Biophysj* **82**, 509-516 (2002).

89. Sakai, R., Repunte-Canonigo, V., Raj, C.D. & Knoepfel, T. Design and characterization of a DNA-encoded voltage sensitive fluorescent protein. *European Journal of Neuroscience* **13**, 2314-2318 (2001).

90. Pollok, B.A. & Heim, R. Using GFP in FRET-based applications. *Trends Cell Biol* **9**, 57-60 (1999).

91. Piston, D.W. & Kremers, G.J. Fluorescent protein FRET: the good, the bad and the ugly. *Trends in biochemical sciences* **32**, 407-414 (2007).

92. Baker, B.J. et al. Genetically encoded fluorescent sensors of membrane potential. *Brain Cell Biology* **36**, 53-67 (2008).

93. Knoepfel, T. Optical recordings of membrane potential using genetically targeted voltage-sensitive fluorescent proteins. *Methods* **30**, 42-48 (2003).

94. Knoepfel, T., Díez-García, J. & Akemann, W. Optical probing of neuronal circuit dynamics: genetically encoded versus classical fluorescent sensors. *Trends in neurosciences* **29**, 160-166 (2006).

95. Dimitrov, D. et al. Engineering and Characterization of an Enhanced Fluorescent Protein Voltage Sensor. *PLoS ONE* **2**, e440 (2007).

96. Murata, Y., Iwasaki, H., Sasaki, M., Inaba, K. & Okamura, Y. Phosphoinositide phosphatase activity coupled to an intrinsic voltage sensor. *Nature* **435**, 1239-1243 (2005).

97. Kohout, S.C., Ulbrich, M.H., Bell, S.C. & Isacoff, E.Y. Subunit organization and functional transitions in Ci-VSP. *Nature Structural & Molecular Biology* **15**, 106-108 (2007).

98. Okamura, Y., Murata, Y. & Iwasaki, H. Voltage-sensing phosphatase: actions and potentials. *The Journal of Physiology* **587**, 513-520 (2009).

99. Perron, A. et al. Second and third generation voltage-sensitive fluorescent proteins for monitoring membrane potential. *Frontiers in Molecular Neuroscience* **2**, 5 (2009).

100. Akemann, W., Lundby, A., Mutoh, H. & Knopfel, T. Effect of voltage sensitive fluorescent proteins on neuronal excitability. *Biophysical Journal* **96**, 3959-3976 (2009).

101. Akemann, W., Mutoh, H., Perron, A., Rossier, J. & Knopfel, T. Imaging brain electric signals with genetically targeted voltage-sensitive fluorescent proteins. *Nature Methods* **7**, 643-649 (2010).

102. Katz, E.B. et al. Cardiomyocyte proliferation in mice expressing alpha-cardiac myosin heavy chain-SV40 T-antigen transgenes. *The American journal of physiology* **262**, H1867-1876 (1992).

103. Stec, D.E., Morimoto, S. & Sigmund, C.D. Vectors for high-level expression of cDNAs controlled by tissue-specific promoters in transgenic mice. *BioTechniques* **31**, 256-258, 260 (2001).

104. Kabaeva, Z., Zhao, M. & Michele, D.E. Blebbistatin extends culture life of adult mouse cardiac myocytes and allows efficient and stable transgene expression. *AJP: Heart and Circulatory Physiology* **294**, H1667-H1674 (2008).

105. O'Connell, T.D., Rodrigo, M.C. & Simpson, P.C. Isolation and culture of adult mouse cardiac myocytes. *Methods in molecular biology (Clifton, N.J.)* **357**, 271-296 (2007).

106. Little, M. & Jones, N. Sparse bayesian step-filtering for high-throughput analysis of molecular machine dynamics. *In Proc. ICASSP*, 4162-4165 (2010).

107. Subramaniam, A. et al. Tissue-Specific Regulation of the Alpha-Myosin Heavy-Chain Gene Promoter in Transgenic Mice. *Journal of Biological Chemistry* **266**, 24613-24620 (1991).

108. Huang, W.Y., Aramburu, J., Douglas, P.S. & Izumo, S. Transgenic expression of green fluorescence protein can cause dilated cardiomyopathy. *Nat Med* **6**, 482-483 (2000).

109. Colomer, J.M., Terasawa, M. & Means, A.R. Targeted expression of calmodulin increases ventricular cardiomyocyte proliferation and deoxyribonucleic acid synthesis during mouse development. *Endocrinology* **145**, 1356-1366 (2004).

110. Arrigoni, C. & Crivori, P. Assessment of QT liabilities in drug development. *Cell biology and toxicology* **23**, 1-13 (2007).

111. Villalba-Galea, C.A. et al. Charge Movement of a Voltage-Sensitive Fluorescent Protein. *Biophysical Journal* **96**, L19-L21 (2009).

112. Bøkenes, J., Sjaastad, I. & Sejersted, O.M. Artifactual contractions triggered by field stimulation of cardiomyocytes. *Journal of Applied Physiology* **98**, 1712-1719 (2005).

113. Cheng, D.K., Tung, L. & Sobie, E.A. Nonuniform responses of transmembrane potential during electric field stimulation of single cardiac cells. *The American journal of physiology* **277**, H351-362 (1999).

114. Sharma, V. & Tung, L. Spatial heterogeneity of transmembrane potential responses of single guinea-pig cardiac cells during electric field stimulation. *The Journal of Physiology* **542**, 477-492 (2002).

115. Tung, L. Response of cardiac myocytes to electrical fields. *Optical mapping of cardiac excitation and arrhythmias* (2001).

116. Cheng, Y., Li, L., Nikolski, V., Wallick, D.W. & Efimov, I.R. Shock-induced arrhythmogenesis is enhanced by 2,3-butanedione monoxime compared with cytochalasin D. *Am J Physiol Heart Circ Physiol* **286**, H310-318 (2004).

117. Hayashi, H. et al. Effects of cytochalasin D on electrical restitution and the dynamics of ventricular fibrillation in isolated rabbit heart. *J Cardiovasc Electrophysiol* **14**, 1077-1084 (2003).

118. Swift, L.M. et al. Properties of blebbistatin for cardiac optical mapping and other imaging applications. *Pflugers Archiv : European journal of physiology* **464**, 503-512 (2012).

119. Brines, L. et al. Modifications of mechanoelectric feedback induced by 2,3-butanedione monoxime and Blebbistatin in Langendorff-perfused rabbit hearts. *Acta Physiol (Oxf)* **206**, 29-41 (2012).

120. Biermann, M. et al. Differential effects of cytochalasin D and 2,3 butanedione monoxime on isometric twitch force and transmembrane action potential in isolated ventricular muscle: implications for optical measurements of cardiac repolarization. *J Cardiovasc Electrophysiol* **9**, 1348-1357 (1998).

121. Brack, K.E., Narang, R., Winter, J. & Ng, G.A. The mechanical uncoupler blebbistatin is associated with significant electrophysiological effects in the isolated rabbit heart. *Exp Physiol* **98**, 1009-1027 (2013).

122. Salmon, A.B. et al. Fibroblast cell lines from young adult mice of long-lived mutant strains are resistant to multiple forms of stress. *American journal of physiology. Endocrinology and metabolism* **289**, E23-29 (2005).

123. Filipczyk, A.A., Passier, R., Rochat, A. & Mummery, C.L. Regulation of cardiomyocyte differentiation of embryonic stem cells by extracellular signalling. *Cellular and molecular life sciences : CMLS* **64**, 704-718 (2007).

124. Somers, A. et al. Generation of Transgene-Free Lung Disease-Specific Human Induced Pluripotent Stem Cells Using a Single Excisable Lentiviral Stem Cell Cassette. *STEM CELLS* **28**, 1728-1740 (2010).

125. Loh, Y.H. et al. Excision of a viral reprogramming cassette by delivery of synthetic Cre mRNA. *Curr Protoc Stem Cell Biol* **Chapter 4**, Unit4A 5 (2012).

126. Christalla, P. in Department Biology, Vol. Ph.D (University of Hamburg, 2010).

127. Rubart, M. et al. Physiological coupling of donor and host cardiomyocytes after cellular transplantation. *Circ Res* **92**, 1217-1224 (2003).

128. Didié, M. et al. Parthenogenetic stem cells for tissue-engineered heart repair. *J. Clin. Invest.* (2013).

129. Deisseroth, K. Optogenetics. *Nat. Meth.* **8**, 26-29 (2010).

130. Rein, M.L. & Deussing, J.M. The optogenetic (r)evolution. *Molecular genetics and genomics : MGG* **287**, 95-109 (2012).

131. Tsutsui, H., Karasawa, S., Okamura, Y. & Miyawaki, A. Improving membrane voltage measurements using FRET with new fluorescent proteins. *Nature Methods* **5**, 683-685 (2008).

132. Mutoh, H. et al. Spectrally-Resolved Response Properties of the Three Most Advanced FRET Based Fluorescent Protein Voltage Probes. *PLoS ONE* **4**, e4555 (2009).

133. Perron, A., Mutoh, H., Launey, T. & Knopfel, T. Red-shifted voltage-sensitive fluorescent proteins. *Chemistry & Biology* **16**, 1268-1277 (2009).

134. Akemann, W. et al. Imaging neural circuit dynamics with a voltage-sensitive fluorescent protein. *Journal of Neurophysiology* **108**, 2323-2337 (2012).

135. Mutoh, H. & Knopfel, T. Probing neuronal activities with genetically encoded optical indicators: from a historical to a forward-looking perspective. *Pflügers Archiv - European Journal of Physiology* **465**, 361-371 (2013).

8. Appendix

A1. Supplement data

Table S-1 Echocardiography data and heart weight to body weight ratio

Line	HR (bpm)	HW/BW (mg/g)	FAS (%)	CO (ml/min)	LVIDd (mm)	LVIDs (mm)	AWThF (%)	PWThF (%)
WT	523.25	4.16	44.19	32.52	5.05	3.81	21.29	23.71
#97	548.88	4.23	38.74	27.89	4.82	3.74	21.75	26.32
#107	521.43	4.38	45.53	32.38	4.94	3.69	25.80	17.58
#108	513.88	4.40	45.01	32.41	5.02	3.72	27.42	25.93
#123	540.25	4.08	41.41	30.40	4.84	3.70	22.29	21.15
	ns	ns	ns	ns	ns	ns	ns	ns

A2. Reagents and medium

For cloning

1X TAE-buffer	mM
Tris-Acetate	40
Sodium-Acetate	20
EDTA, pH 7.5	1

LB-agarose plate (with ampicillin)

Agar	7.5 g
LB-medium	500 ml
Ampicillin stock (100 mg/ml)	500 µl

The LB-agar was autoclaved. After cooled down to around 60°C, LB-agar was poured into 10-cm petri dishes. Plates were stored at 4 °C after the agar had hardened.

LB-medium

Bacto-Tryptone	10 g
Bacto Yeast Extract	5 g
NaCl	10 g

Chemicals were dissolved with 950 ml of ddH_2O and pH was adjusted to 7.4 with 0.1 N NaOH. Final volume was brought up to 1 L and medium was autoclaved. Medium can be kept at 4°C for 3 weeks.

Ampicillin stock (100 mg/ml)

500 mg of Ampicillin was dissolved in 5 ml of ddH_2O. the stock solution was stored at -20°C in 500 µl aliquots.

Buffer for adult mouse cardiomyocytes isolation

Perfusion buffer (1X)	mM
NaCl	120.4
KCl	14.7
KH_2PO_4	0.6
Na_2HPO_4 x 2 H_2O	0.6
$MgSO_4$ x $7H_2O$	1.2
Na-HEPES	10
$NaHCO_3$	4.6
Taurine	30
BDM	10
Glucose	5.5

(1) Sterile filter (0.22 μm filter); (2) Adjust pH to 7.4 with NaOH

Buffers for patch clamp recordings

Bath solution	mM	Pipette solution	mM
NaCl	150	KCl	40
KCl	5.4	K-aspartate	80
$MgCl_2$	2	NaCl	8
Na-HEPES	10	Mg-ATP	5
$CaCl_2$	1.2	EGTA	5
Glucose	5.5	$CaCl_2$	2
		GTP-tris	0.1
		Na-HEPES	10

Buffer for optical mapping in Langendorff perfused hearts

Modified Tyrode's solution	mM
NaCl	130
$NaHCO_3$	24
KCl	4
$MgCl_2$	1
$CaCl_2$	1.8
KH_2PO_4	1.2
Glucose	5.6
BSA	1%
Insulin	5 IU/L
Blebbistatin	$5x10^{-3}$

Media for cell culture

MEF medium

DMEM (+) 4.5 g/l glucose, no pyruvate, with glutamax	
FCS	10%
NEAA (Non Essential Amino Acid, 100x)	1x
Pen/Strep (10,000 IU/l, 10,000 µg/l, 100x)	1x

Feeder layer medium

DMEM (#1960, Gibco)	
FCS (F7524, Sigma)	15%
L-glutamin (200 mM, 100x)	1x

mES medium

DMEM (+) 4.5 g/l glucose, no pyruvate, 25mM Hepes	
FCS (ES-qualified, active)	10%
NEAA (Non Essential Amino Acid, 100x)	1x
Pen/Strep (10,000 IU/l, 10,000 µg/l, 100x)	1x
L-glutamin (200 mM, 100x)	1x
* Nucleosidmix (100x)	1x
2-Mercaptoethanol (50 mM, 1000x)	100 µM
LIF (107 U/ml)	1000 U/ml
Sodium pyruvate	1x

* Nucleosidmix (100x)

Adenosine	30 µM
Guanosine	30 µM
Cytidine	30 µM
Uridine	30 µM
Thymidine	10 µM

Differentiation medium

Iscove medium (1X)	
FCS (ES-qualified, active)	20%
NEAA (Non Essential Amino Acid, 100x)	1x
Pen/Strep (10,000 IU/l, 10,000 µg/l, 100x)	1x
L-glutamin (200mM, 100x)	1x
2-Mercaptoethanol (50mM, 1000x)	100 µM
L-Ascorbic acid 2-phosphate sesquimagnesium salt hydrate	240 µM

Reagents and solutions for isometric force measurement

For making Tyrode's working solution, the following stock solutions should be prepared:

$CaCl_2$ stock (2.25 M)

$CaCl_2$ x 2 H_2O (Mw = 147.02)	165.57 g
ddH_2O	500 ml

$MgCl_2$ stock (1.05 M)

$MgCCl_2$ x 6 H_2O (Mw = 203.01)	106.83 g
ddH_2O	500 ml

Stock I: Ca^{2+} concentration in stock I can be adjusted accordingly.

[Ca^{2+}] (mM)	1.8	0.4	0.2
NaCl (Mw = 58.44)	175 g	175 g	175 g
KCl (Mw = 74.58)	10 g	10 g	10 g
$CaCl_2$ stock	20 ml	4.44 ml	2.22 ml
$MgCl_2$ stock	25 ml	25 ml	25 ml
to up with ddH_2O to	1000 ml	1000 ml	1000 ml

Stock II

$NaHCO_3$ (Mw = 84.01)	50 g
ddH_2O	1000 ml

Stock III

NaH_2PO_4 (Mw = 137.99)	5.8 g
ddH_2O	1000 ml

All stock solutions can be stored at 4°C till required.

Tyrode's working solution (for 8 EHMs)

Stock I	80 ml
Stock II	76 ml
Stock III	20 ml
Glucose	2 g
Ascorbic acid	100 mg
H_2O	to 2 L

9. List of Publication

Original work

Mei-Ling Chang Liao, Hiroki Mutoh, Teun de Boer, Nour Raad, Claudia Richter, Bernhard Unsöld, Iqra Tarrar, Katrin Streckfuss-Bömeke, Stephan Doeker, Stefan Luther, Kaomei Guan, Stefan Wagner, Stephan Lehnart, Lars Maier, Walter Stühmer, Erich Wettwer, Toon van Veen, Michael Morlock, Thomas Knöpfel, Wolfram-Hubertus Zimmermann. Reporting Cardiac Electrical Activity with a Cardiomyocyte Targeted Optogenetic Voltage Indicator. **(In preparation)**

Conference Presentation

Oral

Mei-Ling Chang Liao, Hiroki Mutoh, Yuka Iwamoto, Nour Raad, Peter Christalla, Stephan Doeker, Viacheslav Nikolaev, Stefan Luther, Stephan Lehnart, Thomas Knöpfel, Wolfram-Hubertus Zimmermann. Optogenetic Voltage Sensor VSFP2.3 as a Novel Tool in Cardiac Electrophysiology. *American Heart Association Meeting, Orlando, USA, 2011.* (Circulation, 2011; 124 (21 suppl): A15940).

Mei-Ling Chang Liao, Hiroki Mutoh, Yuka Iwamoto, Nour Raad, Peter Christalla, Stephan Doeker, Viacheslav Nikolaev, Stefan Luther, Stephan Lehnart, Walter Stühmer, Thomas Knöpfel, Wolfram-Hubertus Zimmermann. Towards Optogenetic Cardiography. *Molecular Imaging meeting, Goettingen, Germany, 2011.*

Poster

Mei-Ling Chang Liao, Katrin Streckfuß-Bömeke, Erich Wettwer, Kaomei Guan, Thomas Knöpfel, Wolram-Hubertus Zimmermann. Voltage Sensitive Fluorescent Protein (VSFP2.3) Stably Expressed in Induced Pluripotent Stem Cell derived Cardiomyocytes and Engineering Heart Muscle. Deutsche Gesellschaft fuer Kardiologie Basic Science Meeting, Dresden, Germany, 2013.

Mei-Ling Chang Liao, Hiroki Mutoh, Yuka Iwamoto, Nour Raad, Stephan Doeker, Viacheslav Nikolaev, Stefan Luther, Stephan Lehnart, Teun de Boer, Walter Stühmer, Thomas Knöpfel[5], Wolfram-Hubertus Zimmermann. Optogenetic Cardiac Electrophysiology. Heart Failure Association of the European Society of Cardiology Translational Winter Research Meeting on Heart Failure, Les Diablerets, Switzerland, 2012.

Mei-Ling Chang Liao, Hiroki Mutoh, Yuka Iwamoto, Nour Raad, Stephan Döker, Viacheslav Nikolaev, Stefan Wagner, Peter Christalla, Stefan Luther, Stephan Lehnart, Lars Maier, Walter Stühmer, Thomas Knöpfel, Wolfram-Hubertus Zimmermann. Voltage Sensitive Fluorescent Protein (VSFP2.3) – A Biosensor for Studying the Electrical Activity and Sacrolemma Structure in Mouse Hearts. 9th German-Dutch Meeting of Cardiology Groups. Ulm, Germany, 2011.

Mei-Ling Chang Liao, Hiroki Mutoh, Yuka Iwamoto, Nour Raad, Viacheslav Nikolaev, Stefan Luther, Stephan Lehnart, Stefan Wagner, Lars Maier, Walter Stühmer, Thomas Knöpfel, Wolfram-Hubertus Zimmerman*n.* Voltage Sensitive Protein 2.3: a Novel Tool to Study Sarcolemmal Structure and Electrical Activity in Mouse Heart. *Biophysical Society 55th Annual Meeting, Baltimore, USA.* (Biophysical Journal, 2011; 100 (3 Supp1 1), Pages 575a–576a).